Motor Imagery based Brain-Computer Interface Systems beyond Controlled Environments

Sonal Santosh Baberwal

B.Eng.

A dissertation submitted in fulfillment of the requirements for the award of Doctor of Philosophy (Ph.D.)

DCU
Ollscoil Chathair
Bhaile Átha Cliath
Dublin City University

School of Electronic Engineering
Dublin City University

Supervised by: Dr Shirley Coyle, Prof. Tomás Ward

January 2026

Declaration

I hereby certify that this material, which I now submit for assessment on the programme of study leading to the award of Doctor of Philosophy is entirely my own work, and that I have exercised reasonable care to ensure that the work is original and have conformed to the regulations on the use and declaration of Generative AI, and does not to the best of my knowledge breach any law of copyright, and has not been taken from the work of others save and to the extent that such work has been cited and acknowledged within the text of my work.

Sign: Sonal Santosh Baberwal
ID No.: **21267107**
07/01/2026

Reporting of Generative AI

Tools:	ChatGPT 4.0, 5.0, Grammarly from Jul 2023 to Sep 2025
Outputs:	I used ChatGPT and Grammarly to improve the clarity and academic writing style with grammar throughout the thesis. Also, ChatGPT has been used to improve some parts of the code generated in Chapter 6 and for Statistical Analysis in Chapters 4 and 7.
Prompts:	I asked ChatGPT to "Improve this text grammar, academic style while maintaining flow with the previous paragraph". To improve the code(for Chapter 6) after generating the primary code, I asked ChatGPT, "Can you assist with converting this code into a loop to extract features across all datasets?" For Chapters 4 and 7, I asked ChatGPT, "Can you help me confirm if my code is correct for parametric and non-parametric tests?"
Iterations:	Mostly once for some parts of the thesis where a better flow is required. After a prompt was generated, each part was carefully read and manually edited to fill the gaps while maintaining the correct theoretical background supported with literature. For code, sometimes a few iterations (2 to 3 times) were required to improve the final version as required. Every code is manually checked line by line and validated by running each block. No Gen AI system was used to compose, rewrite, edit, structure, or otherwise create any part of the scholarly narrative, argumentation, analysis, or conclusions presented herein. All intellectual contributions, interpretations, and results are entirely my own, and all work complies with DCU's standards for responsible and ethical use of Gen AI.
Critical Reflection:	As a non-native English speaker, the role of Gen AI has been vital in assisting to improve the clarity and grammar in some parts of the thesis to develop a high-quality and academically sound thesis. Furthermore, the use of Gen AI to improve the code has assisted in focusing more on the core objectives of the project while meeting the deadlines and delivering high-impact outputs.

"When your heart learns to be satisfied with things and shows mercy and love towards all beings, you'd start living life with happiness."

- Mrs. Rajkumari V. Baberwal, On behalf of my Paternal Family.

Dedication

In loving memory of My Dadaji, Maa, Babuji, Nani [grandparents], my Mama (Uncle) and Shiro 🐾

Acknowledgements

Personal: Mumma, Papa and Meenal, thanks a lot to all of you for supporting me through thick and thin with this journey. I can't even imagine pursuing a research career without your support. I'd like to extend my gratitude to my entire family, especially Chachu, Maa, Masi and Shiro. Thank you to team W.e.I.r.D.O.s for all the fun over video calls. I'd like to thank Sia, Veda, Anant and Kanha for all the happiness they bring through their innocence. I'd like to extend my gratitude to Amma, Raj, Suman, Shubham, Amruta, Karan, Sara and Yolande. Thank you for your rock-solid support

At Work: My Biggest thanks go to my Supervisor, Dr. Shirley Coyle, for being my biggest supporter and inspiration. **Shirley, I cannot imagine doing my PhD under any other Supervisor**; you made this journey for me so much worth it. You are my "Wonder Woman". My sincere thanks to Angela Lally; thank you for being the "Dublin Mammy"; you made my journey logistically so much easier. I'm lucky to have you at DCU. Vicky Flanagan, Thank you for making the logistical journey easy. Prof. Tomás Ward, my co-supervisor, thank you for all the valuable insights and for being "Guru". Thank you for all the out-of-the-box ideas and conversations. Dr. Cosimo Della Santina, thank you for having me at TU Delft and making me think beyond my limits. I enjoyed working with you and learning so much about soft robots and writing styles; thank you for the feedback you gave me along the way. I'd like to extend my gratitude to the Exoskeleton group at DCU for all the support with Spinal Cord Injury patients. Luz and Sanjaya, you are the best labmates I could ever ask for. You guys are rock stars! Ebrahim, Daniel and Maxi, thank you for the warmth at TU Delft. Valerio and Taro, thank you for cheering me up in my blues and being just a phone call away!

Bigger Picture: I'd like to thank all the taxpayers in Ireland and each and every individual who participated in the experiments conducted for this research, without whom pursuing this dream was impossible. I'd like to extend my gratitude to Dublin City University, ML-Labs, Insight Research Centre and TU Delft!

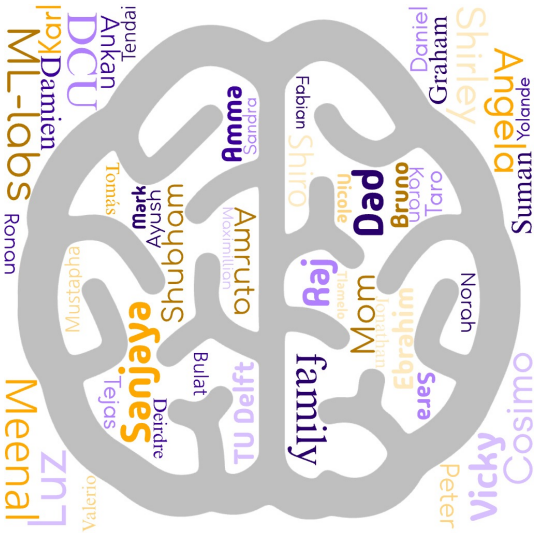
Thank You!
Daniel
Graham
Shirley
Angela
Yolande
Suman
Cosimo
Vicky
Peter
Norah
Ebrahim
Sara
Mom
family
Raj
Dad
Bruno
Koro
Taro
Nicole
Fabian
Shiro
Amma
Sandra
Mark
Ayush
Maximilian
Amruta
Shubham
Tomás
Mustapha
Sanjaya
Deirdre
Tejas
Bulat
TU Delft
Meenal
Luz
Valerio
ML-labs
Ronan
DCU
Karl
Damien
Ankan
Tanbai

Thank You!

List of Publications and Presentations

Journal Publications

1. **Baberwal, S. S.**, Magre, L. A., Gunawardhana, K. S. D., Parkinson, M., Ward, T., & Coyle, S. (2024). Motor imagery with cues in virtual reality, audio and screen. Journal of Neural Engineering, 21(5), 056020.

Conference Publications

1. **Baberwal, S.S.**, and Coyle, S., 2025. GP-based Motor Imagery Classification. In 2025 33rd International Conference on Artificial Intelligence and Cognitive Science (AICS 2025).

2. **Baberwal, S.S.**, Ward, T. and Coyle, S., 2024, August. Single Channel-Based Motor Imagery Classification Using Fisher's Ratio and Pearson Correlation. In 2024 32nd European Signal Processing Conference (EUSIPCO) (pp. 1476-1480). IEEE.

3. Stölzle, M.*, **Baberwal, S.S.***, Rus, D., Coyle, S. and Della Santina, C., 2024, April. Guiding soft robots with motor-imagery brain signals and impedance control. In 2024 IEEE 7th International Conference on Soft Robotics (RoboSoft) (pp. 276-283). IEEE. [Where * represents equal authorship]

4. **Baberwal, S.S.**, Magre, L.A., Gunawardhana, K.S.D., Ward, T. and Coyle, S., 2023, October. Protocol design and testing to investigate motor imagery training using cues in different mediums: A pilot study. In 2023 20th International Conference on Electrical Engineering, Computing Science and Automatic Control (CCE) (pp. 1-6). IEEE.

Contents

List of Acronyms

ADL Activities of Daily Living.

ALS Amyotrophic Lateral Sclerosis.

BCI Brain–Computer Interface.

CNN Convolutional Neural Network.

CSP Common Spatial Patterns.

DCU Dublin City University.

ECoG Electrocorticogram.

EEG Electroencephalography.

ERD Event-Related Desynchronization.

ERS Event-Related Synchronization.

FBCSP Filter Bank Common Spatial Patterns.

fMRI Functional Magnetic Resonance Imaging.

fNIRS Functional Near-Infrared Spectroscopy.

FR Fisher's Ratio.

GP Gaussian Process.

HMI Human Machine Interface.

HSA Handed Shearing Auxetic.

HSD Honestly Significant Difference.

LSTM Long Short-Term Memory.

MEG Magnetoencephalography.

MI Motor Imagery.

MI-BCI Motor Imagery based BCI.

PCC Pearson Correlation coefficient.

SCI Spinal Cord Injury.

TL Transfer Learning.

TLX Task Load Index.

VR Virtual Reality.

XR Extended Reality.

List of Tables

List of Figures

Motor Imagery based Brain-Computer Interface Systems beyond Controlled Environments.

Sonal Santosh Baberwal

Abstract

BCI enable users to control external devices or interact with computer systems through brain activity alone.MI-BCI leverage the imagination of movements—eliciting neural activity akin to actual execution—to provide intuitive, non-muscular control. Inspite significant advances, MI–BCIs remain largely confined to laboratory environments due to challenges in signal reliability, algorithmic robustness, and user engagement.

This PhD thesis investigates how systematic enhancements across the key MI–BCI subsystems—signal acquisition, user training, algorithmic processing, and interface design—can enable reliable, motivating, and practical use outside controlled settings, ultimately supporting Activities of Daily Living (ADL) for both healthy individuals and persons with Spinal Cord Injury (SCI).

Four interconnected research questions are addressed: (1) the feasibility of MI in SCI populations, (2) the influence of instructional medium on MI skill acquisition and engagement, (3) the potential of channel reduction and advanced algorithms to enhance classification and real-time control, and (4) the design of immersive and safe interfaces for real-world ADL tasks. Empirical investigations demonstrate that immersive VR training enhances MI skill acquisition and motivation; single-channel and Gaussian Process–based classifiers enable robust and portable control; and compliant robotic interfaces facilitate continuous, safe interaction with functional tasks.

Collectively, these findings show that MI–BCIs can transition from controlled laboratory paradigms to functional, user-centered systems capable of supporting ADL. By integrating advances across all subsystems, this research provides a methodological framework for translating MI–BCIs into real-world applications—offering tangible benefits for rehabilitation, independence, and quality of life.

Chapter 1

Introduction

"Let your thoughts be good, your actions noble, and your heart kind."
- Mrs. Sunita S. Baberwal

1.1 Motivation

The dream of controlling interfaces or external devices directly by human brain activity is no longer confined to science fiction; it is steadily becoming a reality with the advances in Human Machine Interaction. This is made possible through the design and development of the Brain Computer Interface BCI, which translates neural activity into control signals that can be used as actionable commands to operate external applications. In practical terms, a BCI enables a person to use their thoughts to perform specific tasks, for instance, moving a wheelchair (1), typing with a BCI speller, or controlling a robotic device (2). Such technologies represent a paradigm shift in Human Machine Interface (HMI), as they bypass the traditional reliance on muscles and speech, instead creating a direct link between the brain and external systems in order to augment the capabilities of humans.

At its core, a BCI is a collaboration between the brain and an external device, established through a communication pathway that allows brain activity to be transformed into meaningful outputs. This process involves several interconnected stages: signal acquisition, feature extraction, feature translation, and device output. Signal acquisition is the first and most crucial step, as it involves recording brain activity from activated regions of the cerebral cortex. Depending on the method used, this can be achieved through invasive, semi-invasive, or non-invasive techniques. Invasive methods include sensors used for intracortical recordings (3). Semi-invasive methods include Electrocorticogram (ECoG), where electrodes are placed beneath the skull but outside the brain (4). Non-invasive techniques include EEG, which records electrical activity using electrodes placed on the scalp; Functional Magnetic Resonance Imaging (fMRI), which measures brain activity by detecting changes in blood flow (5); Functional Near-Infrared Spectroscopy (fNIRS), which measures brain activity by detecting changes in blood oxygenation levels using near-infrared light (6); and Magnetoencephalography (MEG), which measures brain activity by detecting the magnetic fields generated by neural activity (7). Invasive methods involve implanting electrodes directly into brain tissue and provide high-quality signals, but they carry surgical risks. Semi-invasive techniques offer a balance between signal quality and safety. Non-invasive techniques avoid surgery and are therefore the most widely used in research and practice.

Among the non-invasive methods, EEG remains the most common and

practical approach (8). EEG measures the brain's electrical activity using electrodes placed on the scalp, capturing the dynamic neural processes (9) that underlie thought, intention, and motor imagery. Despite its relatively low spatial resolution compared to invasive approaches, EEG is favored for its safety, portability, and cost-effectiveness, making it highly suitable for both experimental and applied BCI systems. This is further explained in Section 2.5

Once brain signals are acquired, they must be processed and interpreted (8). This is where feature extraction and feature translation come into play together as Algorithms. Feature extraction refers to identifying the most relevant aspects of the neural signals, for instance, changes in frequency or patterns associated with specific cognitive or motor tasks. Feature translation then converts these extracted features into control commands that can be understood by a computer or device. Together, these steps are enabled by advanced signal processing techniques and machine learning / deep learning algorithms (10), which are trained to recognize patterns in brain activity and later associate them with specific user intentions. The final stage of a BCI system is the device output, where the translated signals are used to control an external application. The entire pipeline is demonstrated as a diagrammatic representation in Fig. 2.5, from Chapter 2, included here to provide a visual overview of the workflow.

The range of possible outputs is diverse and continues to expand with ongoing research. In clinical and rehabilitation contexts, BCIs have been explored to operate assistive technologies for instance, powered wheelchairs, robotic exoskeletons, or spellers that enable communication for individuals with severe motor impairments. Beyond healthcare, BCIs are increasingly being applied in areas for instance, gaming, VR, and HMI, where they allow new forms of immersive control and engagement (11; 12; 13).

In summary, a BCI provides a direct pathway between the brain and external systems, translating thought into action through a structured process of acquisition, interpretation, and execution. By doing so, BCI not only offers life-changing opportunities for individuals with motor disabilities but also opens up new horizons for everyday applications, from assistive devices to entertainment technologies. However, in spite of many decades of BCI research, the majority of BCI systems remain confined to laboratory environments. This limitation arises not from a single technical barrier, but from fragmented progress across multiple subsystems—ranging from signal acquisition and decoding to user training, feedback, and integration with real-world applications (14).

Instead of addressing one isolated challenge and focusing in one avenue, this thesis identifies and examines gaps across these interconnected subsystems and proposes strategies for every sub-system that can be useful in designing future BCI systems. The overarching motivation of the thesis is to move BCI beyond controlled experimental settings and into the domain of ADL, where they can provide meaningful impact in real-world contexts for rehabilitation and everyday assistance.

1.2 Hypothesis, Research Questions, and Objectives

1.2.1 Overall Hypothesis

The central hypothesis guiding this PhD thesis is:

> *Enhancing the key components of MI based BCI systems—including MI signal acquisition, user training protocols, algorithmic processing, and interface design—can facilitate reliable, motivating, and practical MI-BCI use outside controlled laboratory environments, thereby supporting ADL for both healthy individuals and persons with neuromuscular conditions, for instance, Spinal Cord Injury (SCI).*

This hypothesis is grounded in the premise that systematic improvements across all pillars of MI-BCI are essential to enable real-world application. By addressing these components, the project aims to bridge the gap between controlled experimental paradigms and functional BCI systems that can be incorporated into everyday life.

1.2.2 Research Questions

To operationalize this overarching hypothesis, the following research questions have been formulated:

RQ 1: MI and Spinal Cord Injury (SCI) Feasibility *How can motor imagery training be useful for SCI patients?*

Significance: Understanding MI capability in SCI populations is critical because it forms the neurophysiological foundation of MI-BCI systems. Without reliable MI signals, subsequent training, classification, and interface design cannot be effectively implemented. Insights gained here can guide calibration protocols, improve signal acquisition strategies, and ensure that MI-BCI systems are inclusive and beneficial for rehabilitation.

Expected Outcomes: Characterization of MI signal quality in SCI, foundations for how motor imagery training contributes to rehabilitation environments.

Testing and Validation: ERD/ERS analysis, MI classification accuracy, and comparison across SCI participants.

RQ 2: User Training Optimization *Does the medium of instruction (visual, auditory, or immersive VR) influence motor imagery skill acquisition and BCI performance?*

Significance: Effective user training is a critical bottleneck in translating MI-BCIs to real-world use. Optimizing instructional methods can improve MI signal quality, accelerate learning, enhance engagement, and reduce cognitive fatigue. This is particularly relevant for both rehabilitation and general-purpose ADL applications, where user motivation and rapid skill acquisition directly impact adoption.

Expected Outcomes: Enhanced MI signal clarity, improved online control accuracy, and increased participant motivation.

Testing and Validation: Controlled experiments comparing performance and neurophysiological markers across different instructional modalities.

RQ 3: Algorithmic Enhancements for ADL

Part A – Foundational Techniques: *Can combining methods for instance, Fisher Ratio and Pearson Correlation facilitate single-channel MI-BCI classification, thereby reducing the number of electrodes required without compromising performance?*

Significance: Minimizing hardware complexity is crucial for real-world deployment. Single-channel classification reduces setup time, improves comfort, and enhances portability, making MI-BCIs more practical for daily use.

Expected Outcomes: Reliable single-channel classification and identification of most informative electrode sites on offline datasets.

Testing and Validation: Comparative experiments between single- and multi-channel systems, analyzing classification accuracy and signal discriminability.

Part B – Advanced Algorithms: *Can advanced classifiers, such as Gaussian Process (GP) models, improve robustness and real-time control in MI-BCI systems intended for ADL applications?*

Significance: Robust classification under real-world conditions is essential for practical MI-BCI deployment. Advanced algorithms can mitigate noise, inter-subject variability, and non-stationarity, leading to more reliable control of both VR and robotic interfaces.

Expected Outcomes: Improved classification accuracy, reduced latency, and smoother control on offline datasets.

Testing and Validation: Implementation in real-time MI-BCI tasks and benchmarking against conventional LDA/CSP pipelines.

RQ 4: Interface Design and Real-World Application

Part A – VR-Based MI-BCI: *Can MI-BCI performance and user engagement be enhanced through immersive VR tasks, such as a 6° head-down tilt microgravity simulation, embedded within conventional MI-controlled VR paradigms for healthy individuals and SCI patients?*

Significance: Incorporating immersive, ecologically valid VR environments may enhance motivation, engagement, and task-relevant MI signal generation. This is particularly important for rehabilitation, where sustained user involvement is critical, and for translating MI-BCI use to real-world contexts.

Expected Outcomes: Improved MI signal quality, higher online control accuracy, and increased user motivation.

Testing and Validation: Comparative studies between standard VR and immersive microgravity VR tasks.

Part B – Safe Interfaces for ADL: *Can continuous, interactive MI-BCI tasks, implemented via compliant and safe robotic interfaces, enable the execution of real-world ADL tasks beyond discrete interface trials?*

Significance: Real-world ADL applications require continuous, safe, and intuitive control. Compliant interfaces reduce risk, accommodate human variability, and enable effective interaction with objects in dynamic environments. This directly supports the ultimate goal of translating MI-BCIs from controlled

settings to everyday use.

Expected Outcomes: Successful task execution, trajectory accuracy, and user safety and comfort.

Testing and Validation: Real-time control of robotic devices in continuous ADL tasks, with performance metrics including task completion time, error rates, and end-effector stability.

1.3 List of Contributions

1.3.1 List of Publications

Journal Publications

1. **Baberwal, S. S.**, Magre, L. A., Gunawardhana, K. S. D., Parkinson, M., Ward, T., & Coyle, S. (2024). Motor imagery with cues in virtual reality, audio and screen. Journal of Neural Engineering, 21(5), 056020. **[Published]**

2. **Baberwal, S.S.**, Magre, L.A., Gunawardhana, K.S.D., Shahabi, E., Ward, T., Santina, C.D, and Coyle, S., 2025. MI-BCIs Beyond the Lab: A Review of the Key Pillars for Real-World Translation. IEEE Access. **[Submitted]**

3. **Baberwal, S.S.**, Byrne. D.,Awais, M. A.,Vijayvargiya,A., Langan, R., Ward, T., Healy, G. and Coyle, S., 2025. Motor Imagery and Exoskeleton Intervention - a preliminary understanding with Spinal Cord Injury Patients. IEEE Transactions in Neural Systems and Rehabilitation Engineering. **[In Preparation]**

4. **Baberwal, S.S.**, Baberwal. M., Langan, R., Ward, T., and Coyle, S., 2025. Motor Imagery BCI - on Earth and Artificial Microgravity: An initial pilot study. Journal of Neural Engineering. **[In Preparation]**

Conference Publications

1. **Baberwal, S.S.**, and Coyle, S., 2025. GP-based Motor Imagery Classification. In 2025 33rd International Conference on Artificial Intelligence and Cognitive Science (AICS 2025). **[Presented]**

2. **Baberwal, S.S.**, Ward, T. and Coyle, S., 2024, August. Single Channel-Based Motor Imagery Classification Using Fisher's Ratio and Pearson Correlation. In 2024 32nd European Signal Processing Conference (EUSIPCO) (pp. 1476-1480). IEEE.

3. Stölzle, M.*, **Baberwal, S.S.***, Rus, D., Coyle, S. and Della Santina, C., 2024, April. Guiding soft robots with motor-imagery brain signals and impedance control. In 2024 IEEE 7th International Conference on Soft Robotics (RoboSoft) (pp. 276-283). IEEE. [Where * represents equal authorship]

4. **Baberwal, S.S.**, Magre, L.A., Gunawardhana, K.S.D., Ward, T. and Coyle, S., 2023, October. Protocol design and testing to investigate motor imagery training using cues in different mediums: A pilot study. In 2023 20th International Conference on Electrical Engineering, Computing Science and Automatic Control (CCE) (pp. 1-6). IEEE.

Collected Data

1. Dataset 1: Motor Imagery Data (no feedback) collected from 9 SCI patients. [Further discussed in Chapter 4]

2. Dataset 2: Motor Imagery Data (no feedback) collected from 21 healthy subjects across VR, Screen, and Audio. [Further discussed in Chapter 5]

3. Dataset 3: Motor Imagery Data (with feedback) collected from 6 healthy and 3 SCI patients in VR based simulation MI based BCI game for Earth and Space. [Further discussed in Chapter 7]

Awards and Achievements

1. Finalist at Thesis in 3 Competition by EURASIP, 32nd European Signal Processing Conference, France. 3MT. 2024.

2. Best Paper Award at RoboSoft 2024, USA: Stölzle, M.*, Baberwal, S.S.*, Rus, D., Coyle, S. and Della Santina, C., 2024, April. Guiding soft robots with motor-imagery brain signals and impedance control. In 2024 IEEE 7th International Conference on Soft Robotics (RoboSoft) (pp. 276-283). IEEE. 2024.

3. 2nd Position with team in BCI Hackathon sponsored by IEEE Brain and organised by g.tec medical engineering GmbH. 2022.

1.4 Structure of the thesis

This thesis is organized into 8 chapters, as described below.

Chapter 1 – **Introduction** sets the foundation by outlining the motivation and scope of the thesis. The chapter presents the central research questions and gaps that the thesis addresses.

Chapter 2 - **Motor Imagery and BCI Systems** introduces the basics of the human brain, highlighting different types of signal acquisition and fundamentals of MI-BCI research.

Chapter 3 – **Literature Review** is where a comprehensive review of existing work is presented, focusing on key components of MI-BCI: user training, algorithms, interfaces, and their applications. From the gaps identified from the literature review the central research questions of the thesis are presented.

Chapter 4 – **MI and SCI** investigates the role of Motor Imagery in rehabilitation. The hypothesis is presented, the protocol intervention followed, exoskeleton data, and EEG datasets collected. Analytical tools are described, followed by results and discussion on how MI contributes to rehabilitation.

Chapter 5 – **User Training** investigates the role of user training in MI-BCI systems. It presents the hypothesis, the protocol followed, questionnaires used in the experiment, and EEG datasets collected. Analytical tools are described, followed by results and discussion on how training impacts BCI performance.

Chapter 6 – **Algorithms** highlights the computational side of MI-BCI. Different pipelines for signal processing and classification that can be used in Activities of Daily Living ADL BCI systems are explored, where datasets used, analysis tools, and results systematically presented to evaluate their effectiveness in improving decoding accuracy.

Chapter 7 – **Interfaces and Their Applications** examines how MI-BCI can be integrated with external systems. Two key applications listed below are explored: (1) VR and MI-BCI – exploring immersive environments for motor imagery training and rehabilitation. (2) Soft Robots and MI-BCI – investigating soft robotics controlled via motor imagery. Each section follows a structured presentation of hypothesis, dataset, tools for analysis, and results with discussion.

Chapter 8 – **Conclusion** The final chapter summarizes the contributions of the thesis and revisits the identified research gaps. The future of MI-BCI systems is discussed, emphasizing the transition from laboratory-based experiments into adoption in daily living.

Chapter 2

Motor Imagery and BCI Systems

"By educating children, we nurture a society that grows and individuals who evolve."

- Mr. Santosh Baberwal

2.1 Anatomy of the Human Brain

The human brain is a complex and highly connected organ that allows us to sense the world, move our body, experience emotions, and think. Broadly, it is made up of three main parts: the **cerebrum**, the **cerebellum**, and the **brainstem**.

The **cerebrum** is the largest part of the brain. It is responsible for higher functions such as reasoning, memory, language, and voluntary movement. It is divided into left and right halves (hemispheres), which are connected by a bundle of nerve fibres called the corpus callosum. Beneath its surface lie important inner structures: the **thalamus**, which acts like a relay station for sensory and motor signals; the **basal ganglia**, which help control movement and learning of habits; and the **limbic system**, which includes the hippocampus (important for memory) and the amygdala (important for emotions).

The **cerebellum**, located at the back of the brain, helps fine-tune movement, balance, and coordination. The **brainstem**, which connects the brain to the spinal cord, controls essential automatic functions such as breathing, heart rate, and basic alertness (15).

Lobes of the Cerebral Cortex

The outer layer of the cerebrum is called the **cerebral cortex**. It is a sheet of gray matter with many folds and grooves that increase its surface area. Furthermore, the cortex is divided into four main lobes (represented in Fig.2.1), each with specialized functions:

- **Frontal lobe**: Involved in planning, decision-making, problem-solving, attention, social behavior, and voluntary movement. It also plays a key role in imagining and preparing movements.
- **Parietal lobe**: Processes information from different senses and helps us understand the position and movement of our body. It is important for touch, spatial awareness, and coordination between vision and movement.
- **Temporal lobe**: Important for hearing, understanding language, recognizing patterns, and forming memories.
- **Occipital lobe**: Mainly responsible for vision, including the ability to detect shapes, colors, depth, and motion.

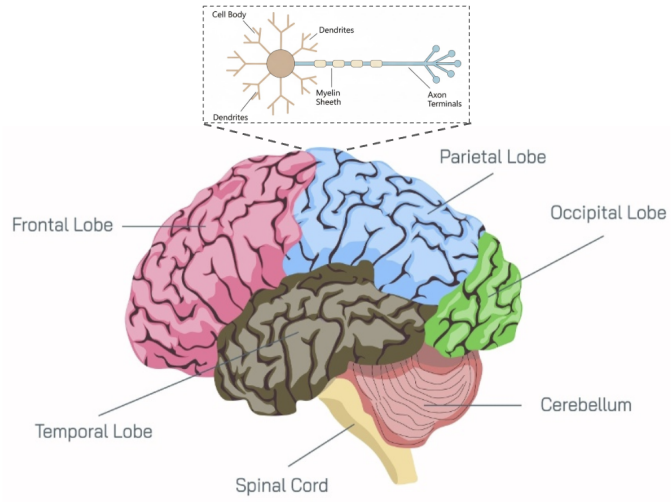

Figure 2.1: Diagrammatic representation of the lobes of the human brain along with the structure of a single neuron, adapted from (16).

Key Brain Systems and Networks

Beyond the division of function within lobes, the brain also works through specialized systems that communicate across different regions:

- **Movement system**: Includes areas that control and plan voluntary movements and those that coordinate with sensory input to generate activity in the muscles.
- **Sensory system**: Includes areas that process touch, body position, and the sense of movement, and combine them to give us a complete body awareness.
- **Visual system**: Includes regions that process visual information and help us recognize objects, colours, and motion, as well as guiding our actions.
- **Auditory and language system**: Includes regions that allow us to hear, process speech, and produce language.
- **Association areas**: Networks that link information from different senses and regions of the brain. These areas support higher functions such as attention, decision-making, working memory, and mental imagery of movement.

Neurons and Emergent Electrical Activity

The brain's outer layer, called the cortex, is made up of billions of **neurons** (shown in Fig. 2.1). These neurons communicate by sending small electrical signals to each other. When many neurons in the same area become active together, their combined activity creates larger electrical patterns that can be detected on the scalp using EEG.

Because many neurons in the cortex are similarly arranged, their coordinated activity appears in the EEG as rhythmic patterns called **brain waves**, which occur at different **frequency bands** (such as delta, theta, alpha/μ, beta, and gamma). For movement and **motor imagery**, the most important of these are the **sensorimotor rhythms** found over the motor areas of the brain. These rhythms change when a person moves or imagines moving (Fig. 2.2). The next section describes how EEG data are recorded, how these frequency bands are defined, and how they are used for BCI applications.

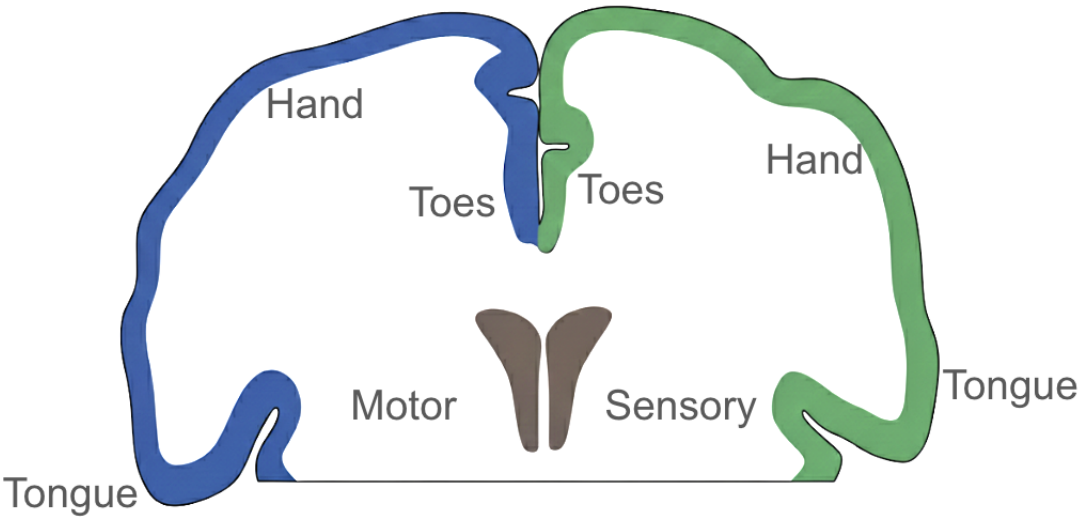

Figure 2.2: Homunculus Model of Motor Cortex adapted from (17)

2.2 EEG and Frequency Bands

As mentioned above, EEG is a widely used non-invasive neuroimaging technique that measures the brain's electrical activity through electrodes placed on the scalp. The recorded signals primarily reflect potentials originating mainly in the cerebral cortex, providing millisecond-level temporal resolution of neural

dynamics. Due to its portability, cost-effectiveness, and safety, EEG has become an essential tool in both clinical and research settings, particularly in the study of motor control, cognitive processes, and BCI.

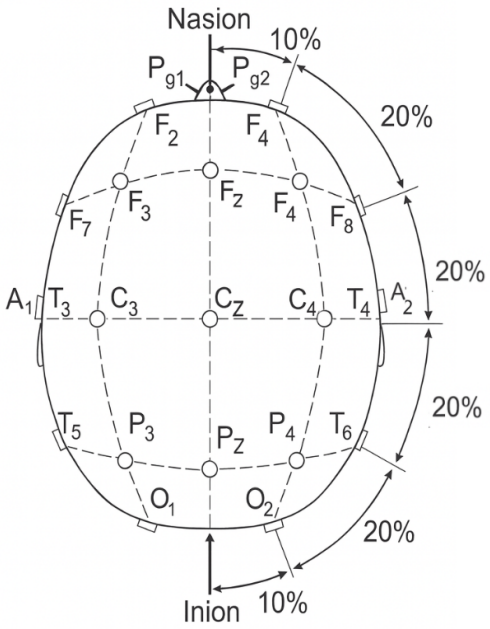

Figure 2.3: Diagrammatic representation of 10-20 system as a top view adapted from (18).

A standardized method for electrode placement (demonstrated in Fig. 2.3) is critical to ensure reproducibility and comparability across studies (18). The most commonly adopted approach is the International 10–20 system (19), which defines electrode positions relative to the size and shape of an individual's head. Electrodes are placed at intervals corresponding to 10% or 20% of the total distance between anatomical landmarks such as the nasion, inion, and preauricular points. Each electrode is designated by a letter indicating the underlying cortical region (e.g., F = frontal, C = central, P = parietal, O = occipital), while odd numbers refer to the left hemisphere, even numbers to the right, and 'z' denotes the midline. This standardized montage facilitates systematic coverage of the scalp and enables cross-subject comparisons. Of particular relevance to motor imagery and sensorimotor rhythm research are the central electrodes (e.g., C3, Cz, C4), which overlay the primary motor cortex and are commonly analyzed in EEG-based BCI studies (20).

EEG signals are typically decomposed into distinct frequency bands, each associated with specific neurophysiological functions and cognitive states. These

oscillatory rhythms reflect the coordinated activity of large neuronal populations and are widely analyzed in both clinical and research contexts. Table 2.1 summarizes the conventional EEG bands.

Table 2.1: Overview of EEG frequency bands and associated functions.

Band	**Frequency Range (Hz)**	**Associated Functions**
Delta	0.5–4	Dominant during deep sleep and unconscious states; linked to slow-wave sleep and cortical inhibition.
Theta	4–8	Related to drowsiness, memory encoding, and attentional processes; often increased during meditative or transitional states.
Mu	8–13	Sensorimotor rhythm originating over the motor cortex; suppressed during actual or imagined movement (ERD), making it highly relevant for motor imagery-based BCI systems.
Alpha	8–13	Prominent in occipital regions during relaxed wakefulness with eyes closed; associated with cortical idling and resting-state activity.
Beta	13–30	Observed during active thinking, sensorimotor processing, and movement execution; highly relevant for motor imagery studies.
Gamma	>30	Associated with perception, attention, and memory integration; more challenging to measure due to susceptibility to noise.

In BCI research, particular attention is given to the *Mu rhythm* (8–13 Hz) and *beta rhythm* (13–30 Hz) over the sensorimotor cortex, as ERD and ERS in these bands are robust markers of motor imagery and movement-related neural activity. This is further described in Section 2.5

2.3 ERD/ERS

ERD/ERS are fundamental concepts used to quantify the modulation of rhythmic brain activity during motor tasks or motor imagery (MI). ERD corresponds to a decrease in power of specific EEG frequency bands relative to a baseline or rest period, indicating cortical activation and neural engagement. Conversely,

ERS represents an increase in power relative to baseline, often reflecting cortical idling, inhibition, or a return to a resting state. These power changes are computed as a ratio between the event-related and baseline spectral power values, providing a normalized measure of brain activity modulation.

Mathematically, ERD/ERS can be expressed as:

$$\text{ERD/ERS}(\%) = \frac{P_{\text{event}} - P_{\text{baseline}}}{P_{\text{baseline}}} \times 100 \tag{2.1}$$

where P_{event} corresponds to the Power Spectral Density (PSD) during the event period (when the cue is presented), and P_{baseline} refers to the PSD during the resting state, where no task is performed.

The average ERD/ERS values are obtained by averaging these ratios across all epochs for each motor imagery condition (e.g., left and right hand) within the Mu (8–13 Hz) and beta (13–30 Hz) frequency bands—bands known to be most responsive to motor-related activity. The resulting ERD/ERS time courses and amplitude maps provide insight into the temporal dynamics of cortical activation and deactivation during MI tasks.

The increase and decrease of these rhythms in terms of amplitude, causing suppression or enhancement (ERS or ERD), are useful in designing BCI systems utilising mental state imagination for the mobility of the left/right hand (21).

2.4 Graz BCI paradigm

The Graz-MI paradigm is a widely used protocol for EEG-based MI/MI-BCI experiments. The paradigm is explained with a customized window frame. For instance, with reference to Figure 2.4, each trial begins with a blank screen (0–2 s), allowing the participant to relax before the next cue. At around 2 seconds, a beep sounds and a fixation cross appears at the center of the screen, helping the participant focus attention and minimize eye movement artifacts. At 3 seconds, a visual cue (arrow) is presented alongside the fixation cross—this arrow indicates the type of motor imagery to perform (e.g., left hand, right hand, or foot). This marks the onset of the motor imagery period (trigger). The participant then engages in the imagined movement for approximately 4 seconds (3–7s) while maintaining gaze on the fixation cross. After the imagery period, the trial ends, and the screen returns to baseline before the next repetition. This structured timing ensures consistent ERD/ERS patterns across trials,

enabling accurate decoding of motor imagery from EEG signals. (22)

The Graz-BCI focuses on differentiating two or more MI-based brain imagination or EEG signals synchronously, i.e., in predefined time windows (20).

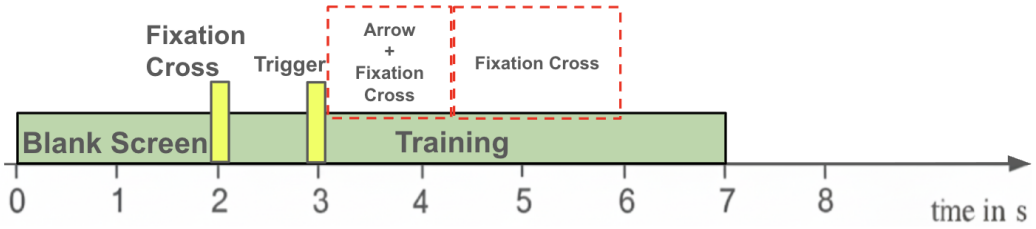

Figure 2.4: An example of a customized Graz-BCI paradigm adapted from (23).

2.5 Motor Imagery based BCI Systems

Imagining the movement of any body part (for instance, hands, legs, tongue) without moving it or the mental rehearsal of a motor act without overt movement execution (24) is termed Motor Imagery. Jeannerd (25) defines MI as the result of conscious access to the content of the intention of a movement, which is usually performed unconsciously during movement preparation. Pfurtscheller (20) shares MI as a mental rehearsal of a motor act without any motor output. The similarity between brain regions involved in the imagination of movements and programming/preparing respective movements is accepted broadly, with the main difference in the later stages of execution, which is blocked at the cortico-spinal level. The neuronal activities observable inside a frequency range of 8 Hz to 13 Hz (Mu) and 13 Hz to 30 Hz (Beta) are associated with cortical areas directly connected to the brain's motor output (activating primary sensorimotor areas that can be modulated with imaginary mental movement in healthy individuals, as well as people with neuromuscular disabilities). Thus, MI-BCI holds a potential application for Neuroprosthetic BCI systems (26) and rehabilitation (27).

MI-BCI systems have significant potential to support individuals with motor disabilities, particularly those affected by conditions like Amyotrophic Lateral Sclerosis (ALS) or SCI. For these populations, BCI offer a pathway to restored autonomy and improved quality of life by enabling control over essential functions that may otherwise be inaccessible.

Motor Imagery is widely used for the BCI systems involved in classification (for instance, classification of hand movement (21) for motion (wheelchair (28), exoskeleton ((29)). One of the well-known systems for using MI to perform respective mental tasks is the Graz BCI paradigm, which reports clinical applications of MI-based BCI systems with operations like controlling a virtual keyboard device and hand orthosis operations.

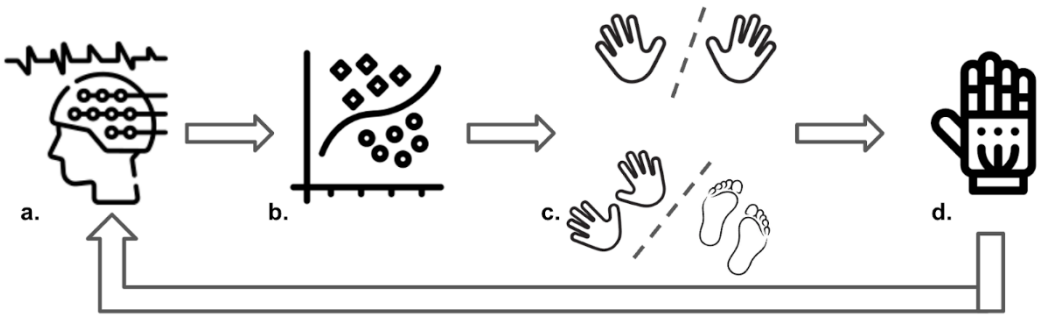

Figure 2.5: Diagrammatic representation: Framework for MI-BCI systems where (a.) EEG signals are collected, (b.) processed, and (c.) classified to operate (d.) an interface.

A typical MI-BCI framework comprises four components (30) that are further explained in Section 3:

Signal Acquisition: As mentioned earlier in Section 1.1, this stage involves capturing neural signals through invasive, semi-invasive, or non-invasive methods. These signals serve as a representation of the user's cognitive or motor intent. Here, the most widely used systems are EEG devices due to their cost-effectiveness and non-invasive approach of signal acquisition.

Feature Extraction: Once signals are acquired, advanced signal processing techniques (31) (explained in Subsection 3.3) are used to extract relevant features. These features represent distinctive patterns associated with specific mental states or intentions.

Feature Translation: In this phase, machine learning algorithms (explained in Subsection 3.3) are used to map extracted features to control commands. This step is critical in interpreting the user's intent and generating meaningful outputs.

Device Output: Finally, the translated commands are applied to external devices (various applications explained in Subsection 3.4). These outputs can support various functions such as the navigation of assistive technologies (e.g., wheelchairs), text input, or the operation of robotic exoskeletons.

Chapter 3

Literature Review

"Embrace opportunities and challenges, taking things one step (or mile) at a time. Keep going and learn from any setbacks along the way. Celebrate what you can make possible and be grateful for the things and more importantly people who bring you joy."

- Dr. Shirley Coyle

Since MI-BCI systems have shown significant potential in rehabilitation, particularly for individuals with SCIs (32), the field has been extensively investigated over the past decade. However, despite this progress, this technology remains largely confined to laboratory settings (33). Various factors contribute to this limitation, including the complexity of user training, safety constraints of the interfaces (e.g., traditional rigid exoskeletons), and the accuracy and reliability of the algorithms. Addressing these challenges is essential for transitioning MI-BCI systems from controlled research environments to real-world applications.

In recent years, these systems have extended their utility to gaming, VR (34), and lifestyle enhancements (35; 36) from traditional setups and interfaces. Emerging studies highlight the transformative potential of MI-BCI systems in diverse domains. For instance, incorporating MI-BCI systems can be productive for healthcare applications such as stroke rehabilitation (37; 27), and also in sports performance (38). The incorporation of VR has been shown to enhance the attention of the user during the imagination of movement (12). Another study suggests that MI-based soft robotic glove rehabilitation holds potential for clinical rehabilitation (39). These advancements indicate a pathway for bringing MI-BCI systems out of laboratories and into practical use. However, significant challenges still exist in bringing the MI-BCI systems outside laboratories for integration into daily activities.

McFarland and Wolpaw refer to User Training, Machine Learning (Algorithms), and Application as pillars of MI-BCI systems (30). Since applications of MI-BCI systems depend on training, algorithms, and interfaces used, a thorough evaluation is needed to investigate the feasibility of bringing them outside laboratories. While there are studies addressing gaps and state-of-the-art in the domain of MI-BCIs, there has been no study on a comprehensive summary of the state-of-the-art across the pillars of MIBCIs with motivation to see their potential outside laboratories and different potential applications for real-world deployment. To the author's knowledge, there have been state-of-the-art reviews on MI-based Interfaces (40), MI-based algorithms (3; 41; 10; 42) and MI-based applications (43; 44). These studies address precise avenues of research which must be considered collectively in order to bring MI-BCI systems outside laboratories.

To address this gap, Section 3 aims to analyse the key pillars that contribute to the efficiency of MI-BCI systems, with particular focus on facilitating their

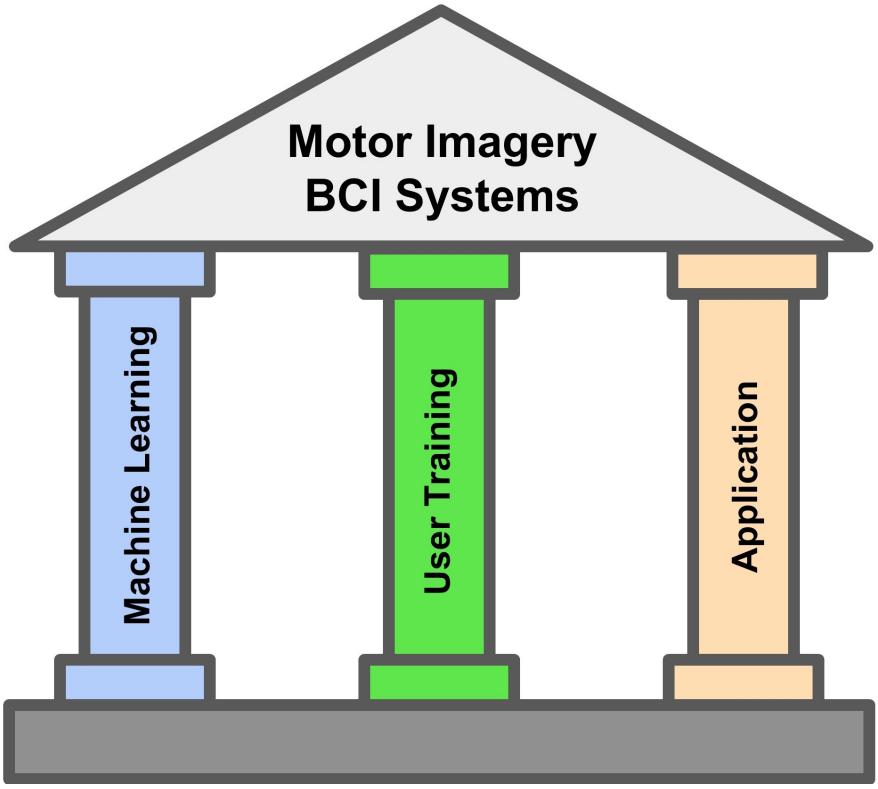

Figure 3.1: The three pillars of MI-BCI Systems: (a.) Machine Learning, (b.) User Training, and (c.) Application for efficient MI-BCI systems, adapted from (30)

transition from laboratory environments to real-world settings.

3.1 Motor Imagery and Spinal Cord Injury

Motor imagery has been explored in individuals with SCI, where research (45) suggests that although SCI alters sensorimotor connectivity and cortical excitability, MI-related neural activity can still be elicited and, in some cases, modulated through training. Systematic evidence indicates that MI interventions in SCI populations have been associated with changes in motor function, pain perception, and neurophysiological markers, even though protocols and outcome measures remain heterogeneous (46).

Several studies have investigated MI-based BCI systems in SCI for assistive control and rehabilitation (46). A single-participant case study showed that an SCI patient could use a motor imagery–based BCI to control a lower-limb exoskeleton, highlighting feasibility but also usability challenges such

as high mental workload, fatigue, and the need for frequent recalibration (47). Case studies and small cohort investigations have demonstrated that individuals with SCI can learn to generate MI-related EEG patterns that are sufficiently separable for device control, including robotic gloves, lower-limb robots, and functional electrical stimulation (FES) systems (48; 49; 50). MI-driven gait and upper-limb rehabilitation paradigms using robotic exoskeletons and neurofeedback have reported modulation of sensorimotor rhythms, changes in brain connectivity, and improvements in clinical or functional indicators, even in individuals with complete or chronic injuries (51; 52; 53). More recent work has also explored non-invasive MI decoding for controlling epidural electrical stimulation and multimodal BCI–FES–exoskeleton systems, highlighting the potential role of MI signals as an interface between intention and assisted movement (54; 50).

At the signal level, advances in machine learning and neural modeling have shown that MI-related patterns in SCI EEG can be decoded with moderate to high accuracy under controlled conditions, including the use of transformer-based architectures, spiking neural networks, and transfer learning approaches (55; 56; 57). Intracortical and EEG studies further suggest that MI in SCI may recruit both shared and imagery-specific neural subspaces, supporting the notion that covert motor representations remain accessible even when overt execution is impaired (58). However, these findings are typically derived from small samples, case studies, or short-term training paradigms, limiting generalizability across the highly diverse SCI population.

SCI is characterized by substantial heterogeneity in lesion level, completeness, chronicity, and secondary complications, all of which may influence MI vividness, cortical reorganization, and EEG signal stability. Fatigue, neuropathic pain, and cognitive load can affect sustained MI performance, particularly during longer or repeated sessions (59; 60). From a practical perspective, donning and doffing of EEG systems, reliance on caregivers, and variability in home or clinical environments pose additional constraints on consistent signal acquisition and training continuity (48; 61). These factors contribute to limited sample sizes, high inter-subject variability, and inconsistent reporting of MI capability.

While prior work provides encouraging indications that MI can be harnessed for assistive and rehabilitative BCIs in SCI, the degree to which MI signals are reliable, trainable, and comparable across individuals remains insufficiently

characterized. A clearer understanding of MI feasibility in SCI is therefore needed to inform calibration strategies, signal processing choices, and interface designs that are appropriate for this population, particularly in rehabilitation-oriented and real-world applications.

3.2 User Training

One of the most popular ways of training users for MI-BCI systems is the Graz BCI protocol. The cue-based paradigm is a structured, time-paced system designed to guide participants through MI tasks using visual cues. This time-paced approach ensures a standardized training environment, allowing reliable decoding of motor intentions and enabling practical BCI applications in areas such as communication and neurorehabilitation (62). Although the training process has been standardized, yet consistent mental imagination and attention to cues are challenging. To enhance the training and usability of MI-BCI systems outside laboratory settings, researchers have explored multiple approaches focusing on feedback modalities, Extended Reality (XR) environments, and cue presentation methods.

One of the most significant findings comes from Korik et al. (63), who demonstrated the impact of real-time biased feedback on improving the performance of a primitive object-imagery BCI. Across four linked studies involving 69 sessions (26 with real-time feedback), the researchers found that decoding accuracy improved significantly when real-time feedback was provided. This suggests that continuous, adaptive feedback can enhance the learning process and optimize MI signal decoding over time. Real-time feedback allows participants to adjust their mental strategies, leading to better performance and greater system adaptability.

Another promising avenue involves the use of XR environments to facilitate MI training. Arpaia et al. (64) developed a wearable MI-BCI that uses visual and vibrotactile feedback in an XR setting. Notably, the study highlighted the subject-dependent nature of optimal feedback modalities, emphasizing the importance of personalized approaches in MI-BCI training. Furthermore, the portability and simplicity of the system underscore its potential for real-world applications, as it does not require complex hardware or extensive setup.

In a related study, Arpaia et al. (65) examined a user-friendly, wearable MI-BCI system designed for tele-rehabilitation. Using eight dry EEG sensors, the

study emphasized the system's high perceived usability, which is a crucial factor for adoption outside controlled laboratory settings. These findings indicate that providing feedback during training significantly improves MI detection, supporting the development of accessible and user-centric BCI systems.

The use of action observation combined with MI (AO+MI) has also shown promise in improving MI-BCI training. Chaisaen et al. (66) investigated the neural correlates of sitting and standing MI using both offline and real-time classification analyses. The results suggest that integrating AO with MI enhances cortical activity, leading to better decoding performance. This combined approach may be particularly useful for developing exoskeleton-based rehabilitation systems, as it closely mimics real-life movement intentions.

Similarly, Choi et al. (12) compared the effects of screen-based and VR MI environments. Their study found that immersive VR headsets improved neural engagement and generated better discriminating spatial features than monitor displays. These improvements are attributed to the sense of embodiment provided by VR, which enhances participants' ability to imagine and control motor actions.

Adham et al. (67) further explored the synergistic effects of visual and proprioceptive (body awareness) feedback in MI-BCI systems. Their EEG study reveals that combining video feedback with vibratory cues enhanced sensorimotor cortex recruitment and improved embodiment. Conditions involving visual feedback elicited stronger ERD in the alpha band, while vibratory feedback increased lateralized beta band activity. The combination of these feedback modalities (IOV condition) provided the most accurate motor validation and the highest degree of embodiment. This multimodal feedback approach has the potential to optimise MI-BCI performance in rehabilitation and other practical applications.

Studies by Korik et al. (63) and Arpaia et al. (64; 65) demonstrate the value of providing continuous, adaptive feedback in improving classification accuracy and user experience. The integration of AO with MI, as shown by Chaisaen et al. (66), further enhances cortical engagement and decoding performance. Additionally, immersive VR environments, as evidenced by Choi et al. (12), significantly improve motor imagery signals and user embodiment. Finally, Ahmed et al. (67) highlight the synergistic benefits of combining visual and proprioceptive feedback to optimize sensorimotor recruitment. These insights pave the way for more effective, accessible, and user-friendly MI-BCI

systems, highlighting the importance of user-interactive training and feedback mechanisms.

Thus, to enhance MI-BCI training for use outside laboratory settings, a personalised and adaptable approach is required, in which elements such as real-time feedback, XR, action observation, multimodal feedback, and optimized cue presentation can be selectively employed according to individual user needs. These insights pave the way for more effective, accessible, and user-friendly MI-BCI systems, highlighting the importance of user-interactive training and feedback mechanisms.

3.3 Algorithms

A BCI system needs the right combination of features and accurate algorithms to enhance the accuracy, robustness, and adaptability of MI classification systems. Classifier design remains an important factor influencing BCI performance, although its effectiveness is strongly coupled with feature extraction, calibration strategies, and user adaptation(20).

Lotte et al. (21) describe a pipeline for an MI-BCI where the μ and β band power features from the motor cortex are extracted and provided to the classifiers for training and application. One of the most popular and promising feature extraction techniques is spatial filtering, (68), which combines several EEG channels into a few channels (depending upon the filter dimensions and number of output channels). Algorithms such as CSP and xDAWN are commonly used algorithms for Spatial Filtering. Ramoser et al., initially introduced using the CSP for multi-channel EEG during imagination of hand movements (69). Despite their high classification performance, CSPs are sensitive to noise and primarily provide spatial, rather than spectral, information. Other approaches select specific channels from all the channels to reduce the dimensionality and complexity. Wang 2006, in their work, proposed channel reduction in MI-BCI. To analyse spatial patterns of imagined hand or leg movements, CSP was used (70).

To address the limitations of CSP and improve robustness, the Filter Bank Common Spatial Pattern (FBCSP) approach was introduced and has since become one of the most widely used feature extraction techniques for online motor imagery–based BCI applications (71). In FBCSP, EEG signals are decomposed into multiple frequency sub-bands using a bank of band-pass

filters, and CSP features are extracted independently from each sub-band. Following feature extraction and selection, the resulting features are fed into a classifier to decode the intended motor imagery. Commonly used classifiers include Linear Discriminant Analysis (LDA) and Support Vector Machines (SVM). An insufficient number of features may fail to capture discriminative information, whereas an excessive number of features can lead to overfitting.

More recently, BCI algorithms leverage advances in machine learning (ML), deep learning (DL), and hybrid models to improve signal processing, feature extraction, and classification accuracy. Several studies have explored innovative approaches, demonstrating the significant potential of these methods in overcoming challenges like low signal-to-noise (SNR) ratios, inter-subject variability, limited dataset sizes, and user variability.

Lawhern et al. (72) introduced EEGNet, a compact convolutional neural network specifically designed for EEG-based BCIs. The model incorporated depthwise and separable convolutions to extract features specific to EEG signals, enabling generalization across various BCI paradigms. EEGNet's ability to perform well with limited training data, coupled with its compact design, positions it as an effective solution for real-time MI classification across different user groups and tasks. This work demonstrated that EEGNet could significantly advance the portability and scalability of BCI systems. This prominent approach has gained attention, thereby providing a foundation for other networks. For instance, Zhao et al. (73) introduced the Convolutional Transformer Network (CTNet), which combines convolutional modules similar to EEGNet for extracting local and spatial features, with Transformer encoder modules for capturing global dependencies in EEG signals.

In contrast, Tibrewal et al. (74) investigated the effectiveness of deep learning models for different user groups, particularly inefficient BCI users who struggle to produce desired sensorimotor rhythms (SMRs). By comparing CNNs with traditional machine learning methods like CSP and LDA, they found that CNNs significantly improved classification accuracy, particularly for low-performing users. This study emphasized the potential of deep learning models to address user inefficiency, a critical challenge in MI-based BCIs. Shallow CNN architectures have been explored as an alternative to more complex deep learning models. Milanés-Hermosilla et al. (75) introduced a shallow CNN model combined with Monte Carlo dropout (MCD) and ensemble methods to quantify predictive uncertainty in MI classification. This approach not only

improved classification accuracy but also enhanced reliability by estimating the uncertainty of predictions, which is a crucial aspect for real-world applications. Their experiments demonstrated the potential of shallow CNNs in improving MI-based BCIs while also providing uncertainty estimation. Amin et al. (76) proposed a multi-layer CNN model for EEG MI classification, integrating multiple CNN architectures to capture both spatial and temporal features from EEG signals. This fusion method demonstrated superior performance compared to traditional machine learning and deep learning techniques, showcasing the effectiveness of multi-layer CNNs in improving classification accuracy.

Ouahidi et al. (77) presented EEG-SimpleConv, a straightforward 1D convolutional network for MI classification. Their architecture, composed of standard layers like 1D convolutions, batch normalization, ReLU activation, and pooling, provided an efficient and easy-to-implement baseline for BCI classification. The approach was evaluated on multiple EEG MI datasets, including simulated online setups, and showed that it performed as well or better than other contemporary methods. This simplicity and efficiency in design make EEG-SimpleConv a promising approach for real-world MI-based BCIs.

Another key advancement in the field is the use of Long Short-Term Memory (LSTM) networks for EEG-based MI classification, as presented by Wang et al. (78). By integrating the one-dimensional aggregate approximation (1d-AX) technique for feature extraction and channel weighting to enhance signal representations, this approach effectively tackled the challenges of temporal and spatial dependencies in EEG signals. This framework outperformed traditional machine learning methods, establishing LSTM as a powerful tool for robust classification. Khademi et al. (79) explored hybrid networks combining CNNs and LSTMs to improve classification accuracy in MI-based BCIs. Their Transfer Learning (TL) approach, utilizing pre-trained CNNs such as ResNet-50 and Inception-v3, achieved impressive results. This approach also addressed the issue of limited dataset sizes by transferring learning from pre-trained models, demonstrating a significant improvement of 7% over previous methods in terms of classification accuracy.

Ensemble methods have also emerged as powerful techniques in MI classification. Subasi et al. (80) proposed an ensemble machine learning-based classification framework for MI tasks, combining multiscale principal component analysis (MSPCA), wavelet packet decomposition (WPD), and statistical fea-

ture extraction. This approach highlighted the benefits of combining multiple classifiers to enhance the robustness and performance of MI-based BCIs. In another study, Chatterjee et al. (81) explored ensemble learning techniques like AdaBoost to improve MI classification in BCI. This study highlighted the advantage of ensemble methods in combining the strengths of various learners to improve classification outcomes for MI tasks.

When BCI systems are moved from laboratory settings to real-world applications, issues such as limited data, inter-subject variability, and low SNR ratios in EEG signals are the main causes of low accuracy. Apart from algorithms designed to overcome these challenges, TL has emerged as an effective approach by leveraging pre-trained models and adapting them to new users or environments with minimal data. Studies like those by Khademi et al. (79) and Parvan et al. (82) show how fine-tuning pretrained CNNs, such as ResNet and Inception-v3, enhances MI classification performance, achieving high accuracy even with limited training data. Furthermore, Zhang et al. (83) demonstrated the effectiveness of TL in adapting CNN-based models to new users, reporting significant improvements in subject-independent performance. TL also offers benefits in reducing calibration time and user fatigue, as highlighted by Wu et al. (84), who integrated TL into multiple components of the BCI pipeline, including data alignment and feature extraction. This multi-level integration contributes to more efficient and user-friendly systems. Additionally, TL-based approaches have shown potential in clinical settings, with Xu et al. (85) proving its utility in stroke rehabilitation, where personalized models can be adapted from limited patient data. Overall, TL is a critical tool for making MI-based BCIs more adaptable, efficient, and suitable for real-world deployment, ranging from wearable systems to clinical applications. By leveraging novel hybrid models, deep learning architectures, and ensemble techniques, these studies are paving the way for more efficient and accurate BCI systems, with the potential for broader applications in rehabilitation and assistive technologies.

3.4 Interfaces and their Applications

In the context of MI-BCI systems, the most advanced and robust applications are found in the domains of wearable devices and VR technologies. These applications are discussed in greater detail in the following subsections.

Exoskeletons are wearable robotic devices (86) that support or enhance

Table 3.1: Summary of BCI classification approaches across various datasets and pipelines.

Author (Year)	**Dataset**	**Classes**	**Accuracy**	**Pipeline**
Zhao et al. (2024) (73)	BCI 4-2a, 4-2b	4, 2	82.52, 88.49	Data Augmentation + CNN + Transformer
Wang et al. (2018) (78)	BCI 4-2a	4	76.47	LSTM-based Classification
Khademi et al. (2022) (79)	BCI 4-2a	4	86	Hybrid Network: CNN + LSTM + TL
Tibrewal et al. (2022) (74)	Data from 54 Subjects	2	69.07	Comparison of CNN with Traditional CSP + LDA
Subasi et al. (2021) (80)	BCI 3	2	94.83	Ensemble Machine Learning Based Classification
Milanés-Hermosilla et al. (2021) (75)	BCI 4-2a, 4-2b	4, 2	77.43, 77.72	Shallow CNN and Ensemble Model
Amin et al. (2019) (76)	BCI 4-2a, High Gamma Dataset	4	75.7, 95.4	Multi-CNN Models with Different Layers + Transfer Learning
Ouahidi et al. (2024) (77)	BNCI2014001, Zhou2016, Cho2017, PhysionetMI	4, 3, 4, 2	72.1, 81.8, 64.6, 75.4	1D Convolutional Architecture
Chatterjee et al. (2019) (81)	BCI 3	2	85.71	AdaBoost Ensemble Learning
Lawhern et al. (2018) (72)	BCI 4-2a	4	-	Conv2D → DepthwiseConv2D → SeparableConv2D
Sreeja et al. (2017) (31)	BCI 4a from Competition 3	2	94.17	Gaussian Naive Bayes Classifier

human movement. Traditional exoskeletons are made from hard materials (87) like metal and use motors to help move the body. Due to its reliability, exoskeletons have gained potential interest and scope to integrate with BCI systems to help with mobility for people with SCI, ALS, or as an assistive device for rehabilitation.

Lee et al. reported the use of MI-BCI systems for a 3-way navigation-based lower limb exoskeleton, a modified version of the Rex (Rex Bionics) system

(29). Its ability to self-balance and self-support makes it suitable for tetraplegic individuals. Using ERD-based strategies, operations such as walking forward, turning left, and turning right were achieved with the help of cascaded binary classification.

The major challenge in this field is the application in day-to-day life, including activities such as climbing stairs, crossing roads, and walking in open areas. One such novel approach using a hybrid BCI and lower limb exoskeleton for climbing stairs was proposed by Li et al. (88). The powered exoskeleton with 6 degrees of freedom(DoF) involves the combination of the MI-BCI system with EMG. The combination of the strength of processed EMG signals and two MI tasks with a powered exoskeleton is used to translate the signals into useful commands for climbing stairs and overcoming the environment and kinematic constraints. Therefore, providing motivation and the possible feasibility of BCI-based exoskeletons outside laboratories.

A full-body exoskeleton that provides complete mobility for upper and lower limbs has also been investigated for BCI system integration. For instance, the Enhancing MobilitY exoskeleton developed by Benabid et al. (89) weighs 65 kg and consists of 14 joints with 14 actuated DoF and a computer station as a backpack, controlled with ECoG signals for upper limb movement and a programmable switch for lower limb, where they are translated into unidimensional (linear, rotation around the axis), bi-dimensional (movements in the plane) and three-dimensional (movements in volume).

Although all these traditional exoskeletons have been researched with a goal towards real-life applications, safety remains an area of concern. The exoskeletons are hard and rigid, which present their own challenges and complications of use in terms of comfort and fatigue from use. They are costly to purchase and maintain, and may not be affordable to everyone. This opens a path to exploring emerging fields that are possibly affordable and safe, such as soft interfaces that can be integrated as wearable technology and VR.

3.4.1 Virtual Reality

The integration of VR and MI has emerged as a transformative approach in the fields of neurorehabilitation and BCIs. VR provides immersive and interactive environments that facilitate MI training by enhancing engagement, motor learning, and neuroplasticity.

For example, Lin et al. (90) developed a VR-based MI training system specifically tailored for post-stroke rehabilitation. This system incorporated real-time EMG and EEG feedback, enabling personalized adjustments based on participants' brain activation in the alpha and beta bands. Similarly, Arpaia et al. (64) introduced multimodal feedback mechanisms in a VR ball game, integrating visual and wearable haptic feedback to enhance neurophysiological detection during MI.

Studies like those of Skola et al. (91; 92) emphasize the role of embodiment in VR environments. Using first-person avatars and vibrotactile feedback, these studies leveraged the sense of ownership, agency, and self-location to strengthen EEG correlates of MI. This embodied VR approach significantly improved training outcomes, as evidenced by higher accuracy rates in MI-BCI tasks compared to traditional methods.

The synergy between immersive VR and MI is further supported by research such as Choi et al. (12). Mahmood et al. (93) expanded on this concept by showcasing a four-class MI paradigm with soft EEG electrodes in a VR cube color game, highlighting advancements in wearable and portable EEG systems for VR-BCI integration.

Several studies focus on using VR for specific patient populations. For instance, Kashif et al. (94) investigated the combined effects of VR and MI for patients with idiopathic Parkinson's disease (PD). Their findings demonstrated significant improvements in motor function, balance, and ADL when VR-MI training was integrated with physical therapy. Xu et al. (95) introduced a novel 3rd-person perspective (3PP) VR paradigm for stroke rehabilitation, utilising full-body illusions to enhance the sense of ownership (SOO) over virtual avatars and improve MI efficacy.

Research by Alsuradi et al. (96) explored neural signatures associated with MI of a virtual supernumerary thumb, offering insights into augmented BCIs for new effectors. Wang et al. (97) proposed a VR game-based adaptive neurofeedback training paradigm, achieving significant improvements in motor cortex activation and MI-BCI performance. These studies highlight the versatility of VR in eliciting distinct neural activations and enhancing MI training across diverse contexts.

Vourvopoulos et al. (98; 99) demonstrated the benefits of multimodal VR feedback and motor priming in optimizing MI-BCI calibration and training outcomes. Their findings emphasize the importance of synchronizing visual,

motor, and sensory inputs to maximize neural engagement and neuroplasticity. Similarly, Fererro et al. (100) employed real-time VR feedback during MI of gait for closed-loop trials.

These studies underscore the transformative potential of VR in MI training and neurorehabilitation. Through advances in feedback modalities, embodiment, and neural activation, VR offers a promising avenue for enhancing MI-BCI systems. Future research can be directed towards exploring the integration of VR with emerging technologies, such as soft EEG electrodes and adaptive neurofeedback, linking it with assistive devices to further optimize rehabilitation outcomes and user experience.

3.4.2 Soft Interfaces

Soft exoskeletons (102; 103; 104; 105; 106), also called exosuits, are different from the traditional ones explained before. They use soft materials like fabrics (107; 108), cables(109), or flexible actuators (110; 111). This makes them much lighter and more comfortable to wear. Soft exoskeletons are designed to move naturally with the body, helping without getting in the way.

While soft exoskeletons already improve comfort and wearability, a deeper focus lies in compliance (how these devices physically adapt to uncertain or imperfect control signals). Compliance is especially important in BCI systems, where MI classification can be inconsistent or delayed. There are several forms of compliance that enhance safety and adaptability: active compliance (112), where rigid systems are made responsive through control algorithms; passive compliance (113), seen in articulated soft robots that use springs or elastic joints; and continuum soft robots, where flexibility is distributed throughout the body. These strategies help absorb errors, reduce risk, and enable more natural interaction. While each approach contributes to safe human-robot collaboration, continuum soft robots (114) hold particular promise in MI-BCI settings, due to their inherent adaptability and gentle interaction with the body.

In the field of BCI-controlled rehabilitation systems, creating safe and effective interfaces is key. As these technologies advance, research continues to focus on improving the usability, safety, and effectiveness of BCIs. Several studies have contributed to the development of these intuitive interfaces by combining various strategies and technologies that ensure safe interaction

Table 3.2: Summary of VR-based MI paradigms across various studies.

Author (Year)	**Application, VR Paradigm**	**Participants**	**Accuracy**
Lin et al. (2022) (90)	Poststroke rehabilitation, Shooting Basketball	8 Post-stroke	-
Choi et al. (2020) (12)	MI, Left/Right Hand Grasping	20	67.85 ± 13.50
Skola et al. (2018) (91)	MI, Left/Right Hand Pressing Button	30	58.30%
Kashif et al. (2022) (94)	Parkinson's disease rehabilitation, -	44 Patients with Idiopathic PD	-
Vourvopoulos et al. (2016) (98)	MI, Left/Right Virtual Hand Mapping	9	53.61
Alsuradi et al. (2024) (96)	MI,Supernumerary Thumb	20	69%
Choi et al. (2020) (101)	MI,Navigation Track	14	53.27
Xu et al. (2024) (95)	Poststroke rehabilitation, 3rd Person Perspective Visually Guided MI	13 Stroke Patients	-
Skola et al. (2023) (92)	MI,Spaceship Control Panel with Vibrotactile Feedback	30	74.4
Ferrero et al. (2021) (100)	MI gait training to use exoskeleton,Walking in Corridor	5	91
Vourvopoulos et al. (2015) (99)	MI,Grasping Control Handles for Opening Garage Door	9	65.6
Wang et al. (2024) (97)	MI,Fruit Cutting	6	83.52
Arpaia et al. (2023) (64)	MI, Ball Game (Left/Right) with Wearable Haptic Feedback	8	70
Mahmood et al. (2021) (93)	MI, VR 4-Class Cube Color Game with Soft EEG Electrodes	N.D.	-

between the user and assistive devices.

One of the foundational studies in the development of BCI-based rehabilitation tools for stroke patients is Vargas et al. (115), which focuses on a soft robotic glove controlled through MI. This study was guided by practical needs, with continuous feedback from physiotherapists. The glove was designed to support rehabilitation while keeping the palm and fingers exposed, enabling natural object interaction. Its lightweight and unobtrusive form makes it well-suited for everyday use beyond clinical settings (115; 116).

Similarly, Li et al. (117) explored the potential of a soft robotic glove to control a Qrobotics manipulator using MI signals. The aim was to develop a straightforward and reliable interface for controlling robotic manipulators in tasks like grasping. Prioritizing usability, the system enables patients to carry out ADLs with safe and controlled support.

Additionally, Zhang et al. (118) developed a more complex multimodal system combining EEG, EMG, and EOG signals to control a soft robotic glove. This approach aimed to improve the precision and safety of the system by integrating multiple signal sources. The study focused on building user confidence, particularly for individuals with physical impairments. Using multiple signal modalities reduced false positives, helping prevent unintended actions. The findings also showed the glove's potential for safe, real-time control in daily activities for people with motor disabilities.

As the technology evolves, researchers have explored combining sensory inputs to further enhance the safety and effectiveness of BCIs. Kwon et al. (119) pioneered the integration of MI with vision-based control to reduce false positive rates (FPR) in soft robotic glove applications. The system combined vision glasses, EEG signals, and a tendon-driven glove to ensure that it responded only when the user's hand was visible. The study showed that vision-based feedback can improve the safety and effectiveness of assistive robotic devices.

Similarly, Mukherjee et al. (120) developed an advanced assistive device for elbow and finger rehabilitation using a low-cost BCI system powered by EEG sensors and deep learning algorithms. With a focus on affordability and ease of implementation, this study presented an interface that is not only safe but also accessible to a broader patient population.

An exciting direction in BCI-assisted rehabilitation is the combination of VR with MI, as seen in the study by Gao et al. (121). By integrating VR with a soft robotic glove, this system added an element of immersion, encouraging patients

to focus more on their movements, thus increasing their brain's participation in the rehabilitation process. The added feedback from the VR environment engaged users by providing real-time information on movements, ensuring they were engaging in safe, controlled exercises. This VR-BCI hybrid system highlights the potential of combining digital environments with real-world interfaces to enhance rehabilitation outcomes and make the experience safer for patients.

The development of safe and effective interfaces for BCI-assisted rehabilitation is crucial to improving the quality of life of individuals with motor impairments, particularly those recovering from stroke.

As these technologies evolve, combining MI with soft robotics and VR offers the potential for safer, more intuitive, and more effective rehabilitation systems. These advances not only increase the accuracy of device control but also enhance patient comfort, ensuring that these systems can be used effectively in both clinical and home settings. With continued innovation, BCI interfaces are becoming more accessible, adaptive, and safer for a wider range of patients, ultimately improving rehabilitation outcomes and enhancing the independence and confidence of individuals with motor disabilities.

3.5 Other Potential Interfaces and their Applications

Beyond motor imagery and exoskeleton-based systems, several other safe and accessible interfaces hold promise for supporting daily living and rehabilitation. These technologies aim to enhance user independence, engagement, and functional recovery by integrating intuitive control, feedback, and assistive mechanisms. Exploring such interfaces helps identify complementary pathways to improve the usability and adaptability of neurorehabilitation tools in real-world contexts.

Knierim et al. (158) compared two dry-electrode EEG systems (the Open ExG headphone EEG and the OpenBCI Ultracortex headset) across both controlled and naturalistic environments involving 50 participants and 146 recordings. Their findings indicate that the EEG headphone system offers significantly improved wearability, with comparable signal quality and recording reliability when used by trained experimenters under laboratory conditions.

Table 3.3: Overview of BCI-based robotic assistive systems using MI strategies.

Author (Year)	**Type of Interface (Strategy)**	**Participants**	**MI Algorithm**	**Accuracy**	**Application**
Vargas et al. (2017) (115; 116)	Soft Robotic Glove (MI)	5	CSP+LDA (16 ch)	73.6–95.4	Potential for Stroke Rehabilitation
Li et al. (2022) (117)	QRobotics Manipulator (MI)	5	CSP+SVM	87	-
Kwon et al. (2022) (119)	Tendon-Driven Soft Robotic Glove (MI, Vision)	6	Shallow ConvNet	-	-
Zhang et al. (2019) (118)	Soft Robotic Glove w/ 5 Flexion Actuators (MI, EMG, EOG)	6	Wavelet, ERD/ERS - SVM	93.83	Potential for Stroke Rehabilitation
Li et al. (2018) (122)	Soft Robotic Glove (MI)	4	CSP+SVM	72 [30 ch]; 76.3 [9 ch]	Potential for Stroke Rehabilitation
Schiatti et al. (2017) (123)	7-DoF KUKA Arm + Pisa/IIT SoftHand (MI, Eye Tracking)	1	-	-	Object Manipulation
Cheng et al. (2020) (124)	Soft Robotic Glove (MI)	11 ($\geq$6 mo post-stroke)	FBCSP-LDA	-	Stroke Rehabilitation
Zhang et al. (2024a) (125)	Bilateral Vibration Tactile Stimulation (MI)	14	CSP-LDA	-	-
Gao et al. (2022) (121)	Soft Robotic Glove (MI)	11 Stroke Patients	PSD-kNN (Riemann)	-	Stroke Support, Rehabilitation
Mukherjee et al. (2024) (120)	Elbow and Finger Assistive Device (MI)	15	CNN-TLSTM	98.66	-
Zhang et al. (2024b) (39)	Robotic Glove (MI, SSVEP)	12 Healthy, 9 Stroke	FBCSP, FBCAA	81.7 $\pm$ 15.6%, 95.1 $\pm$ 7.5%	Stroke Rehabilitation
Tang et al. (2022) (126)	Supernumerary Robotic Limb (MI)	10	GNN	86.44	-
Araujo et al. (2021) (127)	Robotic Glove (MI)	1	-	-	Stroke Rehabilitation

Table 3.4: Possible future interfaces for MI.

Application	**Literature**
Wearable electrodes, Smart glasses / VR	(128; 129; 130; 131; 132)
Soft upper body exoskeleton	(48; 133; 134; 135; 136; 137; 138; 139; 140)
Smart Hug Vest, Wearable textiles	(141; 142; 143; 144; 145)
Wearable Haptics	(146; 147; 148; 149; 150; 151; 152)
Wearable lower-body exoskeleton	(153; 154; 155; 156; 157)

In particular, the EEG headphones also maintained reliable classification of cognitive load in field settings, even after participant-led setup at home. These results underscore the growing feasibility of deploying dry-electrode EEG for MI-BCI applications in everyday life, where ease of use and comfort are essential. When paired with MI tasks such as imagining reaching, grasping, or walking, these wearable systems could enable continuous at-home BCI operation for individuals with motor impairments. This could support hands-free control of assistive technologies, smart home devices, or exoskeletal systems, promoting greater independence and quality of life in daily routines. The implications of the study point toward a future in which MI-based BCIs, powered by dry EEG technologies, become seamlessly integrated into users' real-world environments. Another possibility could be using clinical EEG systems in the laboratory and clinical setups for training the highly advanced algorithms, such as Transfer Learning, and then using the wearable dry EEG as an application to control everyday interfaces. In this way, the user gets familiar with the systems involved under supervision and thereafter can use the MI-BCI systems independently.

The development of wearable haptic interfaces has significant potential for enhancing MI-BCI applications, particularly in rehabilitation and VR contexts. For instance, Sonar et al. (159) presented a soft pneumatic actuator (SPA)-based skin interface capable of simulating tactile sensations such as roughness, shape, and size with high fidelity. Integrating such feedback with MI paradigms can strengthen sensorimotor integration by coupling imagined movements with congruent somatosensory feedback, which has been shown to enhance neural plasticity and motor recovery, especially in patients with neurological impairments such as stroke or SCI. Furthermore, combining SPA-skin feedback with MI could improve BCI training by increasing vividness and engagement of MI, ultimately leading to better decoding performance. This integration also

supports applications in VR-based skill training and telepresence, where users can mentally simulate interactions while receiving realistic haptic feedback, creating a closed-loop system that bridges cognitive intention and sensory perception.

Deep Pressure Stimulation (DPS) is another avenue that has been shown to produce calming effects, particularly in individuals experiencing elevated anxiety, and its integration with BCI paradigms presents new opportunities for enhancing emotional regulation during MI tasks. Bontula et al. (160) evaluated the effects of a soft-robotic DPS device, the AID Vest, on individuals with moderate to high anxiety. Comparing it to the widely used weighted blanket, their study demonstrated that both DPS modalities reduced anxiety, as measured by biosignals and one-shot self-reports, with the AID Vest demonstrating particularly promising outcomes. These findings support the potential of the AID Vest as a portable and responsive anxiety-regulation tool. Integrating such DPS technologies with MI-based BCIs could offer dual benefits: enhancing user comfort and emotional stability during MI tasks, and improving BCI performance by mitigating anxiety-induced variability in EEG signals. This is especially relevant in real-world BCI applications, such as assistive control or rehabilitation, where a consistent mental state is essential for reliable decoding. The AID Vest could be incorporated into closed-loop systems where DPS is dynamically modulated based on real-time brain or physiological signals, supporting a more stable and user-friendly MI-BCI experience.

The integration of MI-based BCI control with wearable exoskeletons presents promising avenues for the rehabilitation of individuals with gait impairments, such as dropfoot. Zhang et al. (161) developed a soft ankle exoskeleton designed to provide assistance in two DoF—dorsiflexion and eversion—through a dual-motor actuation system and a cable-based transmission mechanism. Their design includes a force-free controller that effectively compensates for device resistance, and proof-of-concept experiments demonstrated its capability to restore more normative ankle kinematics in simulated dropfoot conditions. Integrating this exoskeleton with MI-BCI systems could enable users to control the timing and degree of ankle assistance using imagined dorsiflexion and eversion movements, thus fostering active neural engagement during gait rehabilitation. This combination of volitional neural input with robotic assistance could enhance motor recovery by reinforcing the sensorimotor loop and promoting cortical reorganization. Furthermore, MI-driven control could allow for more

intuitive, user-adaptive assistance during walking, reducing dependence on pre-programmed gait phases and enabling real-time modulation of support based on the user's intent and capability. Such a system holds promise for restoring more natural and personalized locomotion in individuals with post-stroke gait disorders.

Another avenue with MI-based control for assistive exoskeletons offers an intuitive and neurologically engaging strategy to reduce physical strain while supporting motor function. Nassour et al. (162) introduced Carry, a soft exoskeleton designed to assist the elbow joint during load holding and carrying tasks using soft pneumatic actuators and a compliant HMI. These outcomes underscore the device's potential to mitigate fatigue and injury risks associated with repetitive or prolonged upper limb exertion. When integrated with MI-based BCI control, users could initiate or modulate exoskeleton assistance through imagined elbow flexion or extension, allowing for a more seamless and adaptive user experience. This MI-driven approach could not only reduce the need for manual or sensor-based triggering but also promote active motor planning and cortical engagement during task performance, which is particularly valuable in rehabilitation settings. Such synergy between neural intent and physical assistance opens the door to more ergonomic, user-centred support systems for both clinical and occupational use cases.

Recent advancements in soft wearable robots provide new avenues for integrating MI-BCI control, enabling more intuitive and adaptive human-robot interaction. Varghese et al. (140) introduced a bio-inspired kinematic sensing framework for a multi-DoF shoulder exosuit, designed to accurately capture joint kinematics through compliant sensing mechanisms. Drawing inspiration from the embodied organization of muscles and synergies involved in shoulder movement, their tendon-routing-based sensor system was validated using motion capture data, achieving low root mean square errors for azimuth and elevation angles. Unlike rigid sensing and actuation systems, this compliant and biologically informed design facilitates naturalistic motion tracking, which is essential for intuitive control. When paired with MI-based BCI systems, such sensing mechanisms could enable users to modulate exosuit behavior through neural intent, allowing real-time adjustments in joint angles or support level without physical exertion. This closed-loop neuro-robotic system has the potential to enhance user comfort, promote cortical engagement, and reduce the cognitive and physical burden of control. Moreover, the biomimetic

approach supports the development of more personalized and responsive rehabilitation tools, aligning assistive outputs with the user's imagined movements to accelerate motor recovery and foster adaptive motor learning.

Advances in soft sensor technology have expanded the capabilities of HMIs for assistive control, and their integration with MI-BCIs could enable more intuitive and multimodal control systems. Liu et al. (163) presented a soft HMI composed of silicone-based soft sensors and IMUs that translates shoulder movements into continuous 2D control commands, targeting users with severe motor impairments such as amputees and individuals with quadriplegia. The interface employs both rule-based and intent-inference-based decoding strategies, and further enhances control by incorporating a shared autonomy framework that integrates user-specific performance priors. Their experimental validation, spanning target-reaching and virtual wheelchair navigation tasks, demonstrated the system's effectiveness in generating reliable, real-time interaction commands. Integrating this soft-sensor-based control with MI-BCI inputs could facilitate hybrid control schemes, where shoulder gestures and neural intent collaboratively guide assistive devices such as wheelchairs, robotic arms, or soft exosuits. Such a system could increase precision, reduce cognitive load, and offer redundancy for users with fluctuating motor or neural reliability. Moreover, shared control blending physical gestures with MI would support adaptability in real-world scenarios, further enhancing autonomy and usability for individuals with complex physical impairments.

3.5.1 Summary

In summary, the reviewed state-of-the-art literature motivates the investigation of motor imagery–based BCI systems at the subsystem level and underpins the research questions outlined in Chapter 1. These research questions collectively address the pillars required to bring MI-BCIs from laboratory paradigms to practical applications in daily life. Significance is embedded in each question, highlighting why foundational understanding, user training, algorithmic improvement, and interface design are crucial for real-world deployment. RQ1 establishes neurophysiological feasibility, RQ2 optimizes user training, RQ3 develops robust and practical algorithms, and RQ4 translates control into safe, interactive ADL tasks, ultimately advancing MI-BCI applicability for rehabilitation and daily living.

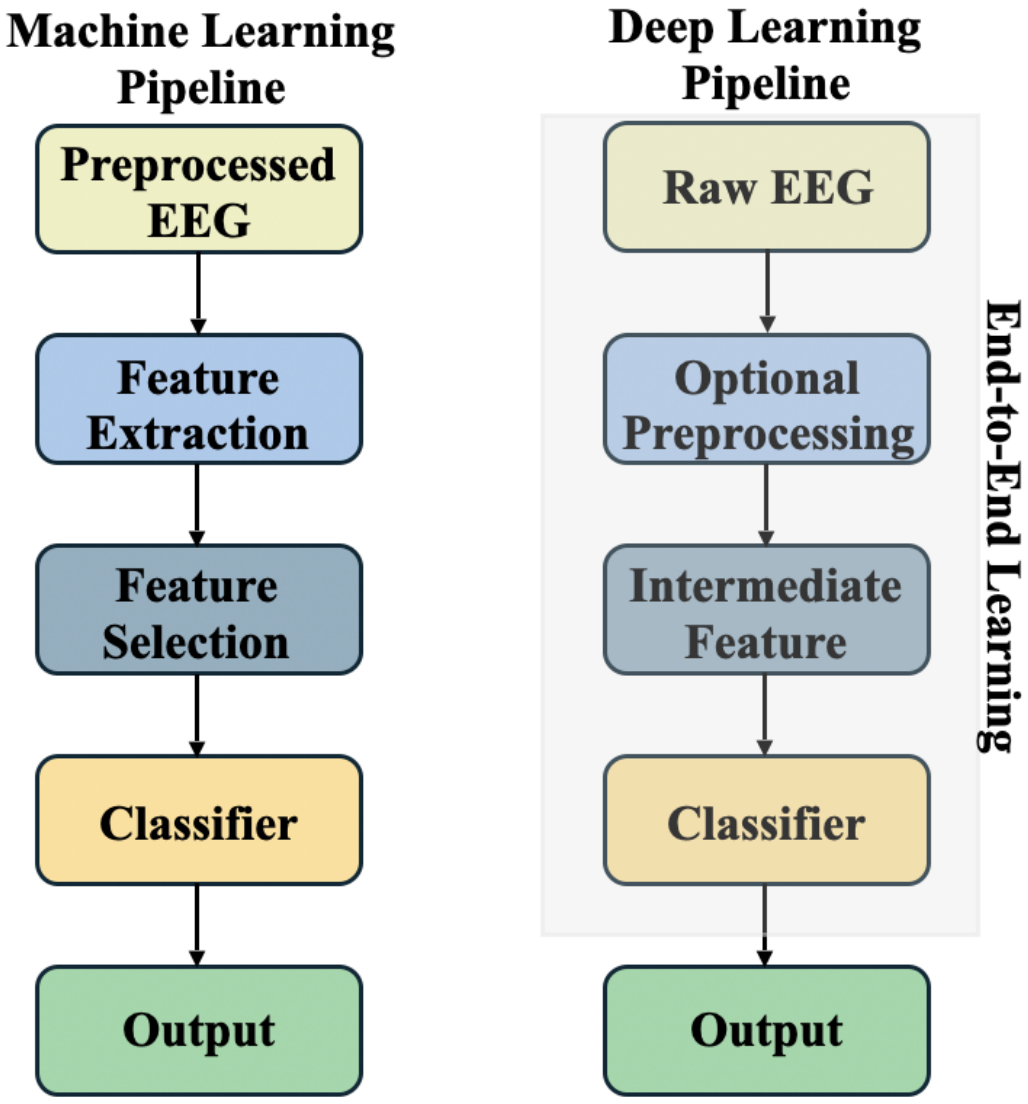

Figure 3.2: MI Classification Pipeline for Machine Learning (where Preprocessed EEG(Filtered and Normalized data) is passed for Feature Extraction (CSP, FBCSP, channel selection) and selected features are passed on to Classifier (SVM, LDA, Ensemble Learning) resulting in Output (Binary/Multi) (Left/Right/Foot/Tongue classification)) and Deep Learning (where Raw EEG (with optional preprocessing) with Intermediate Features (Spatial/Temporal) e.g. CNN, Transformers is passed to Classifier (CNN, RNN, Hybrid), resulting in Output (similar to ML pipeline).

Chapter 4

Motor Imagery and Spinal Cord Injury

"In research, if you never fail, you are just not trying hard enough!"
- Prof. Tomás Ward

RQ 1: MI and SCI Feasibility *How can motor imagery training be useful for SCI patients?*

Significance: Understanding MI capability in SCI populations is critical because it forms the neurophysiological foundation of MI-BCI systems. Without reliable MI signals, subsequent training, classification, and interface design cannot be effectively implemented. Insights gained here can guide calibration protocols, improve signal acquisition strategies, and ensure that MI-BCI systems are inclusive and beneficial for rehabilitation.

Expected Outcomes: Characterization of MI signal quality in SCI, foundations for how motor imagery training contributes towards rehabilitation environments.

Testing and Validation: ERD/ERS analysis, MI classification accuracy, and comparison across SCI participants.

Systematic reviews and clinical studies indicate that MI may be beneficial for patients with SCI and can positively influence motor function, pain modulation, and neurophysiological responses, although study heterogeneity remains high (46; 60; 164; 61). Recent EEG studies highlight MI-related alterations in connectivity and oscillatory activity, including differences linked to neuropathic pain, underscoring MI's potential both as an intervention and as a measure of neuro-rehabilitation (60; 164; 61).

Robotic exoskeletons (165) have emerged as powerful tools for gait rehabilitation after SCI, enabling upright, repetitive, and task-specific walking that promotes mobility gains and neuroplasticity (166). In contrast, upper-limb rehabilitation robotics and therapist-mediated feedback systems (53; 167) emphasize fine motor control, user engagement, and adaptive feedback to foster voluntary motor relearning. While exoskeletons focus on large-scale, lower-limb movement and locomotion, upper-limb and feedback-driven systems target precision and cortical activation—together representing complementary pathways toward functional recovery and neuroplastic reorganization after SCI.

Importantly, engagement during exoskeleton training—such as during motor imagery—can be influenced by how feedback, control, and interaction are designed, suggesting that combining brain signals with robotic assistance may improve rehabilitation outcomes (167).

BCI systems (168; 40; 165) based on MI-related EEG activity have been used to link the user's motor intentions with control of robotic exoskeleton execution. MI-BCI-based control of exoskeleton has been demonstrated in people with SCI during gait training. In these studies, MI classifiers were applied to control robotic exoskeletons, achieving reliable classification of gait imagery. The provision of real-time feedback enabled participants to learn to modulate Alpha/Beta rhythms (52; 51). These studies demonstrate the translational potential of MI-BCI exoskeleton systems to support the brain's adaptive plasticity through neurofeedback-based protocols. (52; 51).

When it comes to SCI based progress in this field, EEG-based MI classification has advanced considerably, with methods such as time-varying autoregressive spectral analysis (169), graph-attention networks integrating temporal–frequency–spatial features (170), spiking neural networks (56), and Transformer-based models leveraging probabilistic attention or Mixture-of-Experts mechanisms (171; 55; 57). Hybrid paradigms have also gained attention, for instance, brief BCI-FES priming before rehabilitation therapy improved

outcomes in small runs (59), multimodal EEG–fMRI BCIs synchronized with FES/exoskeletons yielded functional recovery in chronic cervical SCI (50). Other studies illustrate broader applicability, including EEG-driven robotic controllers during lower-limb pedaling (172). Research further demonstrates rapid expansion of SCI-BCI research and a shift toward translational and clinical integration (173).

Despite these advances, current exoskeleton protocols focus largely on peripheral execution, often underutilizing the user's motor intent. Integrating MI practice directly with exoskeleton-assisted walking—particularly when scheduled before and after sessions—offers a unique opportunity to couple central and peripheral processes, reinforcing top-down intention and bottom-up sensory feedback. The present study addresses this gap by implementing a co-created rehabilitation protocol in which individuals with SCI perform MI immediately before and after exoskeleton-assisted walking.

Only a limited number of studies have examined MI-BCI approaches for lower-limb rehabilitation in individuals with SCI, with most existing work focusing on *online* MI-based control or neurofeedback during exoskeleton-assisted gait training (52; 51). In these studies, MI is directly coupled to robotic execution following offline classifier training. By contrast, the role of structured MI practice scheduled *before* or *after* exoskeleton-assisted walking—without direct online control—has received comparatively little attention, despite related evidence from MI-only and MI–FES priming studies (59).

The contributions from this chapter are:

1. To test the hypothesis whether engaging in MI practice before and after exoskeleton-based walking will enhance the efficacy of exoskeleton-based rehabilitation.

2. To evaluate whether the exoskeleton-assisted walking will, in turn, modulate post-intervention MI performance.

By examining MI-related EEG activity across sessions, the aim is to explore whether integrating MI sessions before and after exoskeleton training can create a bidirectional enhancement and lay a foundation for future closed-loop MI–BCI–exoskeleton rehabilitation strategies.

4.1 Methodology

4.1.1 Participants

30 participants were recruited from the DCU exoskeleton clinic for this study. Of the 30 participants, 3 were excluded due to severe contractures, 2 due to restricted range of motion, 3 due to cognitive impairments that prevented them from following directions, and 1 due to exceeding the body weight limit of 100 kg during the initial assessment. This resulted in 21 eligible participants at study entry. Of these, 1 participant withdrew during the familiarization session due to difficulty committing to the study schedule, and 2 participants withdrew after the first intervention session for reasons including transportation difficulties, fatigue, and personal circumstances unrelated to the study.

The final sample comprised 18 participants, with 9 allocated to the experimental group (with motor imagery) and 9 to the control group (without motor imagery). The experimental group consisted of newly recruited participants, whereas the control group was formed using 9 participants from a previous study who underwent the same exoskeleton intervention protocol without the motor imagery protocol; no randomization procedures were applied. Injury details are classified by neurological level and American Spinal Injury Association (ASIA) impairment grade (174), whereby level refers to the segment of the spinal cord affected, and the ASIA grade is a standard clinical classification of the severity of sensory and motor impairment following SCI.

The experimental group had a mean age of 46.3 ± 10.8 years compared to 51.7 ± 14.5 years in the control group, with no statistically significant difference (Welch's t-test: $p = 0.389$, i.e., $p > 0.05$). Sex distribution (Experimental: 9M/0F; Control: 8M/1F) showed no significant group difference (Fisher's exact test: $p = 1.000$, i.e., $p > 0.05$). ASIA grade profiles (Experimental: A=3, C=5, D=1; Control: A=4, C=3, D=2) were also comparable (chi-square test: $p = 0.614$, i.e., $p > 0.05$), and baseline step rate/motor-severity data were not available for statistical testing. Based on descriptive comparisons, the two groups appear generally similar in age, sex distribution, ASIA severity, and injury level. The differences observed are small and not indicative of major baseline imbalance, although the sample size does not allow for strong statistical conclusions.

Before Session 0, the participants were first exposed to the study protocol,

during which they completed initial assessments and were introduced to the exoskeleton setup. Ethical approval for the study was obtained from the Research Ethics Committee at DCU (DCUREC/2023/155).

The current sample was drawn exclusively from the DCU Exoskeleton Clinic, which operates at a capacity of approximately 25 sessions per week and serves individuals with a range of gait-affected neurological disorders. For the present study, only participants with a spinal cord injury were included. However, due to the clinic's limited capacity, the resulting sample was heterogeneous in terms of injury levels. Importantly, this heterogeneity reflects the real-world diversity of individuals undergoing exoskeleton training and thereby enhances the ecological validity of the study findings.

4.1.2 Experimental Protocol

This study was designed to compare the effects of standard exoskeleton gait training with and without the addition of MI. The experiment consisted of two groups: a control group, which served as baseline, which performed exoskeleton walking only, and an experimental group designed with the control group as baseline, which performed MI sessions immediately before and after selected exoskeleton walking sessions (sessions 0 and 4). The decision to include only two motor imagery sessions was based on pragmatic considerations related to clinic scheduling, participant fatigue, and the structure of the exoskeleton rehabilitation programme, and was not intended to produce long-term motor changes.

The experimental protocol is illustrated in Figure 4.1, where I represents the experimental group procedures, and II represents the control group procedures.

- **Control Group Procedure:**

  The control group (n = 9) completed four exoskeleton-assisted walking sessions over a period of 4–6 weeks using the Ekso-NR device in a previous study, which served as baseline for this study.

- **Experimental Group Procedure:**

  The experimental group (n = 9) followed the same exoskeleton walking protocol as the control group. In addition, they performed MI tasks

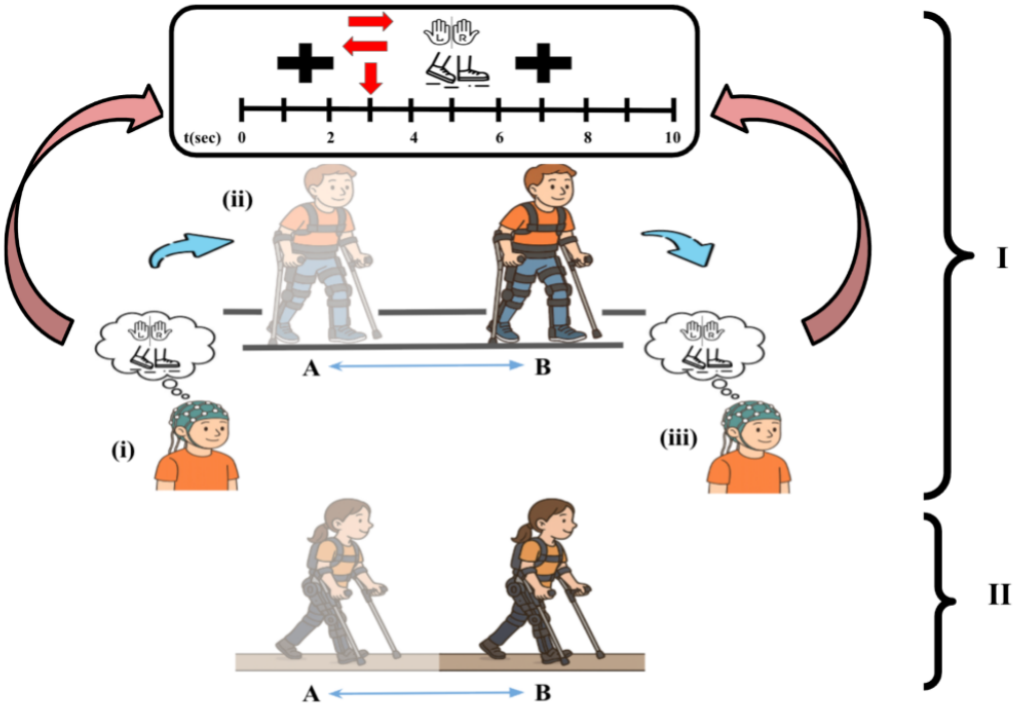

Figure 4.1: Experimental Protocol: Where I is the experimental group where participants perform (i) Motor Imagery session, followed by (ii) exoskeleton walking intervention from distance of A to B, and later followed by (iii) Motor Imagery session. II represents the control group that performs only the exoskeleton walking intervention from distance A to B.

immediately before and after exoskeleton walking during sessions 0 and 4.

4.1.3 Tools used

The details of the devices used to test the hypothesis is listed below. Figure 4.2(a) illustrates the MI experiment, in which the participant performs imagery tasks while EEG signals are recorded, and Figure 4.2(b) demonstrates the exoskeleton walking intervention, where the participant engages in gait training with the Ekso-NR device.

Exoskeleton

The exoskeleton walking was conducted using the Ekso-NR device (Ekso Bionics, Inc., Richmond, CA, USA) (175). The Ekso NR (176; 166) is an exoskeleton framework for the lower limbs, equipped with actuated hip and knee joints

(a) Motor Imagery

(b) Exoskeleton Intervention

Figure 4.2: Demonstration of the experiment where (a) Participant performs Motor Imagery and (b) Participant performs exoskeleton intervention

and passive spring-loaded ankle joints. The participant is required to weight-shift laterally and forward to initiate stepping of the robotic exoskeleton, and depending on the degree of paralysis and subsequent robot settings, effort from the participant's legs may also be required. A trained handler stands at the back, physically and verbally guiding the user. Ambulation assistance and exoskeleton settings vary based on the individual's gait specifics and training progress.

Each exoskeleton walking session lasted approximately 20–45 minutes, excluding the time required for device setup. Actual walking duration varied across participants depending on individual fatigue, discomfort, or pain levels. All sessions were supervised by the physiotherapist and a trained handler, who assisted with balance and adjusted device settings using a wired rear controller. Where necessary, participants also used walking aids such as canes, crutches, or a frame, as demonstrated in Figure 4.2(b). Exoskeleton-assisted walking was performed with clinical therapist assistance. Apart from the steps/min data, details regarding mode, speed, and other device parameters are beyond the scope of this study.

EEG Device

For the EEG data, MI EEG was recorded using an EEGO 32-channel EEG system (ANT Neuro, Enschede, The Netherlands) (177). Data acquisition was done using OpenVibe software, and electrode impedance was maintained below 5 kOhms. During each run, participants were presented with a random 15 cues for right-hand movement, 15 cues for left-hand movement, and 15 cues for

feet movement. Each participant completed two runs before their exoskeleton walking session, and two runs post walking session.

4.2 Evaluation Matrix

4.2.1 Exoskeleton Walking Performance

Data relating to the participants' exoskeleton walking performance was obtained from a designated cloud to which the Ekso NR exoskeleton automatically uploads after each walking session. This data includes steps/min and the total number of steps per session.

For each session, the number of steps and the total walking time were recorded directly from the exoskeleton system. These measures were used to calculate walking cadence, expressed as steps per minute, for evaluation, as session performance is quantified by:

$$\text{Performance}_{i,s} = \frac{N_{i,s}}{T_{i,s}} \quad \text{(steps per minute)} \tag{4.1}$$

where $N_{i,s}$ = total number of steps in session s for participant i,
and $T_{i,s}$ = duration of that session in minutes.

4.2.2 Motor Imagery EEG data

The Graz-BCI MI paradigm was used to collect MI data from the experimental group. In this paradigm, participants were instructed to imagine performing specific limb movements— left hand, right hand, or foot movement—while maintaining physical stillness. The three most commonly studied motor imagery tasks—left-hand, right-hand, and feet (22; 178) were used based on the well-established Graz BCI paradigm. While these movements are not exclusively linked to gait, it was hypothesized that engaging general motor networks via these tasks could support motor outcomes during exoskeleton-assisted walking.

The motor imagery protocol used the Graz BCI paradigm with 15 runs each of left-hand, right-hand, and feet imagery, repeated twice. Each run began with 0–1s rest, 1–3s fixation cross, followed by a 3–6s MI cue (arrow at 3s), followed by imagine window presented via OpenViBE, and 6–9s rest. Participants were instructed to vividly imagine the indicated movement, without prior MI ability screening. The imagery tasks were cued visually, with arrows within a

precisely timed trial structure that includes a fixation period, a cue presentation, an imagery phase, and a rest phase. In the present work, this paradigm is adopted to evoke and analyze MI-related brain activity across Mu and Beta bands both before and after exoskeleton-assisted gait sessions. The EEG data are evaluated using two approaches: (i) ERD/ERS analysis and (ii) machine learning techniques. These are described in the following sections:

EEG Preprocessing and Artefact Handling

Prior to evaluation of EEG, EEG signals were preprocessed to improve signal quality and reduce artefacts prior to feature extraction. A band-pass filter between 8–30 Hz was applied to focus on the frequency range relevant for motor imagery, and a 50 Hz notch filter was used to suppress power-line noise. Bad epochs containing prominent artefacts were identified and discarded manually through visual inspection. Independent Component Analysis was subsequently applied to remove remaining ocular and muscular artefacts. Preprocessed signals were then used for ERD/ERS feature extraction.

ERD/ERS

MI induces systematic modulations of brain rhythms and oscillations, particularly within the sensorimotor cortex. These modulations are characterized as ERD and ERS, reflecting changes in the amplitude of neuronal oscillations in specific frequency bands. The most prominent effects occur in the μ-rhythm (8-13 Hz) and β-rhythm (13-30 Hz), which are closely associated with sensorimotor processing (179; 180).

Mathematically, ERD/ERS can be expressed as a relative change in band power with respect to a pre-stimulus or resting baseline. For a given frequency f and time t, the ERD/ERS percentage is defined as:

$$\text{ERD/ERS}(f,t) = \frac{P(f,t) - P_{\text{ref}}(f)}{P_{\text{ref}}(f)} \times 100\%, \tag{4.2}$$

where $P(f,t)$ denotes the time-varying spectral power and $P_{\text{ref}}(f)$ is the mean reference power during a baseline period. A negative value of $\text{ERD/ERS}(f,t)$ corresponds to ERD, indicating a decrease in oscillatory power and reflecting increased cortical activation through the desynchronization of neuronal populations. Conversely, a positive value indicates ERS, corresponding to an increase

in oscillatory power and often interpreted as cortical idling or post-movement rebound.

During motor imagery, contralateral sensorimotor areas typically exhibit pronounced ERD in the μ and β bands, resembling patterns observed during actual movement execution. This similarity underscores the functional relevance of ERD as a neural correlate of imagined movement, making it a key feature for analysis. By quantifying ERD/ERS dynamics, the temporal evolution of cortical activation can be extracted and used as features for the classification of MI class. Baseline and task windows were defined for feature extraction, with a baseline period of 0.5s implemented at the 3rd second of each trial, and a task window spanning 3–6s used to capture motor imagery-related activity.

Machine Learning Classification

To discriminate between different MI classes, efficient feature extraction and robust classification methods are required. Common Spatial Patterns (CSP) (70) is a widely used supervised spatial filtering technique that enhances class-discriminative oscillatory features by maximizing the variance for one class while minimizing it for another. In the case of three-class MI (left hand, right hand, foot), a one-vs-rest (OVR) strategy is typically employed to extend CSP to multiclass problems (181; 182).

Given multi-channel EEG data $\mathbf{X} \in \mathbb{R}^{C \times T}$ with C channels and T time samples, the class-specific spatial covariance matrix for class k is computed as

$$\mathbf{C}_k = \frac{\mathbf{X}_k \mathbf{X}_k^\top}{\mathrm{tr}(\mathbf{X}_k \mathbf{X}_k^\top)}, \tag{4.3}$$

where $\mathbf{X}_k$ denotes the EEG trials belonging to class k and $\mathrm{tr}(\cdot)$ is the matrix trace. For binary CSP, the composite covariance $\mathbf{C} = \mathbf{C}_1 + \mathbf{C}_2$ is used to solve the generalized eigenvalue problem:

$$\mathbf{C}_1 \mathbf{w} = \lambda \mathbf{C} \mathbf{w}, \tag{4.4}$$

where $\mathbf{w}$ are the spatial filters maximizing variance for one class, while minimizing it for the other. In the OVR setting, this procedure is repeated for each class (left, right, foot) against the pooled data from the remaining classes, yielding three sets of filters. The log-variance of the filtered signals is then

extracted as discriminative features:

$$f_i = \log\left(\frac{\mathrm{var}(\mathbf{w}_i^\top \mathbf{X})}{\sum_j \mathrm{var}(\mathbf{w}_j^\top \mathbf{X})}\right). \tag{4.5}$$

The extracted feature vectors are subsequently classified using a Support Vector Machine (SVM). For a given class k, the SVM solves the optimization problem

$$\min_{\mathbf{w},b,\xi} \quad \frac{1}{2}\|\mathbf{w}\|^2 + C\sum_{i=1}^{N}\xi_i \tag{4.6}$$

$$\text{s.t.} \quad y_i(\mathbf{w}^\top \phi(\mathbf{x}_i) + b) \geq 1 - \xi_i, \quad \xi_i \geq 0, \tag{4.7}$$

where $\mathbf{x}_i$ and $y_i \in \{-1, +1\}$ denote the training samples and labels for class k versus rest, $\phi(\cdot)$ is a kernel mapping, and C is the regularization parameter. The decision functions from the three OVR SVMs are combined, and the class with the maximum decision score is selected as the predicted label.

4.3 Results

4.3.1 Exoskeleton Walking Performance (n=18)

As mentioned in Section 4.2.1, to evaluate the impact of the exoskeleton-assisted training program, gait performance was quantified as steps per minute before and after 5 sessions of exoskeleton training (Week 0 and Week 4) and compared between the experimental and control groups.

Given the repeated-measures design, with steps per minute measured at two time points in the same participants, within-group changes were analyzed using paired statistical tests, while between-group comparisons involved independent groups. Normality of the steps-per-minute data was assessed using Shapiro–Wilk tests, with no violations observed (experimental group: Week 0, $p = 0.51$; Week 4, $p = 0.20$; control group: Week 0, $p = 0.27$; Week 4, $p = 0.95$). Therefore, parametric statistics were deemed appropriate, and non-parametric alternatives were not required.

At baseline (Week 0), the experimental group exhibited slightly higher step rates than the control group, averaging just above 30 steps per minute compared to the control group's approximately 27.5 steps per minute. The distribution of

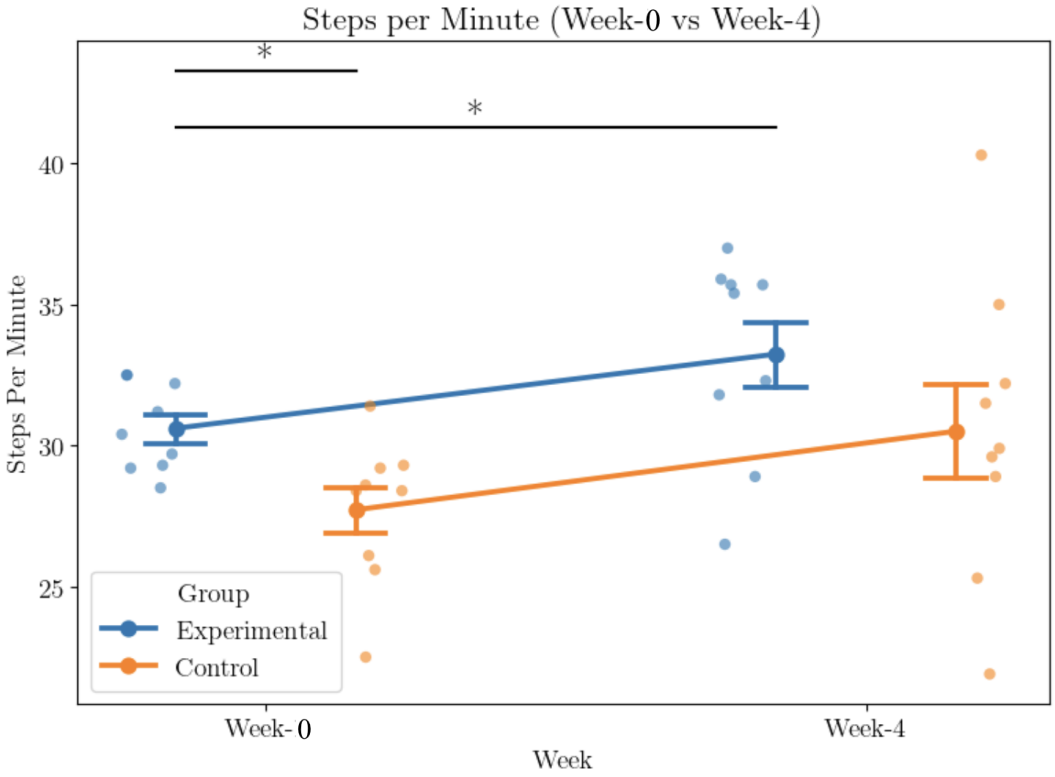

Figure 4.3: Average steps per minute at Week 0 and Week 4 for experimental and control groups. Error bars represent standard deviation. Observed differences are preliminary and exploratory.

change scores (Delta steps/min) is presented in Figure 4.4. The experimental group showed consistently higher delta values relative to the control group, with most participants demonstrating positive gains in walking speed over the course of the intervention.

These observations suggest that MI combined with exoskeleton training may be associated with greater improvements in gait performance; however, as this is a pilot study, results must be interpreted cautiously due to the small sample size, non-random group allocation, and baseline differences between groups. As shown in Figure 4.3, both groups improved in steps per minute from Week 0 to Week 4; however, between-group differences should be considered exploratory and preliminary, and may have been influenced by external factors due to the time difference between the collection of data between the 2 groups. While the experimental group demonstrated a greater average magnitude of improvement, the higher variability observed in the control group indicates that larger Delta steps/min values are not necessarily indicative of poorer performance and may

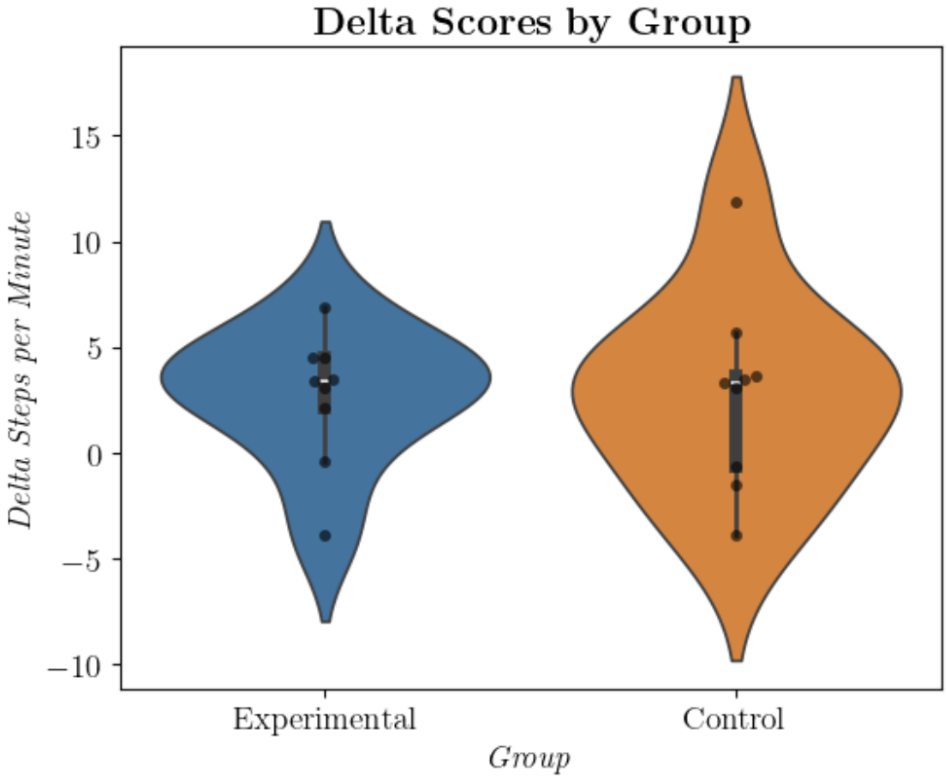

Figure 4.4: Distribution of change in steps per minute (Δ steps/min) for experimental and control groups. Positive values indicate improvement from Week 0 to Week 4. Observed differences are exploratory and should be interpreted cautiously.

reflect individual response differences. By Week 4, both groups improved, with the experimental group reaching an average above 33 steps per minute, while the control group increased more modestly to 30 steps per minute.

Paired t-tests were used to assess within-group longitudinal changes from Week 0 to Week 4. The experimental group showed a trend-level increase in steps per minute ($t(9) = -2.14$, $p = 0.061$), with a medium–large effect size (Cohen's $d_z = 0.68$), whereas the control group showed no statistically significant change ($t(9) = -1.50$, $p = 0.17$; $d_z = 0.47$). To control for multiple testing across the two within-group comparisons, a Bonferroni correction was applied (adjusted $\alpha = 0.025$), under which neither comparison reached statistical significance. Effect sizes were therefore reported to characterize the magnitude of observed changes in order to identify potential trends in the participants' responses.

4.3.2 Motor Imagery EEG (n=9)

ERD/ERS

ERD was used to evaluate two areas: (i) changes w.r.t. class (i.e. left/right and feet) for Week 0 and Week 4 before and after exoskeleton intervention, (ii) changes in motor area responsible for motor movement (primarily around channels C3,C4 and Cz) for Week 0 and Week 4, before and after exoskeleton intervention.

Analysis of ERD revealed clear improvements following the exoskeleton-assisted walking intervention. Across conditions, participants demonstrated stronger desynchronization after training, reflecting enhanced motor cortical engagement during imagined movements.

Short-term (within Week 0) changes: For the **foot** condition, ERD did not significantly change between before and after the first session (Week 0). For the **left hand**, ERD increased after the first training session (Week 0) with a small-to-moderate effect (d = 0.42), suggesting heightened cortical activation. However, at Week 4, no significant short-term (within-session) changes were detected. For the **right hand**, a similar pattern was observed: ERD increased after the first session (d = 0.38), while Week 4 showed no clear short-term effect.

Long-term (across 5 sessions): The **foot** condition showed the clearest long-term improvement. ERD magnitude increased from before Week 0 to before Week 4 with a moderate effect size (d = 0.49, mean difference = +0.20, 95% CI: -0.05–0.45), indicating progressive strengthening of motor cortex desynchronization over the intervention period. The **left hand** condition showed a decreasing trend from after Week 0 to Week 4 (d = -0.54, mean difference = -0.23, 95% CI: -0.55–0.09), although this did not reach significance. The **right hand** condition did not demonstrate significant long-term changes (d values close to zero).

Topographical perspective: At the electrode level (C3, C4, Cz), group-level analysis showed a significant strengthening of ERD/ERS from after Week 0 to after Week 4, particularly at C3 and C4 ($p < 0.05$, paired t-test). This supports increased motor cortex involvement following repeated exoskeleton-assisted walking.

The positive ERD values in Figure 4.6 arise from the log-ratio definition used, where values closer to zero or positive can still reflect reduced desynchro-

nization rather than true ERS. The group-level shift toward positive values is further influenced by inter-individual variability and mixed ERD/ERS responses. Additionally, the long task window (3–6s) may dilute early ERD and pull the averaged values upward, making the grand-average appear less negative despite clear ERD in individual traces.

Overall for the ERD results, the most consistent and robust long-term ERD enhancement was observed for the foot condition, while hand-related ERD effects were present acutely (after Week 0) but not sustained over the longer training period. Channel-level analysis confirmed that repeated training enhanced desynchronization in motor cortical areas, particularly contralateral to the trained movement.

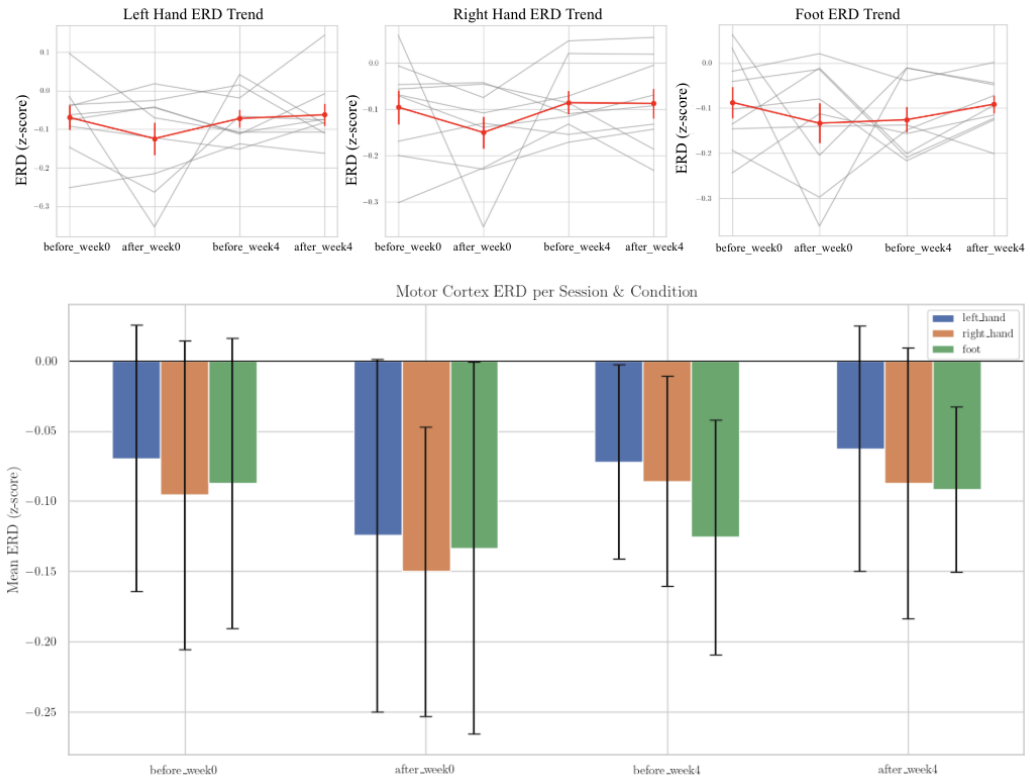

Figure 4.5: Mean ERD z-score for Left, Right and Feet Motor Imagery along with their trends for Week 0 and Week 4, before and after exoskeleton intervention

Machine Learning Classification

The analysis of the experimental group's MI classification performance before and after exoskeleton-assisted walking is demonstrated using Fig.4.7,4.8.

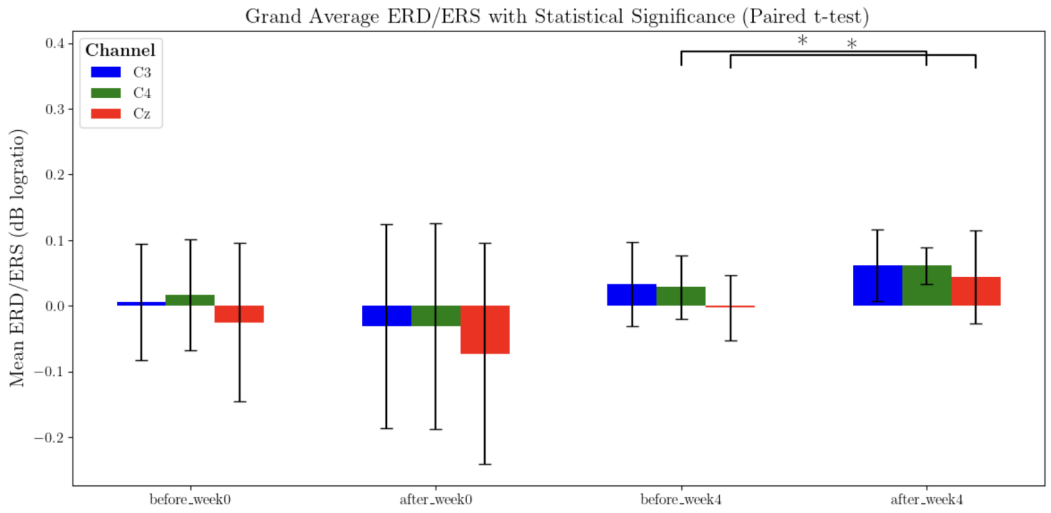

Figure 4.6: Mean ERD/ERS values for channel C3, Cz and C4 for Week 0 and Week 4, before and after exoskeleton intervention

The majority of participants fall within the limits of agreement, suggesting a relatively stable decoding performance across sessions. However, certain individuals (e.g., p10 and p12) deviate more strongly, pointing toward heterogeneous responses to the intervention. The aggregated OVR accuracies by session and target (Figure 4.8) reinforce this interpretation. Across the four time points, mean accuracies remain around 55–60% for all MI classes (foot, left hand, right hand), with standard deviations overlapping across conditions, suggesting no significant group-level gain in classification following exoskeleton use. Nevertheless, class-specific patterns emerge: left-hand imagery shows a slight upward trend after both interventions (Week 0 and Week 4), while foot imagery displays a small decline at after Week 4, hinting that certain MI classes may interact differently with the exoskeleton training. At the participant level (Figure 4.7), performance variability becomes more evident. Some participants, such as p02, p05, and p07, demonstrate noticeable improvements after exoskeleton sessions, while others (e.g., p06, p10) exhibit inconsistent or even reduced accuracies. Importantly, most participants maintain accuracies in the 55–65% range, which is above chance but still reflects the well-known challenge of inter-subject variability in MI-BCI performance.

Taken together, these results suggest that while the exoskeleton intervention did not produce a uniform accuracy improvement across the experimental group, it may have facilitated subtle class-specific or individual-level benefits.

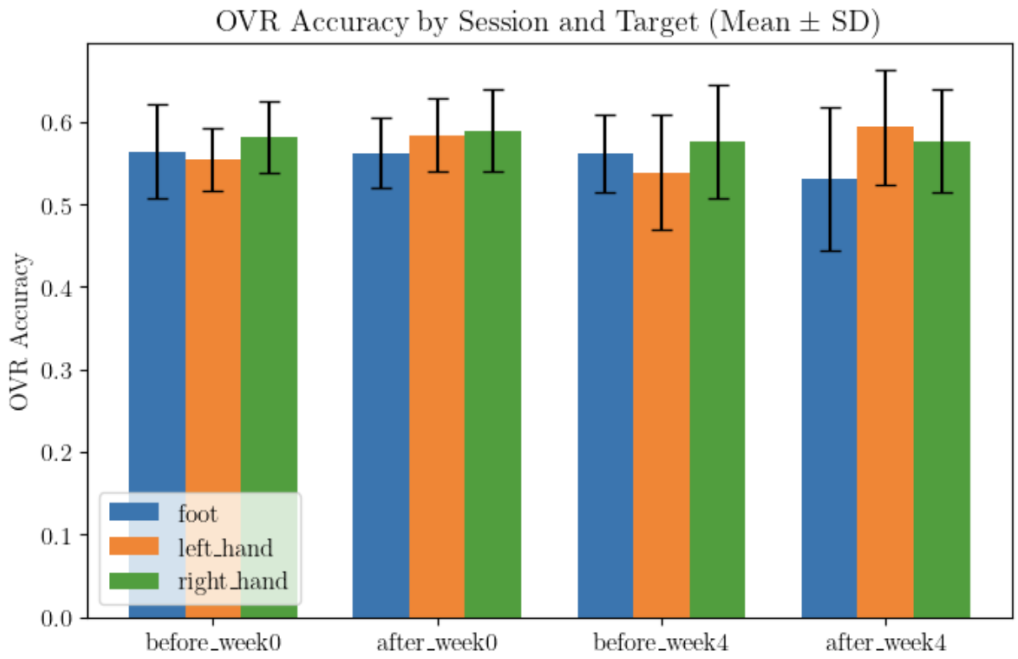

Figure 4.7: Grand Average OVR Accuracies per week w.r.t. condition(Feet, Left Hand, Right Hand)

4.4 Discussion

In a subset of analysis (n=9), strengthening of ERD was observed following both short-term (1-session) and longer-term (5-sessions over 5 weeks) training, indicating increased involvement of contralateral motor areas after exoskeleton training.

The present findings indicate that exoskeleton-assisted training elicited both neurophysiological and behavioral benefits in the experimental group. On the neural level, ERD increased after training, particularly for the foot condition, where a moderate strengthening of desynchronization was observed over the intervention period. These changes suggest enhanced recruitment of motor cortical areas and reflect short-term plasticity in response to repeated practice. Similar, though smaller, improvements were also evident for hand motor imagery immediately following training sessions, highlighting the sensitivity of upper-limb cortical networks to exoskeleton exposure.

However, it is important to note that post-session Week 4 ERD results for the foot condition did not show the same clear short-term increase observed at Week 0. It is important to note these weaker post-session effects to evaluate

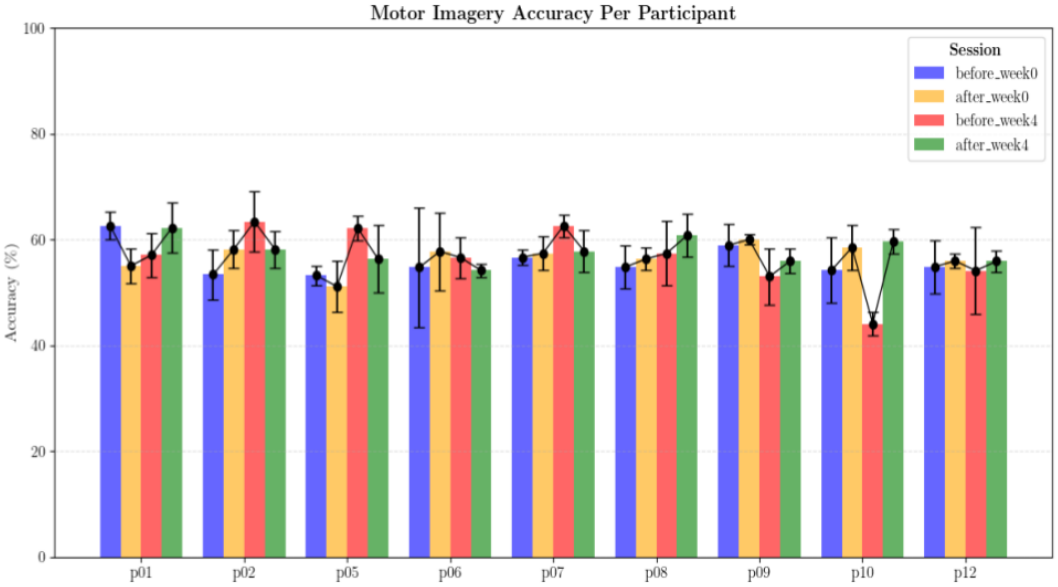

Figure 4.8: Grand Average OVR Accuracies per participant along with trends for Week 0 and Week 4

the overall training-related changes. Although long-term strengthening was evident when comparing pre Week 0 to pre Week 4, the immediate post Week 4 responses were more variable and in some cases attenuated. This suggests that the intervention may have produced modest but non-linear changes rather than uniformly increasing ERD across all sessions.

Taken together, these results demonstrate a convergence between neural markers of motor cortical engagement (ERD) and exoskeleton walking performance outcomes. The strengthening of motor imagery–related desynchronization, particularly for the foot, in parallel with the observed improvements in step rate, suggests that the exoskeleton training may enhance walking performance and also reinforce cortical representations of movement. From this preliminary work, the combination of exoskeleton-assisted intervention along with MI as a rehabilitation approach may improve training effects and thereby the exoskeleton walking performance.

Short-term changes With regards to the short-term (within session), significant strengthening was seen in both upper and lower limb conditions. These early changes point to short-term neurophysiological adaptations triggered by the training.

In terms of changes in upper limb motor imagery (left and right hand conditions), significant ERD strengthening was seen at session 1 (week 0) but

not at session 5 (week 4). In contrast, for the lower limbs (foot condition), significant strengthening was seen at session 5 (week 4) but not at session 1 (week 0). The shift in ERD strengthening from the upper to the lower limbs over the course of the intervention may be explained by the impact of the exoskeleton training sessions. Given that individuals with spinal cord injury predominantly rely on their upper limbs, this initial neural connection is reflected in the motor imagery findings in session 1.

Long-term changes After 5 sessions of exoskeleton training (Week 0 - Week 4), ERD magnitude increased (+0.20), reflecting a progressive strengthening of motor cortex desynchronization over the four weeks of training. Importantly, this suggests that repeated exposure to exoskeleton-assisted walking may have reinforced foot-related cortical representations, which are often more difficult to modulate in motor imagery tasks. Both Situations give rise to the ability to plan, improve, and execute movement.

However, the long-term increase should be interpreted alongside the more variable post Week 4 effects. The combination of a moderate pre–post long-term gain with weaker immediate post-session responses suggests that cortical changes may have stabilized or plateaued by the final week. While the results are encouraging, the limited sample size and study duration prevent definitive conclusions and warrant further investigation with larger cohorts and longer follow-up periods.

4.5 Summary

This study investigated the combined effects of MI and exoskeleton-assisted walking in individuals with SCI, focusing on both behavioral and neurophysiological outcomes during exoskeleton intervention.

Exoskeleton Walking Performance (n=18): From Week 0 to Week 4, the experimental group increased their average step rate from 30 steps/min to >33 steps/min, compared to the control group's more modest gain from 27.5 to 30 steps/min.

Motor Imagery EEG (n=9): ERD analysis revealed condition- and session-specific effects. In the short-term, ERD strengthened for left (d = 0.42) and right (d = 0.38) hand imagery immediately after the first training session (Week 0). Over the longer term, the foot condition demonstrated the clearest enhancement, with ERD magnitude increasing across 5 sessions (d = 0.49,

mean difference = +0.20), particularly at contra-lateral motor sites (C3, C4; $p < 0.05$). These findings indicate progressive strengthening of motor cortical desynchronization associated with repeated exoskeleton-assisted practice.

Despite the long-term effects observed, the post-session Week 4 ERD responses showed weaker or more variable short-term effects compared to Week 0. These effects need to be considered as part of the overall evaluation of the effect of the exoskeleton training intervention. The combined pattern—moderate long-term gains but weaker immediate post Week 4 responses—suggests that cortical adaptation may taper or plateau toward the end of the intervention.

Classification Performance: Machine learning analyses yielded stable decoding across sessions, with mean OVR accuracies in the 55–60% range for all MI classes with negligible systematic change between pre- and post-sessions (Week 0 mean difference = –0.008; Week 4 = –0.012), though individual variability was pronounced. Certain participants (e.g., p02, p05, p07) demonstrated improvements, while others (e.g., p06, p10) showed inconsistent performance.

Taken together, these preliminary results suggest that the exoskeleton-assisted walking intervention combined with MI improved steps/min performance and also enhanced ERD, more notably for foot MI. While classification accuracies remained stable at the group level, individual- and class-specific trends point toward heterogeneous responses to the intervention. Further investigation is needed over a longer time period with more subjects to consider the neural changes throughout the intervention given the stronger long-term foot ERD increases and the weaker post-session Week 4 effects.

Chapter 5

User Training

"“Try Again. Fail Again. Fail Better.” -(Samuel Beckett). For me, it’s a reminder that failure is also success, because it means you dared to attempt hard things."

- Dr. Cosimo Della Santina

RQ 2: User Training Optimization *Does the medium of instruction (visual, auditory, or immersive VR) influence motor imagery skill acquisition and BCI performance?*

Significance: Effective user training is a critical bottleneck in translating MI-BCIs to real-world use. Optimizing instructional methods can improve MI signal quality, accelerate learning, enhance engagement, and reduce cognitive fatigue. This is particularly relevant for both rehabilitation and general-purpose ADL applications, where user motivation and rapid skill acquisition directly impact adoption.

Expected Outcomes: Enhanced MI signal clarity, improved online control accuracy, and increased participant motivation.

Testing and Validation: Controlled experiments comparing performance and neurophysiological markers across different instructional modalities.

As discussed in Section 3.2, MI training plays a significant role in clinical applications involving rehabilitation (183). Although MI-BCI systems are considered intuitive, i.e., no external stimuli are required, these signals require extensive training in the imagination of limb movements. For instance, to enhance MI signals, training typically involves a set of instructions on a screen to imagine the movement of the left or right hand. One of the most popular setups is the Graz MI paradigm (22) that is widely used in BCI research, and has been proven effective in providing precise temporal boundaries for experimental paradigms.

The most common approach to motor imagery (MI) training relies on visual, yet alternative mediums—such as auditory, haptic, or immersive feedback—offer promising advantages for engagement and learning. With the training required for MI, there are possibilities of having instructions over different mediums; for example, the work of Varona et al. (1) tested the feasibility of two-class MI using audio cues for wheelchair navigation. Velasco et al. (184) provide an audio-based navigation paradigm to operate a wheelchair in two scenarios, where the user switches from a graphical to an audio-cued interface and real-world environment. Audio-based scripts for instructions have also been used for kinesthetic MI training in Parkinson's disease (36). Recent trends suggest enhancement of MI signals when cues are presented in VR headsets, making the process of imagination interactive(94; 12; 34; 92; 185; 186). Choi et al. (12) compare the possibility of enhancement of MI signals when the cues were presented in VR in comparison to the screen. These studies emphasise the significance of the training requirements for MI. Training requirements must take into account a variety of factors including training instructions (187), feedback (188; 64; 189), and also possibly the medium in which the instructions are presented Although the medium of instruction has been explored, there has been no distinct comparison of the influence of possible mediums on MI signals. Also, having feedback-integrated MI signals can enhance the experience of the participant (64), which can possibly create a bias during comparison.

By only changing the medium of instruction and keeping training constant across mediums, this study explores the concept of engaging participants in MI tasks without explicit feedback, instead relying on their own subjective assessments of performance—an approach that offers an intriguing perspective on self-perceived engagement and motor imagery ability. The significance lies in exploring the cognitive aspects of MI, where participants, lacking external

feedback, must rely on their internal representations and self-perceptions. This approach allows the examination of the interplay between subjective judgments and neural activity during MI. By probing participants on their perceived performance, the study not only delves into the accuracy of self-assessment without external cues but also sheds light on potential discrepancies between subjective evaluations and objective measures. Understanding how individuals gauge their own performance during MI tasks can offer valuable insights into the cognitive processes underlying this mental simulation, contributing to the broader debate on self-awareness and metacognition in the context of motor cognition research. Additionally, the findings may have implications for the design of MI interventions or neurofeedback approaches, emphasising the importance of aligning participants' subjective experiences with neurophysiological responses for more effective applications in fields such as sports training or neurorehabilitation.

Consequently, a comparison with no feedback may be used to determine whether the medium of instruction influences MI signals. A thorough study of specific mediums will contribute towards the design of MI-BCI rehabilitation systems based on user preferences and performance. The purpose of this study is to compare the MI signals when instructions are presented by three different mediums. - VR headsets, screens and audio. In order to assess the efficacy of each medium, the hypothesis is tested by evaluating performance using multiple criteria, i.e., exploring ERD/S, Machine Learning, statistics, and questionnaires.

The contributions from this chapter are:

1. To conduct an extensive user study to examine the impact of varied cue presentation mediums, specifically considering their relevance to ADL and MI training.

2. To perform qualitative and quantitative analysis to ascertain user preferences and validate the hypothesis through diverse evaluation metrics.

3. To perform analysis based only on three channels to minimise the number of electrodes, in order to promote MI-BCI training in ADL, which would be more feasible for a real-world implementation.

5.1 Methodology

5.1.1 Pilot Study

A preliminary pilot study was conducted to evaluate the feasibility of the designed protocol and to estimate the expected effect size for sample size determination. The pilot involved presenting motor imagery (MI) cues through three different modalities—computer screen, virtual reality (VR) headset, and auditory speakers—to compare their influence on MI-related brain activity. Power spectral features were extracted from the alpha and beta frequency bands, and a one-way ANOVA was performed to assess differences in mean power across the three cueing conditions. This analysis yielded a large effect size ($\eta^2 = 0.895$), indicating substantial variation between modalities.

Using this effect size, the required number of participants for the main study was estimated with G*Power, setting the significance level (α) at 0.05 and the desired power ($1 - \beta$) at 0.9 for a one-way ANOVA with three groups. The calculation suggested a minimum of 21 participants to achieve sufficient statistical power. To account for potential attrition, an additional 10% was added to the target sample size, ensuring the robustness and reliability of the final dataset.

5.1.2 Participants

A total of 21 healthy individuals (12 males and 9 females, age = 28±5) were invited to participate in a study conducted in a comfortable room. The participants were briefed on the experimental procedures and were given a clear understanding of what their involvement would entail. Following this explanation, each participant provided written consent, indicating their voluntary agreement to participate in the experiment. To ensure the ethical standards of the study, prior approval was obtained from the Research Ethics Committee at Dublin City University (DCU). The committee carefully evaluated the research protocol, considering various ethical aspects such as participant welfare, informed consent procedures, confidentiality, and potential risks or benefits associated with the study. Upon review, the committee granted ethical approval, affirming that the research was conducted in accordance with established ethical guidelines.

5.1.3 Experimental Protocol

The study incorporated three distinct mediums for presenting cues: visual cues on a computer screen, audio cues over speakers, and immersive cues through VR headsets. Each medium consisted of two runs, and each run lasted for approximately 7 minutes. Following every two runs, before the protocol changed to a different medium, participants were given a short break of 2-3 minutes to ensure their comfort and reduce fatigue. During each run, participants were exposed to a total of 40 events, with 20 left-hand cues/commands and 20 right-hand cues/commands presented randomly. To control the temporal aspects of the experiment, each event was presented within a fixed time window of 9 seconds, as per the Graz paradigm. In each event, the cue is presented at the 4th second, and the participant is asked to rest at the 6th second. Data collection was conducted across six runs, encompassing all three scenarios for each participant. This comprehensive approach allowed for a thorough investigation of the impact of different mediums on cue perception and response. Over the course of the entire experiment, each participant was exposed to 80 cues presented on the computer screen, 80 auditory cues delivered over the speakers, and 80 immersive visual cues experienced through the VR headsets. From the participant's perspective, a black screen appears for the immersive and visual cues at 0s, and both hands appear for the immersive and visual cues and beep for auditory cues at 1s. Random left- or right-hand instructions appear at 4s for immersive and visual cues, and a synthetic voice commands random left/right for auditory cues. Similarly, both hands appear for the immersive and visual cues; beep for auditory cues at 6s; black screen appears for the immersive and visual cues at 9s. This process repeats 40 times, comprising 40 events per run.

Three scenarios were evaluated where the cues were presented by either a screen, audio, or a VR headset.

1. Scenario 1: The only active medium is the screen, and the participants were asked to follow the instructions on the screen while the Graz BCI paradigm in OpenVibe was used to collect data.

2. Scenario 2: The only active medium is VR, and the participants were asked to wear VR headsets and follow the cues that appeared in the headsets. In this scenario, the instructions and the cues were designed as a video for Meta Quest 2.

3. Scenario 3: The only active medium is the speakers, and the participants were asked to follow the auditory instructions and cues provided by the speakers. Here, the instructions were designed with the help of synthetic voice makers, i.e., converting text to audio.

The participants had cues presented in these scenarios one after the other, with a break after every scenario. These three scenarios were followed sequentially for every participant using the William Square method (190) to eliminate as much learning effect as possible. The possible scenarios in sequence are Scenario 1,2,3, Scenario 2,3,1 and Scenario 3,1,2, where the 21 participants followed this sequence, resulting in 7 participants involved in every sequential order. The Experimental protocol can be seen in Fig. 5.1

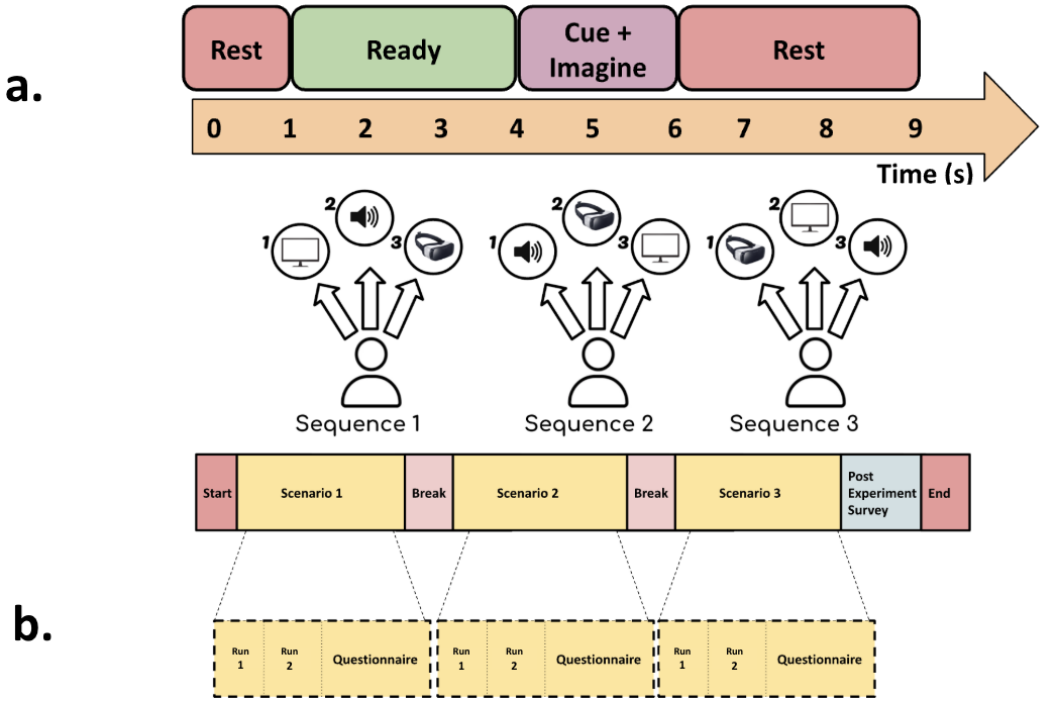

Figure 5.1: Experiment protocol, a. represents one single event of Graz-BCI Motor Imagery where random left or right-hand instruction appears at 4s for the immersive and visual cues, a synthetic voice that commands left/right for auditory cues. This process repeats 40 times, comprising 40 events per run. Where b. Two runs per medium are designed using William Latin square, and questionnaires follow post Scenarios.

5.1.4 Tools used

EEG device and recording:

The FlexEEG Neuroconcise device (191; 192) was used to collect the data. The device was further linked with OpenVibe software using the Lab Streaming Layer (LSL), where the data was recorded, and cues were presented. The sampling frequency was set to 250 Hz. Electrode impedance was not checked during EEG data collection since the equipment does not support the feature. Instead, the data was visually inspected for artefacts, following the protocol directed in the manual, which included testing jaw clenching, eye blinks, etc., before collecting the data. The conductive gel was used to ensure low contact impedance and high stability at the scalp interface. While impedance checking is generally recommended to ensure the highest quality data, these measures taken ensured the reliability of the results. The EEG system is a bipolar system containing seven electrodes, FC3-CP3, FCz-CPz, FC4-CP4 and the bias AFz as ground (Fig. 5.2). Later, data processing employed artefact removal techniques such as Independent Component Analysis(ICA) and bandpass filtering to remove the aforementioned artefacts. The EEG recordings were further processed using a bandpass filter between 7-38 Hz and saved.

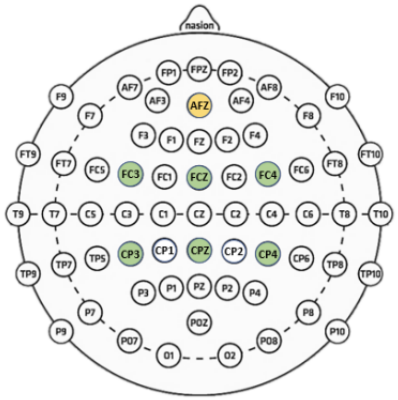

Figure 5.2: Electrode placement for the study, using a bipolar channel system where Afz is biased and the 3-channel system comprises FC3-CP3, FCz-CPz, FC4-CP4 inspired by (191).

Questionnaires:

In order to support the study, every participant was requested to answer a set of questionnaires after performing MI training in each medium and after

completing the entire experiment, followed by a post-experiment survey with a questionnaire and feedback about the entire experiment and preferences.

5.2 Evaluation Matrix

This section describes the different evaluation methods used to analyse the collected data and test the hypothesis. A robust evaluation is performed on the signal processing and machine learning techniques, along with the user study.

5.2.1 Motor Imagery EEG data

Event-Related Synchronization/Desynchronization:

Initially, to explore the data, the alpha band was examined. The focus was on the mean power of 21 participants over time. This data was plotted for a specific time window, between 3.0 and 6.0 seconds, as illustrated in Figure 5.4. This exploration aimed to understand the behaviour and variations of mean power within this time frame, providing insights into the collective neural activity of the participants during the specified interval. The graphical representation in Figure 5.4 serves as a visual summary of the average alpha power dynamics over the chosen period, identifying the underlying patterns and trends present across the different medium used to give instructions - Screen, VR, and Audio. Later, ERD/ERS were performed to understand the statistical significance of the collected data.

Although CSP is widely used in the motor imagery literature for extracting spatially discriminative features (21), it was not employed in this study because the focus was on understanding the ERD/ERS response. ERD/ERS (179; 180) is a phenomenon observed in EEG signals that reflects changes in neural oscillatory activity during cognitive and motor processes. ERS refers to an increase in power or synchronization of neural oscillations, typically in the alpha or beta frequency bands, while ERD signifies a decrease in power or desynchronisation. These dynamic modulations in neural oscillations are associated with various cognitive functions, such as attention, perception, and motor planning. Researchers use ERS/ERD analysis to investigate the temporal dynamics of brain activity in response to external stimuli or tasks, providing insights into the neural mechanisms underlying complex cognitive processes. Examining

ERS/ERD patterns contributes to the understanding of brain function and has applications in fields ranging from neuroscience to neurorehabilitation.

ERD/ERS from the electrodes C4 and C3 placed over the motor cortex are studied for analysis. These ratios are calculated, keeping the baseline as a reference. These can be further explained by equation 1:

$$ERD/ERS\% = \frac{1}{n}\sum_{e,f}^{n}(\frac{P_{event} - P_{baseline}}{P_{baseline}}) \times 100$$

Where,

e represents left or right;

n: total number of epochs;

f: over the frequency bands;

P_{event}: PSD from the time when the cue is presented;

$P_{baseline}$: PSD, when the participant is at rest state, i.e., no event is happening (180).

The average ERD/ERS has been calculated by finding the average of these ratios across all the epochs for left, and right-hand MI signals over the alpha and beta bands, respectively.

ERD/ERS was computed using a baseline of -1s immediately before the cue at 4s, and averaged over the 4–6 s interval across all epochs and all mediums. Finally, the average ERD/ERS ratios, i.e., amplitude plots of ERD/ERS over a range of frequencies for electrodes C3 and C4, have been calculated and plotted for left and right-hand MI signals, respectively, over the time period of 7s when cues were presented in three different mediums at the 4th second.

Feature Extraction and Machine Learning

For the data in each medium for all the participants, statistical and spectral features were extracted where frequency analysis involved computing the Power Spectral Density (PSD) (193) within the alpha and beta band (8-30 Hz) for each channel, providing insights into the spectral characteristics associated with MI. Additionally, statistical features, including mean, variance, and skewness, were computed for each channel, offering a multi-faceted representation of the EEG data.

For the machine learning classification, an AdaBoost classifier was used as it effectively combines multiple weak learners to improve accuracy and reduce

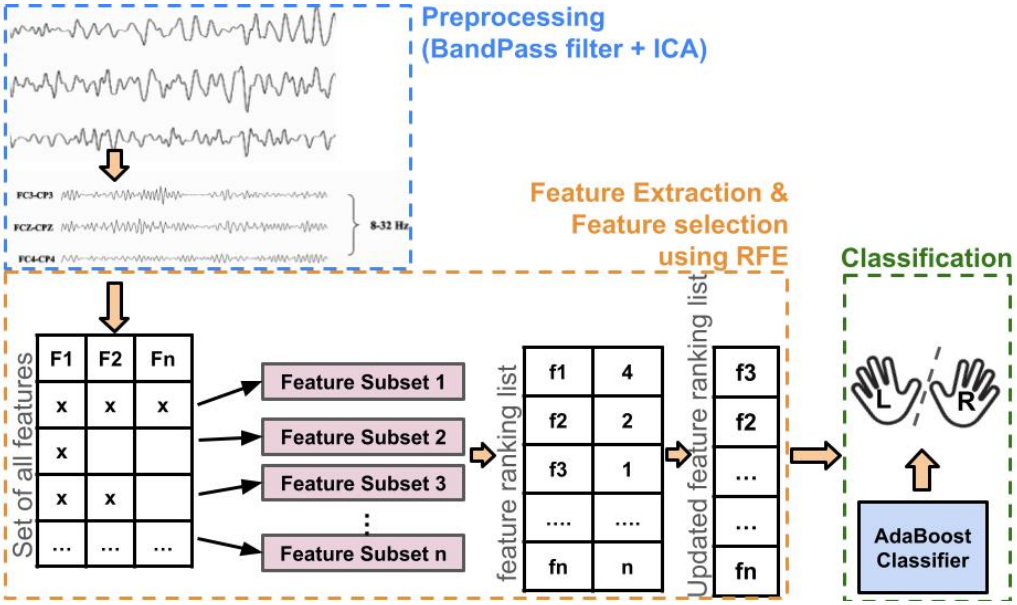

Figure 5.3: Machine Learning Pipeline using Recursive Feature Elimination(RFE) and AdaBoost for left and right-hand classification, with number of features selected as n=5; and cv = 10

overfitting (186; 194), leveraging its ensemble learning capabilities to enhance classification performance. Feature selection was carried out using Recursive Feature Elimination (RFE) with n=5, a technique that systematically identified and retained the most relevant features for classification. The robustness of the model was evaluated using Stratified k-fold cross-validation of 10x10, ensuring an unbiased assessment of classifier performance across different subsets of the dataset. The pipeline can be seen in Fig. 5.3

In the evaluation and results presentation, mean cross-validation accuracy scores were utilised as the primary performance metric to quantify the classification accuracy of the AdaBoost model. The mean accuracy and standard deviation across folds were computed for each participant, providing a comprehensive overview of the classifier's consistency and generalisation of performance across multiple iterations. These evaluation steps contribute to a thorough understanding of the model's effectiveness in discerning MI patterns from EEG data, laying the foundation for insightful interpretations and comparisons across participants.

5.2.2 Questionnaire

A questionnaire adapted from NASA-Task Load Index (TLX) (195) was employed to gauge the mental workload following MI runs in each medium. After completing runs across the three scenarios, participants were tasked with filling out a survey to evaluate their self-perceived performance in each medium. The survey together encompassed inquiries about their focus, stress levels, engagement, understanding of experimental procedures, and ease of comprehension. Additionally, participants provided insights on their preferred medium for receiving instructions, perceived attentiveness, and interactivity. The questionnaire also covered feedback on the experimental setup, and to understand their choice among the three mediums. The post-experiment questionnaire included the following questions:

1. What has been the most feasible/comfortable medium for presenting the instructions?
2. Instructions in which medium have made you feel more attentive while imagining hand movements?
3. Instructions in which medium made you feel more interactive?
4. Instructions in which medium would you recommend?

5.3 Results

5.3.1 Motor Imagery EEG

Event Related Synchronization Desynchronization:

In Fig. 5.4, representing the Alpha wave analysis during cumulative left and right Motor Imagery over time, participants display the strongest Alpha activity when cues are presented in the VR medium. The Alpha activity strength was highest for VR, followed by audio, and then screen.

Subsequently, in Fig. 5.5, illustrating cumulative ERD/ERS results over time for right-hand and left-hand MI using the dominant channels FC3-CP3 and FC4-CP4, participants consistently perform at their best when cues are presented in the VR medium. Following VR, audio is the next preferred

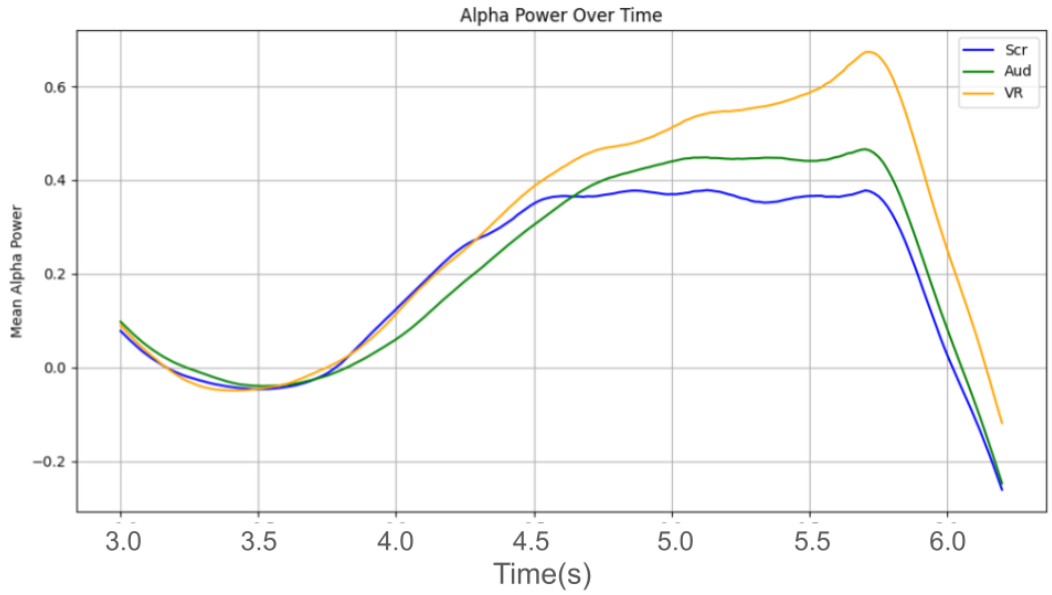

Figure 5.4: Representation of mean power (microvolts squared per Hertz) of the Alpha band over time for the different mediums of cue presentation

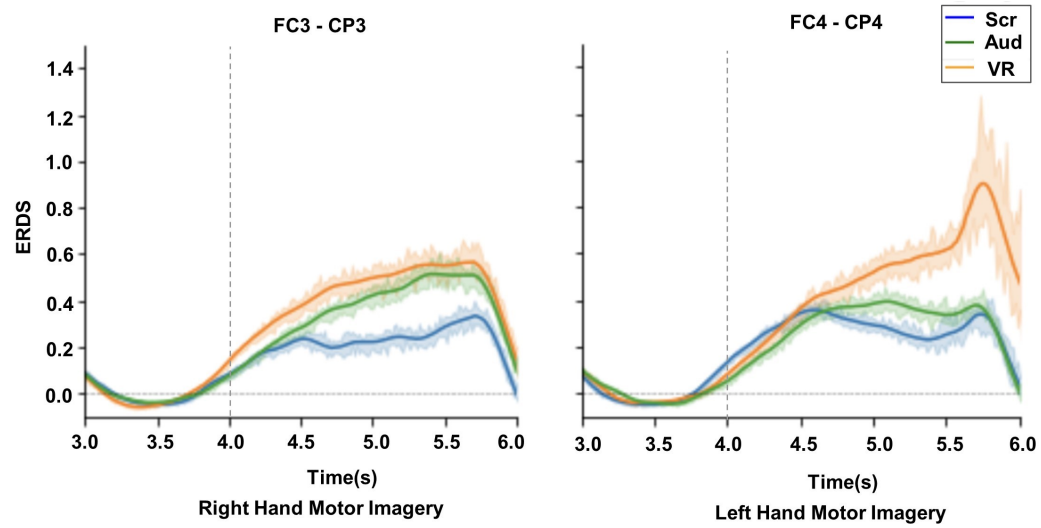

Figure 5.5: Event Related Synchronization/De-Synchronization for Left and Right Hand Motor Imagery Signals; where FC3-CP3 represents the dominant channel for Right Hand motor imagery and FC4-CP4 represents the dominant channel for Left Hand Motor Imagery

medium, with the screen observed as the least favoured, indicating a consistent trend across both Alpha and ERD/ERS analyses.

One-way ANOVA was applied to the mean ERD/ERS values over a time interval from 4.5 to 6 seconds across the three scenarios (audio, screen, and VR). This approach allowed for a comprehensive analysis of the ERD/ERS values within the specified time window, providing a robust comparison of the different mediums of instruction. The F-statistic was calculated to be 11.7193, with a corresponding p-value of 1.0168×10^{-5}, signifying a statistically significant difference among the group means. When the statistical significance of $p<0.05$ was observed, a Tukey Honestly Significant Difference (HSD) post hoc test was employed to identify specific pairwise differences and to understand the statistical significance with groups such as VR-Audio, VR-Screen, and Screen-Audio as demonstrated in Table 5.1.

The results of statistical significance by One-way ANOVA and Tukey HSD test, i.e., the comparison between the *audio* and *screen* groups, revealed a mean difference of -0.0194 with a non-significant p-adj value of 0.6323, suggesting no statistically significant distinction between these two groups. Conversely, the comparisons of *audio* vs *VR* and *screen* vs *VR* exhibited mean differences of 0.0776 and 0.097, respectively, both accompanied by significantly low p-adj values (0.0008 and 0.0). These outcomes indicate a notable dissimilarity between the *audio* group and both the *VR* and *screen* groups. Overall, the one-way ANOVA and Tukey HSD analyses collectively support the presence of significant differences in MI signals when cues are presented in different mediums of instruction.

Machine Learning

Fig. 5.6 illustrates a detailed description of subject-wise accuracies obtained from machine learning classification, as described in 5.2.1, when cues were presented through different mediums of instruction. The dot in the figure represents mean accuracies derived from cross-fold validation, while the error bars convey the corresponding standard errors (5.6.a).

Upon analysis, the average cross-validation accuracy across all participants (mean $\pm$ standard error) was 69.24 ± 3.12 when the medium of instruction was VR. For audio-based instruction, the accuracy was 68.69 ± 3.3, and for screen-based instruction, the accuracy was 66.1 ± 2.59, as illustrated in Fig. 5.6. Given

that this is a 2-class MI task with a theoretical chance level of 50%, these values indicate above-chance performance across all three media. However, differences between VR, audio, and screen accuracies were not statistically significant. With approximately 80 trials per medium, these accuracies should be interpreted as feasibility evidence rather than strong proof that VR dramatically improves classification.

Fig. 5.6.a illustrates the average cross-validation accuracy of motor imagery tasks across three different mediums: screen, audio, and VR. The accuracy values fluctuate over the 21 participants, with variations observed within each medium. The accuracies range from approximately 55 to 75, indicating variability in task performance across participants and mediums.

Fig. 5.6.b demonstrates the paired comparison of mean accuracy distributions between different mediums, with each medium's distribution depicted via violin plots. For the audio medium, the distribution appears relatively symmetrical with a slight peak around the median, suggesting a moderate concentration of accuracy values around the central tendency. In contrast, the screen medium's distribution exhibits a broader and flatter profile, indicating a wider spread of accuracy values and potentially greater variability in task performance. The VR medium, in turn, displays a more pronounced peak and narrower shape compared to audio, suggesting a higher concentration of accuracy values around the central tendency and more consistent task performance within this medium. These descriptive differences, however, did not reach statistical significance.

In comparison, a VR-based MI-BCI system on three channels with feedback exhibits average accuracies of 71.8 (193) and 66 (196), while the approach for training without feedback in this study demonstrates an accuracy of 69.24.

It is important to note that the relatively modest accuracies of the machine learning algorithms reflect the limited amount of data (80 events per medium). Care was taken not to increase the runs to avoid mental fatigue, as participants underwent training in three different media. Thus, the observed accuracies should be viewed as preliminary indicators of feasibility rather than conclusive evidence of medium-dependent performance advantages.

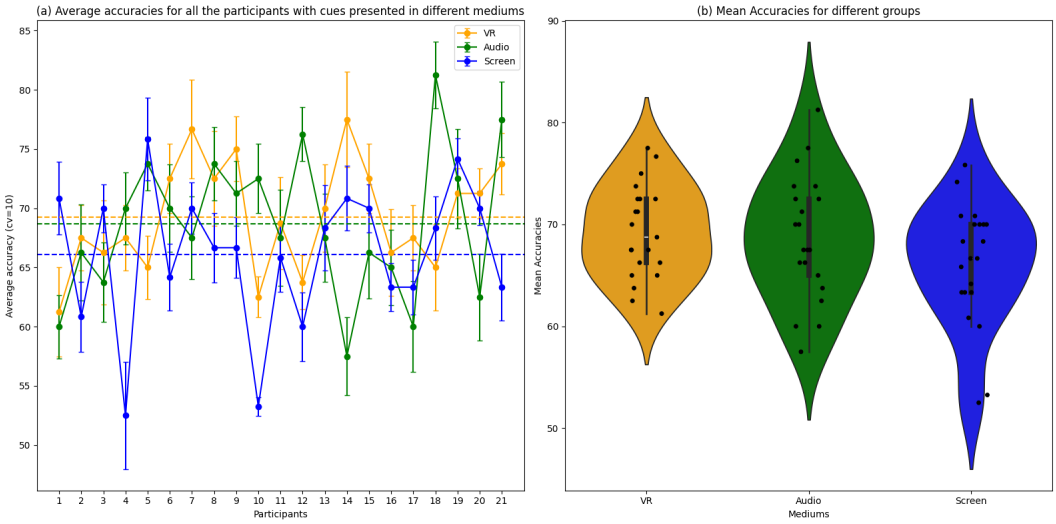

Figure 5.6: Machine learning subject-specific mean cross-validation accuracies (Mean ± Std. Error; $cv = 10$) across different mediums: (a) Average of cross-validation accuracy across participants and mediums, (b) Paired comparison of mean accuracy distribution across Screen, Audio, and VR mediums.

Table 5.1: ANOVA and Tukey HSD Results for comparing mean ERD/ERS power values with statistical significance of p<0.05

Comparison	ANOVA		Tukey HSD	
	F-statistic	p-value	Mean Difference	p-adj
Audio vs. Screen			-0.0194	0.6323
Audio vs. VR	11.7193	1.0168e-05	0.0776	0.0008
Screen vs. VR			0.097	0.0

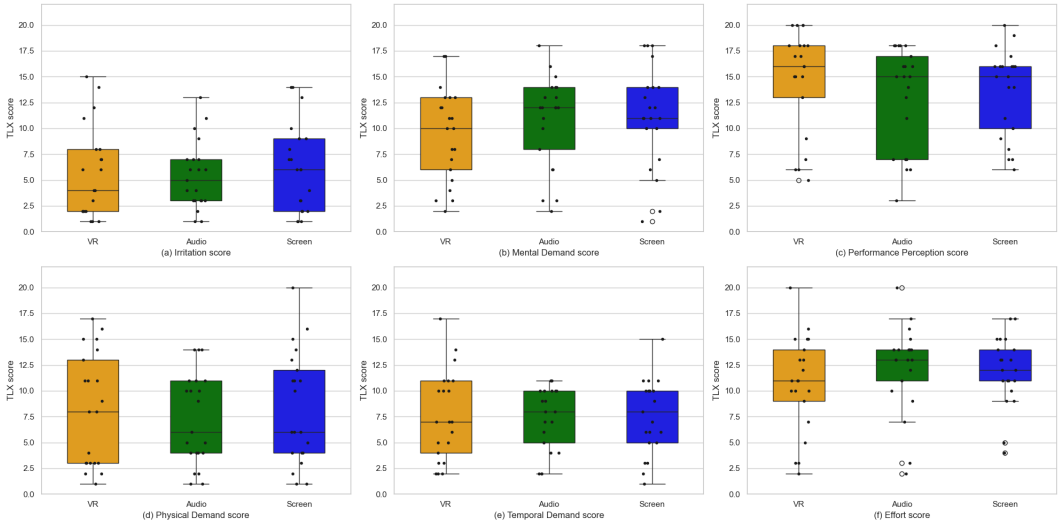

Figure 5.7: NASA-TLX Scores from 21 participants for (a) Irritation, (b) Mental Demand,(c) Performance Perception, (d) Physical Demand, (e) Temporal Demand and (f) Effort

5.3.2 Questionnaire Data Analysis

After analysing the responses gathered from 21 participants through post-experimental questionnaires (Section 5.1.4) and NASA-TLX scores, a distinct pattern emerged in their preferences for different mediums of instruction. Although no statistically significant differences were found ($p > 0.05$), exploratory trends suggest varying preferences across participants.

Among the participants (Table 5.2), 11 individuals showed a strong inclination towards VR as their preferred medium for receiving instructions. The immersive and interactive nature of VR resonates with these participants. Conversely, 6 participants leaned towards audio-based instruction, highlighting the significance of auditory experiences. This preference suggests an appreciation for learning through audio, which may be beneficial in scenarios where visual or hands-on engagement is challenging. Interestingly, 4 participants expressed a preference for screen-based instruction. These participants may find traditional screen-based learning methods effective.

These diverse preferences underscore the importance of accommodating various mediums of instruction and preferences when designing MI-based training. While these patterns are exploratory and not statistically significant, they suggest that participants may feel they performed best when cues were presented in VR.

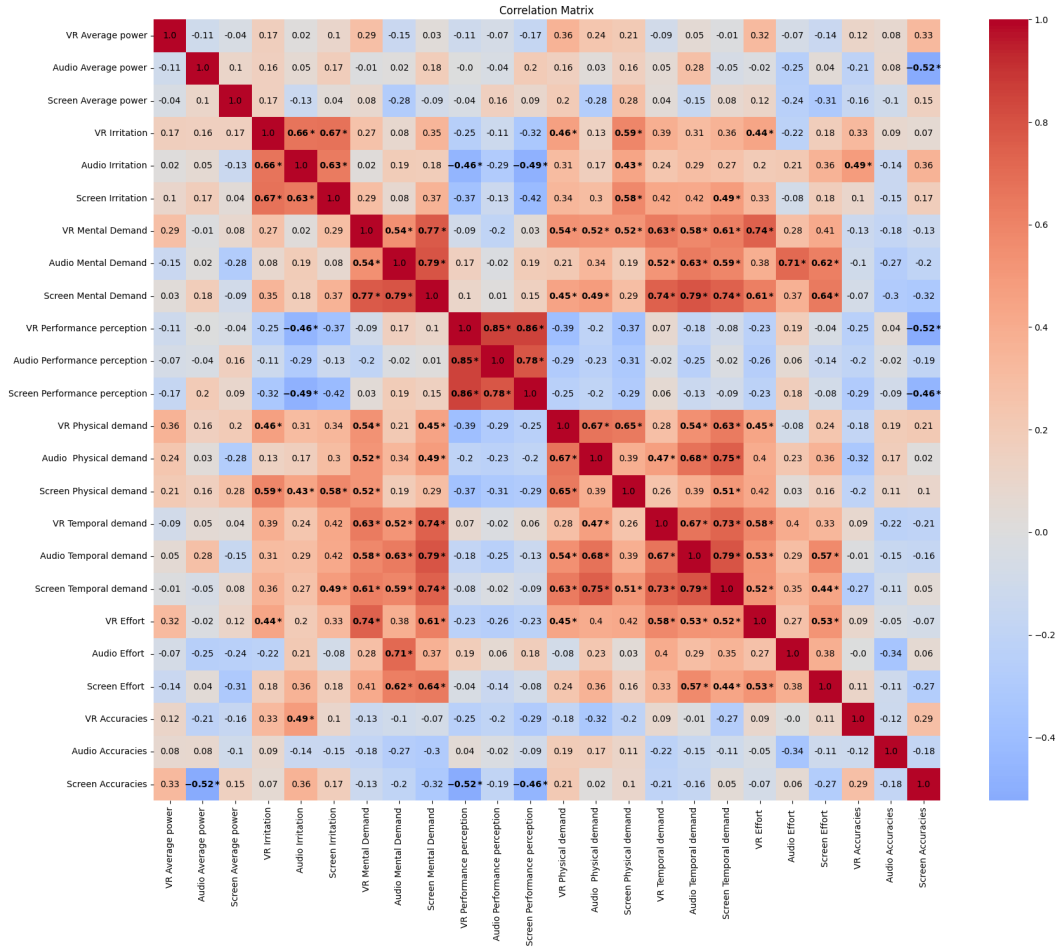

Figure 5.8: Pairwise Pearson's Correlation Analysis for all 21 participants with Average Power Values, NASA-TLX Questionnaire and Machine Learning Accuracies, where * represent statistical significance ($p<0.05$)

When it comes to irritation, the Screen (128) was ranked highest, followed by VR (118), and the least was seen in Audio (114). A similar trend is observed for Physical Demand with Screen (175), VR (172), and Audio (152). The highest Mental Demand is seen in Screen (235), Audio (226), followed by VR (199). For performance perception, participants scored highest for VR (309), followed by Screen (286) and Audio (274). Conversely, in terms of Effort, Audio (258) was scored highest, followed by Screen (251) and VR (225). Temporal Demand was highest for VR (160), Screen (159), and Audio (156). These differences should be interpreted as descriptive trends only.

A Shapiro-Wilk test was applied to test normality; later, statistical significance was assessed at $p < 0.05$. However, no statistically significant differences were identified across the mediums. Therefore, the following interpretations remain exploratory and descriptive rather than confirmatory. The box plots in Fig. 5.7 show an overall comparison of different aspects (Irritation, Mental Demand, Performance Perception, Physical Demand, Temporal Demand, and Effort).

Regarding mental demand, VR and audio show similar levels of Mental Demand, while Screen appears slightly lower. Conversely, VR has the highest perceived performance, followed by audio and screen. For irritation, audio and screen show similar levels, while VR appears slightly lower. These trends, although not statistically significant, align descriptively with the grand average ERD/ERS values, where VR shows the highest ERD/ERS values, followed by Screen and Audio.

When it comes to overall comparison, based on the relative positions and areas covered by the lines for each medium in Fig. 5.7, VR performs well in terms of ERD/ERS values and performance perception, with moderate Mental Demand and lower Irritation. Audio reflects moderate performance in ERD/ERS values and Mental Demand, with lower Performance Perception and Irritation. Screen cues show moderate ERD/ERS values and Perceived Performance, with lower Mental Demand and Irritation. Again, these observations remain exploratory due to the absence of significant differences.

Finally, Pearson's Correlation test was applied to quantitative and qualitative data, indicating several correlations between performance criteria. Some relationships reached statistical significance ($p < 0.05$), but these should still be interpreted with caution due to the small sample size and the exploratory nature of the study. For instance, those who scored low across questionnaires

or MI power values tended to exhibit similar behaviour across all mediums, and vice versa. An overall correlation matrix is shown in Fig. 5.8.

The correlation relationships between dimensions of demand, effort, and irritation across VR, audio, and screen tasks reveal several insights into user experience and task performance. VR irritation is moderately correlated with both VR physical demand (r = 0.46) and VR effort (r = 0.44), suggesting that higher irritation may align with increased physical demands and effort. Screen irritation shows a strong correlation with screen physical demand (r = 0.58) and screen temporal demand (r = 0.49). VR mental demand correlates with VR physical demand (r = 0.54), VR temporal demand (r = 0.63), and VR effort (r = 0.74).

In the audio context, audio mental demand correlates with audio temporal demand (r = 0.63) and audio effort (r = 0.71). Screen mental demand correlates with screen temporal demand (r = 0.74) and screen effort (r = 0.64). Interestingly, screen performance perception is negatively correlated with screen accuracies (r = -0.46). VR physical demand also correlates with VR effort (r = 0.45). Audio physical demand correlates with audio temporal demand (r = 0.68), and screen physical demand correlates with screen temporal demand (r = 0.51). VR temporal demand correlates with VR effort (r = 0.58), and screen temporal demand correlates with screen effort (r = 0.44).

These correlations highlight potential relationships but should be interpreted as exploratory patterns rather than definitive findings. Together, they provide preliminary insights into how different task demands interact within VR, audio, and screen contexts.

Table 5.2: Post-experimental questionnaire scores for 21 participants.

	VR	**Audio**	**Screen**
Preference	11	6	4
Comfort	10	5	6
Attentive	10	6	5
Interactive	15	3	3

5.4 Discussion

The significance of the medium of instruction in MI tasks is a pivotal aspect that shapes the effectiveness and outcomes of applications such as BCI systems

and rehabilitation programs. This study delved into the intricate relationship between cue presentation media and the resulting MI signals, shedding light on their impact and broader implications for human–computer interaction and rehabilitation.

The results indicate that VR tended to perform best among the tested media, showing a small but consistent advantage across several outcome measures. Specifically, VR elicited the strongest average amplitude responses (Fig. 5.4), achieved a mean classification accuracy of 69 ± 3.12% (Fig. 5.6), and was the most preferred medium according to participant ratings (score = 11; Table 5.2). However, effect sizes were modest, classification accuracies overlapped across media, and not all observed differences reached statistical significance. The immersive nature of VR environments may increase engagement and attentional focus, which could translate into enhanced MI-related neural activity (12). The three-dimensional and interactive aspects of VR may facilitate more vivid mental rehearsal, potentially contributing to improved performance trends rather than unequivocal performance gains. Overall, these findings suggest that VR represents a promising cue presentation medium for MI tasks, while its advantages should be interpreted as incremental rather than definitive.

A second noteworthy observation concerns the impact of auditory cues on MI outcomes. Although auditory presentations did not outperform VR, they demonstrated comparable effectiveness, with relatively high amplitude responses (Fig. 5.4), a mean accuracy of 68.69 ± 3.3% (Fig. 5.6), and the second-highest preference score (6; Table 5.2). This aligns with previous work emphasizing the role of auditory stimuli in facilitating MI processes (197). While differences between auditory and VR modalities were generally small and often not statistically significant, these results highlight audio cues as a viable alternative, particularly in contexts where immersive systems are impractical.

Screen-based presentations also demonstrated measurable effectiveness, with a preference score of 5, which was close to that of the auditory modality (Table 5.2). However, they elicited lower average amplitudes (Fig. 5.4) and classification accuracy (66 ± 2.59%; Fig. 5.6) compared to both VR and audio conditions. These differences were primarily descriptive in nature rather than statistically robust. This observation underscores the importance of contextual factors—such as task complexity, user familiarity, environmental distractions, and accessibility—when selecting a cue presentation medium. Screen-based cues may therefore benefit from tailored implementation strategies to maximize

their effectiveness (198; 199).

Collectively, these findings underscore the broader importance of considering the medium of instruction in the design of MI-BCI systems and rehabilitation interventions. Rather than identifying a single universally superior medium, the results suggest that different modalities offer complementary strengths. Tailoring interventions to individual preferences and practical constraints, informed by both quantitative performance measures and subjective workload and preference data, may enhance user engagement and overall system usability.

Looking ahead, this study provides a foundation for future research exploring innovative cue presentation strategies. As immersive and interactive technologies continue to evolve, combining modalities—such as VR with auditory or haptic feedback—may further enhance MI engagement and robustness. Investigating these combinations in larger and more diverse cohorts will be essential to determine whether observed trends translate into reliable performance benefits.

Overall, the discussion of cue presentation media in MI tasks extends beyond direct performance comparisons. It emphasizes the importance of user-centered design, adaptability, and cautious interpretation of modest effect sizes. Understanding the nuanced relationship between presentation medium and MI signal characteristics is key to advancing MI-based applications in rehabilitation and human–computer interaction.

5.5 Summary

To summarize, this study investigated the influence of different cue presentation media—audio, screen-based, and VR—on no-feedback MI tasks, providing insights relevant to human–computer interaction and rehabilitation.

The results indicate that VR showed a small overall advantage across several outcome measures, including MI-related neural amplitude, classification accuracy, and subjective preference ratings. However, these advantages were modest, with overlapping accuracy distributions across media and limited statistically significant differences. Consequently, VR should be viewed as tending to perform best rather than unequivocally outperforming alternative modalities.

Auditory cue presentation followed VR closely in performance and was well accepted by participants, supporting its role as an effective and accessible MI

cueing strategy. Screen-based presentations, while slightly lower in performance on average, still contributed meaningfully to MI task execution and may remain appropriate in settings where immersive or auditory systems are constrained.

Overall, this work highlights the importance of carefully selecting and tailoring cue presentation media in MI-BCI system design. Rather than demonstrating a clear superiority of one modality, the findings emphasize descriptive trends, user preferences, and practical considerations. Future research with larger samples and randomized designs will be critical to determine whether the observed advantages of VR translate into robust and generalizable benefits for MI-based rehabilitation and functional applications aimed at improving ADL.

Chapter 6

Algorithms

"All models are approximations, and effective algorithms adapt to this imperfection" an ode to George E.P.Box

- Dr.Raj Thilak Rajan

RQ 3: Algorithmic Enhancements for ADL

Part A – Foundational Techniques: *Can combining methods such as Fisher Ratio and Pearson Correlation facilitate single-channel after multi-channel preprocessing* MI-BCI classification, thereby reducing the number of electrodes required without compromising performance?

Significance: Minimizing hardware complexity is crucial for real-world deployment. Single-channel classification reduces setup time, improves comfort, and enhances portability, making MI-BCIs more practical for daily use.

Expected Outcomes: Reliable single-channel classification after multi-channel preprocessing and identification of the most informative electrode sites on offline datasets.

Testing and Validation: Comparative experiments between single- and multi-channel systems, analyzing classification accuracy and signal discriminability.

Part B – Advanced Algorithms: *Can advanced classifiers, such as GP models, improve robustness and real-time control in MI-BCI systems intended for ADL applications?*

Significance: Robust classification under real-world conditions is essential for practical MI-BCI deployment. Advanced algorithms can mitigate noise, inter-subject variability, and non-stationarity, leading to more reliable control of both VR and robotic interfaces.

Expected Outcomes: Improved classification accuracy, reduced latency, and smoother control on offline datasets.

Testing and Validation: Implementation in real-time MI-BCI tasks and benchmarking against conventional LDA/CSP pipelines.

Emerging algorithms play a significant role in safe interaction beyond laboratory constraints. As previously discussed in Section 3.3, since Algorithms involve feature extraction and classification, this majorly depends on spatial and temporal information. Spatial information is linked with data from the number of channels, and temporal information is linked to time windows, time points, and bandwidths. These features thereby create robust algorithms. Despite being robust, the challenge of reducing the number of channels and adaptive classifiers yet remains a challenge. The contributions from this chapter are:

1. Part A: To evaluate whether single-channel based feature extraction,after multichannel preprocessing, yields robust classification accuracies on datasets and report the channel commonly used.

2. Part B: To understand the concept of adaptive classifiers and threshold setting from emerging algorithms, such as GP, and report the offline classification accuracies.

Part A: Fisher's Ratios- Pearson's Correlation

The personalized nature of motor imagery has been regarded as requiring subject-specific customization in order for the accuracy and efficiency of a BCI system to be enhanced. Common applications for MI-BCIs are generally found in neurorehabilitation, prosthetic control, and assistive technology. Mental exercises that simulate physical movements have been shown to promote neural plasticity and contribute to the restoration of motor functions, which is considered beneficial for individuals recovering from neurological disorders or injuries. Recent trends in MI-BCI applications have been characterized by significant activity in Stroke Rehabilitation, particularly with upper-limb and hand exoskeletons. Significant improvements have been reported for hand exoskeletons controlled by MI signals (200). This has been taken as evidence that the scope of BCI systems extends not only to SCI but also to broader medical applications such as Stroke Rehabilitation, which affects individuals worldwide. As a result, MI-based BCI systems have been viewed as having the potential to support neuroprosthetic control and rehabilitation beyond research laboratories and to enable motor imagery-based BCIs to assist individuals during ADL.

The integration of Brain-BCI systems into daily routines, particularly in uncontrolled environments, has been acknowledged as a complex task. Among the challenges encountered, issues related to device portability, channel count, user acceptance, and the need for continuous improvements in system robustness have been consistently identified. Consequently, channel reduction has been increasingly regarded as a promising avenue, particularly for BCIs intended for ADL.

While prior studies have explored single-channel MI decoding, current literature does not clearly examine how statistical channel-selection methods can structure a systematic path from multi-channel to minimal-channel MI classification. As a result, the relationship between multichannel discriminability, progressive channel reduction, and eventual single-channel feasibility remains insufficiently understood. In particular, it is unclear how well-established statistical measures—such as Fisher's Ratio and Pearson Correlation Coefficient together can be systematically combined to preserve discriminative information while progressively reducing spatial dimensionality, especially in the context of subject-specific variability and practical deployment constraints.

Research on single-channel-based motor imagery classification has been presented in several studies. For instance, a hybrid MI–SSVEP system using a single channel (C3 or C4) for Motor Imagery and SSVEP, respectively, was developed by Ko et al. using Short Time Fourier Transform (STFT) (201). A real-time single-channel system using STFT and the Grey Level Co-occurrence Matrix (GLCM) was described by Camacho et al. (202). A comprehensive comparison of features (primarily GLCM, log-variance, and single-channel CSP) and classifiers (LDA, k-NN, GMM, RF, MLP, SVM) for single-channel MI classification was performed by Kanoga et al. (203).

Fisher's ratio and Pearson Correlation coefficient (PCC) have been recognized as powerful methodologies used for channel, band, or feature selection. For example, Fisher's ratio was used by Thomas et al. to determine an optimal band from C3 or C4, after which features from this band across all channels were provided to CSP for classification (204). A similar approach was implemented by Thomas et al. to identify discriminative channel sets before extracting CSP features for classification (205). A subject-specific use of Fisher's ratio for optimal channel-set and band identification was also reported by Thomas et al. (206).

Similarly, PCC was employed by Dhiman et al. and Yu et al. for optimal channel selection (207), (208). Gaur et al. used PCC to determine an optimal channel among C3, Cz, and C4, extract relevant information, and use it as a reference (209). Additional work combined squared PCC with other feature-extraction techniques (210). A framework incorporating PCC-based channel selection, power-spectrum–based subband selection, and relevance- plus Fisher's-ratio–based feature selection was proposed by Meng et al. (211).

Although Fisher's ratio has been widely applied for channel selection (205), (212), variability in the number of retained channels across subjects has been frequently observed, and single-channel implementation remains insufficiently explored. Furthermore, the combined use of Fisher's ratio and PCC has been considered capable of identifying efficient features.

Here, the space is further explored by examining how FR and PCC can structure a principled approach for selecting or reducing channels toward single-channel decoding.

A deeper investigation into single-channel-based classification,after multi-channel preprocessing, is carried out in this work through the development of an integrated framework based on Fisher's Ratio and Pearson Correlation. The

framework is evaluated using two open-source datasets and data collected from 21 participants. A comparison with state-of-the-art algorithms is subsequently provided. The hypothesis regarding improved performance under certain classification sets is examined, and the optimal channel across 39 subjects (combining all datasets) is investigated.

6.1 Methodology

6.1.1 Dataset

One of the well-known systems for using MI to perform respective mental tasks is the Graz paradigm, which reports clinical applications of MI-based BCI systems with operations like controlling a virtual cursor and hand orthosis operations. The Graz paradigm differentiates two or more MI-based brain imagination or EEG signals synchronously (in predefined time windows) (179). To evaluate the proposed methodology, the proposed framework has been tested on the following datasets:

1. Dataset 1: The BCI IV-2a dataset encompasses EEG recordings from 9 subjects, employing a cue-based BCI paradigm featuring four distinct motor imagery tasks. Subjects engaged in the mental simulation of movement for the left hand (Class 1), right hand (Class 2), both feet (Class 3), and tongue (Class 4). Recorded over two sessions on different days for each participant, each session comprised six runs with short breaks in between. Within each run, 48 trials were conducted, with 12 trials for each of the four possible classes, resulting in a cumulative total of 288 trials per session (62).

2. Dataset 2: The BCI IV-2b dataset comprises EEG recordings from 9 healthy participants. Participants performed motor imagery tasks involving left and right-hand movements. Each trial consists of a 6-second baseline, followed by 4 seconds of motor imagery, and annotations indicate the onset of these tasks. The dataset includes three recording training sessions for each participant, providing a total of 316 motor imagery trials across all subjects (178).

3. Dataset 3: The data collected at DCU, as a part of an experiment (Chapter 5), approved by the Ethical Committee at DCU, Ireland. The

data consists of a total of 21 healthy individuals. The data was collected using the Neuroconcise 3-channel EEG system. The EEG system used is a bipolar system containing seven electrodes, FC3-CP3, FCz-CPz, FC4-CP4, and the bias AFz as ground, with a sampling rate of 125 Hz. The motor imagery training data is recorded in OpenVibe and using Graz-BCI as a reference paradigm (22) for left and right-hand motor imagery.

6.1.2 FRPC- Feature extraction-based Integrated Framework

In the preprocessing phase, initially, a notch filter is applied to eliminate unwanted frequency components from the raw data, such as power line interference, at 50 and 100 Hz. Subsequently, an Independent Component Analysis (ICA) is employed to mitigate artifacts and enhance the separability of motor imagery conditions. In every cross-validation fold, ICA was trained on the training set only. No test data were used when estimating ICA. The resulting preprocessed data is then focused on three chosen EEG channels, specifically C3, Cz, and C4, which are most popularly known for Motor Imagery (213).

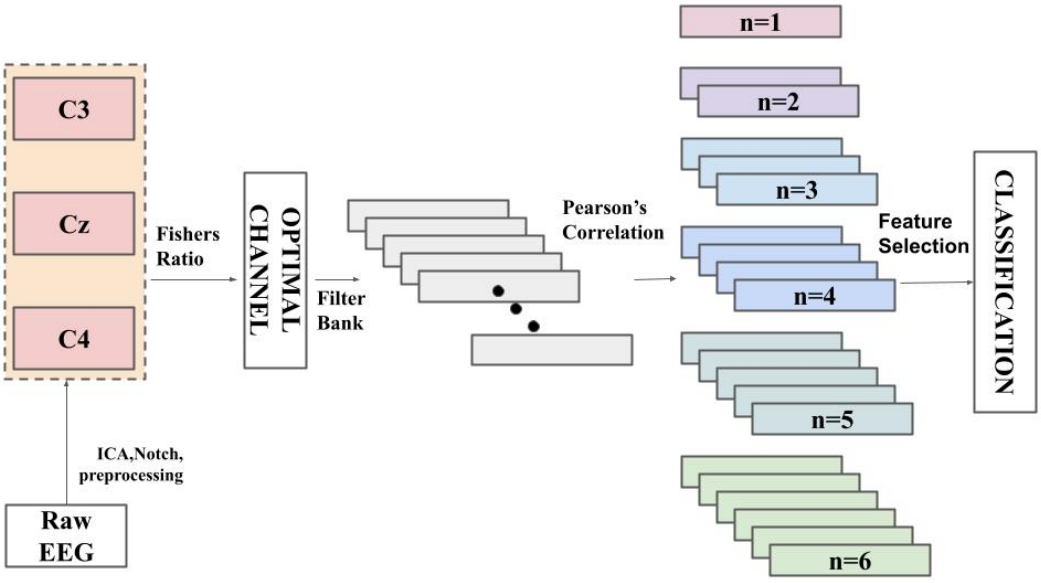

Figure 6.1: Proposed framework

In the proposed method, an integrated framework is initiated by conducting channel selection using Fisher's Ratio (FR) and selecting one optimal channel. The primary goal here is to identify the most discriminative EEG channel for

subsequent motor imagery classification. FR, denoted as FR, serves as the quantitative measure to assess the separability of the data within each channel under all motor imagery conditions.

In Motor Imagery, FR is classically defined as a *between-class separability measure*, quantifying how well a given EEG channel discriminates between motor imagery classes.

For a given EEG channel i and two classes, c_1 and c_2, the Fisher's Ratio is computed as:

$$FR_i = \frac{(\mu_{i,c_1} - \mu_{i,c_2})^2}{\sigma_{i,c_1}^2 + \sigma_{i,c_2}^2} \tag{6.1}$$

where μ_{i,c_k} and σ_{i,c_k} denote the mean and standard deviation of the signal power (or feature of interest) for channel i and class c_k, respectively.

This formulation explicitly measures *between-class variance relative to within-class variance*, with higher FR values indicating greater discriminative power of the channel for separating motor imagery classes. Channels exhibiting consistently higher FR values are therefore considered more informative for MI classification and are commonly selected for subsequent feature extraction and classification stages.

Following the selection of the optimal EEG channel, advancement to sub-band decomposition has been done to capture frequency-specific information. This crucial step involves applying a wavelet transform, a widely used technique for this purpose, to segment the EEG signal into distinct frequency bands. Mathematically, the resulting sub-bands are denoted as $X_{i,j}$, where i represents the chosen EEG channel, and j indexes the sub-band.

The wavelet transform can be expressed as:

$$X_{i,j}(t) = \int_{-\infty}^{\infty} x_i(\tau) \cdot \psi^* \left(\frac{t - \tau}{s_j} \right) d\tau \tag{6.2}$$

Here, $x_i(\tau)$ is the EEG signal from channel i at time τ, ψ is the mother wavelet function, and s_j denotes the scale parameter related to the frequency band of the sub-band j. The integral captures the convolution of the EEG signal with the scaled and translated wavelet function. The sub-bands are divided into frequency ranges from 8 Hz to 40 Hz with intervals of 4 Hz.

This process results in a set of sub-bands $X_{i,j}(t)$, each representing a different frequency range. These sub-bands are essential for extracting spectral features

relevant to motor imagery conditions, providing a detailed representation of the EEG signal's frequency content.

Within each sub-band, the Pearson Correlation Coefficient (PCC) is used to rank the features based on their linear relationship with the target variable. The Pearson correlation ($r_{i,j}$) for a feature $x_{i,j}$ in sub-band j is defined as:

$$r_{i,j} = \frac{\sum_{k=1}^{n}(x_{i,j,k} - \bar{x}_{i,j})(y_k - \bar{y})}{\sqrt{\sum_{k=1}^{n}(x_{i,j,k} - \bar{x}_{i,j})^2}\sqrt{\sum_{k=1}^{n}(y_k - \bar{y})^2}} \tag{6.3}$$

Here, $x_{i,j,k}$ represents the k^{th} sample of feature $x_{i,j}$, and y_k denotes the corresponding class label or target value. $\bar{x}_{i,j}$ and $\bar{y}$ are the mean values of the feature and target, respectively. The resulting correlation coefficient $r_{i,j}$ ranges from -1 to $+1$, where values closer to $+1$ or -1 indicate a stronger linear relationship between the feature and the target. Features with higher absolute correlation values are ranked higher for further analysis.

In the final step, the bands are grouped and ranked (n=1 (top 1 band), n=2 (top 2 bands) ... n=6 (top 6 bands)) in ascending order, and the top 6 bands are selected with high correlation. A within-subject 10×10 cross-validation scheme is used, where each subject's trials are randomly partitioned into 10 folds and repeated 10 times; cross-validation is applied immediately after epoching so that all subsequent data-driven steps occur strictly within each fold. For each fold, all procedures—including Fisher's Ratio computation, PCC-based ranking, sub-band selection, feature extraction, and AdaBoost training—are performed exclusively on the training portion, and the resulting selections and models are applied only to the held-out fold to prevent information leakage. Later, temporal and spectral features (Band Power features) from each sub-band are extracted with respect to their ranking and are fed into an AdaBoost classifier with a crossfold of 10×10, reporting the mean accuracies. This comprehensive framework, integrating Fisher's Ratio for channel selection, sub-band decomposition, Pearson's Correlation for feature ranking, and a machine learning classifier, constitutes a robust methodology for subject-specific motor imagery classification. The pipeline, from raw EEG data to classifier input, leverages both spatial and spectral information to enhance classification performance. The proposed framework for a time window of 0.5 to 2.5s is applied, after the event occurs, for every participant and across all datasets.

6.1.3 Evaluation Matrix

The framework is tested on these datasets, and the results have been reported. The results are compared with the work of Oikonomou et al. (214) for Datasets 1 and 2, for performance to achieve near-accuracy, and Kanoga et al. (203) for comparison for Dataset 2, Dataset 3 with all channel ERD/ERS - AdaBoost. Furthermore, all combinations of 2 classes are explored from Dataset 2.

Table 6.1: Comparison of accuracies (in %) for BCI IV-2b dataset.

Subject ID	**eLDA (214)** (22 channels)	**Proposed FRPC Framework** (One channel)	**Selected channel, no. of bands**
B01	73.13	54.68	C3, 6
B02	61.79	51.56	C3, 1
B03	56.25	58.12	C4, 3
B04	96.25	80.39	C4, 2
B05	91.25	52.81	C3, 6
B06	82.19	63.12	Cz, 6
B07	73.75	63.12	C3, 6
B08	91.56	65.63	C4, 1
B09	85.94	64.37	C3, 6
Average	79.12	62.29	

6.2 Results

For Dataset 1, as seen in Table 6.1, the eLDA framework achieves an average accuracy of 79.12%. In comparison, the proposed system demonstrates an average accuracy of 62.29%. The accuracy was high only for one participant, B03, where the proposed framework achieved 58.12%, whereas (214) reports 56.25%. These results indicate that the proposed approach performs similarly to an existing single-channel baseline for some subjects, while remaining below the performance of multichannel methods, which is expected given the substantial reduction in spatial information.

For Dataset 2, the results in Table 6.2 compare the proposed framework against eLDA. eLDA achieves an average accuracy of 68.37% using 22 channels, whereas the proposed framework attains 66.68% while using only one channel.

Table 6.2: Comparison of accuracies (in %) for BCI IV-2a dataset.

Subject ID	**eLDA (214)** (three channels)	**Proposed FRPC Framework** (One channel)
A01	72.22	72.41
A02	49.31	62.06
A03	86.11	72.41
A04	58.33	86.20
A05	73.61	59.92
A06	56.25	60.68
A07	63.89	61.96
A08	84.72	61.70
A09	70.83	62.80
Average	68.37	66.68

The performance is therefore comparable in numerical terms despite the substantially reduced channel count. Subject-specific results indicate variability, suggesting that the proposed framework can approach eLDA-level performance in some cases, though not consistently across all subjects. Later, a comparison is also made with another single-channel framework (203). Kanoga et al. selects optimal channels among all available channels, whereas in the proposed framework, the channel is restricted to C3, Cz, or C4. Table 6.2 shows that the proposed framework achieves an average accuracy of 66.68%, compared to 63.5% reported for PS-SVM. This reflects a modest improvement over the specific single-channel baseline, while not implying overall superiority across all approaches.

On BCI IV-2b, the overall performance remains clearly lower than established multichannel baselines. This is likely due to the loss of spatial resolution inherent to single-channel classification, the reduced robustness to artefacts, and the difficulty of capturing distributed motor-related activity from a single electrode location.

Later, the FRPC integrated framework was tested on Dataset 2 to examine the classification of all possible two-class combinations. Table 6.4 shows that certain subjects exhibit higher accuracy for specific motor tasks. The average scores indicate that the Right Hand–Tongue set achieves 72.8%, followed by the Tongue–Feet set at 66.68%. These findings suggest that, within the constraints of a single-channel system, after multichannel preprocessing, some class pairs

Table 6.3: Comparison of accuracies (in %) for collected data.

Subject No.	**ERD/S-AdaBoost**	**Proposed FRPC Framework**	**Selected channel & no. of bands (ch, n)**
01	55.00	61.66	C4, 3
02	68.75	40.00	C3, 1
03	63.75	82.50	C4, 5
04	58.75	71.60	C3, 6
05	56.25	68.33	C3, 2
06	56.25	69.16	C4, 6
07	60.00	66.66	C3, 1
08	61.25	61.66	Cz, 6
09	67.52	84.16	Cz, 1
10	65.00	80.83	Cz, 6
11	60.00	64.16	C4, 5
12	63.78	71.66	C4, 4
13	65.00	70.08	C4, 2
14	56.25	72.50	C3, 6
15	61.25	74.90	C3, 2
16	71.25	59.10	C4, 6
17	63.75	60.00	C3, 1
18	55.00	59.00	Cz, 2
19	60.00	72.50	C3, 1
20	58.76	75.83	Cz, 1
21	58.75	53.33	C3, 2
Average	61.21	67.60	

Table 6.4: Comparison of accuracies (in %) for within-group BCI IV-2a dataset using the proposed FRPC framework.

Subject ID	**L/R**	**L/F**	**L/T**	**R/F**	**R/T**	**T/F**
A01	72.40	68.90	75.86	82.70	93.10	82.70
A02	62.06	55.17	41.37	51.72	68.62	65.51
A03	72.41	65.51	72.41	65.51	75.86	65.51
A04	86.20	68.96	62.06	55.72	51.72	58.62
A05	59.92	64.46	64.39	60.15	67.87	63.25
A06	60.68	64.92	59.39	58.10	70.45	58.10
A07	61.96	72.12	73.71	67.80	79.24	75.60
A08	61.70	62.72	74.01	60.45	74.92	75.60
A09	62.80	65.68	85.90	63.63	79.00	74.00
Average	66.68	65.38	67.67	62.86	72.80	68.70

are more distinguishable than others. Understanding these variations is essential for refining the capabilities of single-channel systems, after multichannel preprocessing, particularly for targeted interventions.

For Dataset 3, EEG data from three channels for 21 subjects were analysed using ERD/ERS features fed to an AdaBoost classifier. Table 6.3 shows subject-level variability. The average accuracy of the ERD/ERS approach is 61.21%, while the proposed framework achieves 67.6%. This represents a numerical improvement over the specified method, without implying broader superiority. These findings highlight the usefulness of focusing on subject-dependent frequency bands from the best channel. Combining all 3 datasets (39 subjects), the optimal channel was most frequently C3, followed by C4 and Cz. Since C3 lies over the left motor cortex, typically dominant for right-hand movement, its higher selection frequency likely reflects underlying neurophysiological asymmetries rather than a method-specific preference.

6.3 Discussion

This study introduces an integrated framework for motor imagery classification that systematically selects the optimal channel and uses Pearson correlation for filter bank selection to extract spectral and temporal features. The framework is tested on two publicly available datasets and one collected dataset,

demonstrating its applicability across different recording setups. Rather than asserting performance advantages, the study demonstrates comparable performance with improvements over a specific channel-reduced baseline. The framework is benchmarked against eLDA for Datasets 1 and 2 and a PSD–SVM single-channel framework for Dataset 2. Beyond classification performance, this study examines the repeated selection of C3 as the optimal channel across subjects, contributing insight into subject-specific neural patterns. Additionally, the analysis highlights the class combinations where the single-channel framework, after multichannel preprocessing, demonstrates higher efficiency, particularly for Tongue–Feet motor imagery.

6.4 Summary

Channel reduction is an important factor in making EEG-BCI systems suitable for daily-life applications. Although MI classification heavily depends on spatial information, channel-reduced classification remains an important direction for practical systems. Since Fisher's Ratio and Pearson Correlation are widely used measures, we propose an integrated framework (FRPC integrated framework) combining Fisher's Ratio for channel selection and Pearson correlation for optimal filter bank selection and feature extraction. The framework is evaluated for 2-class MI classification on two public datasets and one collected dataset, and compared with relevant baselines. Overall, the results suggest that the proposed approach can achieve comparable performance to some existing methods under channel reduction constraints, while providing improvements over a specific single-channel baseline, without claiming broad superiority. The study also investigates optimal channel selection across subjects and the class combinations for which the single-channel framework, after multichannel preprocessing, performs more effectively.

Part B: Gaussian Process-based classification

One of the major challenges in BCI systems is the variations in subject-specific motor imagery signals with a limited dataset, which could either be due to the limitations in the number of trials for training or the number of subjects. The main drawback of motor imagery classifiers is their sensitivity to noise and variability in EEG signals, which can reduce classification accuracy. These classifiers often require extensive training (168; 215) and careful feature extraction (216; 217) to perform well. Also, these solutions struggle with real-time processing demands due to computational complexity, especially in dynamic or adaptive systems. Precision in classification accuracy is paramount for MI BCIs, as misclassifications can result in incorrect commands being sent to connected devices, compromising the system's reliability and user experience. Therefore, ensuring high precision in classification is imperative to enhance the usability and safety of BCI systems.

Since classifiers have become a focal point of research (218; 219), one promising avenue could be implementing Gaussian Processes(GP) for robust classification (220), which provide a probabilistic framework that could capture uncertainty in Motor Imagery classification, offering better interpretability and confidence in predictions compared to many deterministic classifiers. GPs (221) can model complex, non-linear relationships in the data through their kernel functions(linear, RBF, etc.). This can potentially lead to higher accuracy and robustness in Motor Imagery tasks where signal patterns can be highly variable (222; 223). Furthermore, GPs can facilitate adaptive learning, allowing BCI systems to continually adapt to changes in neural activity patterns, thereby improving overall performance and usability.

GPs have garnered attention as a potential classifier for MI-based BCIs (220; 224), since they aid in setting decision thresholds and model uncertainty, which is inherent in neural data. However, Zhong et.al, studied BCI IV (finger movement), III, and II datasets as experiments but reported results on one of them (224). On the other hand, Wang et.al. implement GP on BCI on dataset BCI IIIb and report the prediction time. After these significant contributions, the field remains largely unexplored for MI. Despite the promise of GPs in improving decision-making and uncertainty quantification for MI-based BCIs, there is still a need for comprehensive studies that thoroughly investigate GP applications across diverse datasets. To explore various classes in Motor

Imagery with One vs. All (OvA) strategy on the BCI IV-2a dataset. Since the Mean Accuracy of cross-fold validation demonstrates the robustness of the classifier, binary classification, and OvA strategies for every class, and exploring 3 main kernels, which have not been previously reported in the literature. In this work, an exploratory study with a CSP-GP-based classification is carried out with the motivation to explore the potential for GPs in the BCI field.

The contributions from this work are:

1. Application of a GP-based classification for binary classification and OvA strategy, and comparing mean accuracies with state-of-the-art accuracies from different classifiers

2. Exploring different kernels for CSP-GP.

6.5 Methodology

6.5.1 Dataset

The BCI IV-2a dataset encompasses EEG recordings from 9 subjects, employing a cue-based MI paradigm featuring four distinct motor imagery tasks. Subjects engaged in the mental simulation of movement for the left hand (Class 1), right hand (Class 2), feet (Class 3), and tongue (Class 4). Recorded over two sessions for each participant, each session comprised 6 runs. Within each run, 48 trials were conducted, with 12 trials for each of the four possible classes, resulting in a cumulative total of 288 trials per session (62).

6.5.2 Framework

The pipeline of the framework is proposed, which includes pre-filtering and CSP, followed by the Gaussian Process Classification (GPC) as described below:

Pre-Processing

In the preprocessing phase, a Band-pass filter of $7 - 32$ Hz is employed to mitigate artefacts and enhance the separability of MI conditions. Furthermore, the EEG data is segmented into a time window of $1 - 4$ seconds after the event has started, and the baseline is set to None. The resulting pre-processed data is then focused on three chosen EEG channels, specifically C3, Cz, and C4,

which are most popularly known for Motor Imagery (213). The data is then passed to the feature extraction phase.

Common Spatial Pattern (CSP)

CSP (71) is a widely used technique for feature extraction and dimensionality reduction in EEG, particularly for MI classification. CSP identifies spatial filters that enhance the discriminative information between two conditions by maximizing the variance of EEG signals in one class and minimizing it in another. To understand CSP, considering one of the classification strategies, for instance, OvA, where, for instance, LH vs. All as discussed in Section 6.5.2

Given the data dimensions:

- **Input data**: $X \in \mathbb{R}^{288\times3\times751}$ (288 events, three channels, and 751 time points),
- **Covariance matrices** C_1 and C_2 are computed for two classes and are of size 3×3, representing the covariance across the three EEG channels (C3, Cz, and C4) for each class.

Mathematically, CSP solves the following generalized eigenvalue problem $C_1 = W^T S W, \quad C_2 = W^T S' W$, where $S \in \mathbb{R}^{3\times3}$ and $S' \in \mathbb{R}^{3\times3}$ are the covariance matrices for each class. The objective is then to solve

$$C_1 W = \lambda C_2 W \tag{6.4}$$

where λ is a diagonal matrix containing the eigenvalues. The spatial filter matrix $W \in \mathbb{R}^{3\times3}$ is obtained by solving this eigenvalue problem. The eigenvectors corresponding to the largest and smallest eigenvalues are selected to derive the most discriminative spatial patterns. After applying CSP, the transformed data $X_{\text{CSP}} \in \mathbb{R}^{288\times2}$ contains the two most discriminative components, one maximizing the variance for the first class and the other for the second class.

Gaussian Process Classification

GP classification involves modeling the relationship between input data points and their corresponding class labels as a stochastic process (222; 223), and offers a principled framework for probabilistic classification, leveraging prior

distributions, kernel functions, and Bayesian inference to model complex relationships in data. The mathematical underpinnings of GP classifiers focus on the formulation of the prior distribution, kernel functions, and the predictive distribution, as listed below.

(a) Prior Distribution At the heart of a Gaussian Process is the prior distribution over functions, which encapsulates the beliefs about the underlying structure of the data before observing any training examples. Mathematically, a GP prior is defined as:

$$f(\mathbf{x}) \sim \mathcal{GP}(m(\mathbf{x}), k(\mathbf{x}, \mathbf{x}')), \tag{5}$$

where $m(\mathbf{x})$ is the mean function, and $k(\mathbf{x}, \mathbf{x}')$ is the covariance (kernel) function.

(b) Kernel Functions The kernel function is fundamental in defining the covariance structure between different input data points in Gaussian Processes. It allows the model to capture various types of relationships and dependencies between the data. Commonly used kernel functions include the Radial Basis Function (RBF) kernel, the Matérn kernel, and the Dot Product kernel.

The RBF kernel, also known as the Gaussian kernel, is defined as:

$$k(\mathbf{x}, \mathbf{x}') = \sigma^2 \exp\left(-\frac{\|\mathbf{x} - \mathbf{x}'\|^2}{2l^2}\right) \tag{6}$$

where σ^2 controls the overall variance of the functions, and l determines the length scale, regulating the smoothness of the sampled functions. The RBF kernel assumes that the covariance between two points decreases exponentially with their distance, providing a smooth and continuous function.

The Matérn kernel is a generalization of the RBF kernel that introduces an additional parameter ν to control the smoothness of the function. It is defined as:

$$k(\mathbf{x}, \mathbf{x}') = \\ \sigma^2 \frac{2^{1-\nu}}{\Gamma(\nu)} \left(\frac{\sqrt{2\nu}\|\mathbf{x} - \mathbf{x}'\|}{l}\right)^{\nu} K_\nu \left(\frac{\sqrt{2\nu}\|\mathbf{x} - \mathbf{x}'\|}{l}\right) \tag{7}$$

where K_ν is the modified Bessel function of the second kind, $\Gamma(\nu)$ is the gamma function, σ^2 is the variance, l is the length scale, and ν controls the smoothness. The Matérn kernel allows for varying degrees of differentiability and smoothness,

making it flexible for different types of data.

The Dot Product kernel, also known as the Linear kernel, is defined as:

$$k(\mathbf{x}, \mathbf{x}') = \mathbf{x}^T \mathbf{x}' + c \tag{8}$$

where c is a constant that controls the offset. This kernel measures the similarity between two vectors as the inner product and is useful for modelling linear relationships in the data. It assumes that the covariance between two points is directly proportional to their dot product, making it a straightforward choice for linear patterns.

Predictive Distribution

Given a set of training data points $\mathbf{X} = \{\mathbf{x}_1, \mathbf{x}_2, ..., \mathbf{x}_N\}$ and corresponding class labels $\mathbf{y} = \{y_1, y_2, ..., y_N\}$, the goal of GP classification is to infer the posterior distribution over functions conditioned on the observed data. The predictive distribution for a new input data point $\mathbf{x}_*$ is given by:

$$p(y_*|\mathbf{x}_*, \mathbf{X}, \mathbf{y}) = \int p(y_*|\mathbf{x}_*, f)p(f|\mathbf{X}, \mathbf{y})df \tag{9}$$

where $p(y_*|\mathbf{x}_*, f)$ is the likelihood function capturing the relationship between function values and class labels, and $p(f|\mathbf{X}, \mathbf{y})$ is the posterior distribution over functions obtained through Bayesian inference.

Threshold Setting and Decision Making

In practice, GP classifiers provide probabilistic predictions in the form of class probabilities for each input data point. To make binary classification decisions, a decision threshold τ is typically applied to the predicted probabilities. For instance, if $p(y = 1|\mathbf{x}) > \tau$, the input data point is classified as belonging to Class 1; otherwise, it is classified as belonging to Class 0.

The pre-processing and feature extraction are done using MNE Python (225), and Gaussian Process Classification is implemented using the Gaussian Process Classifier Library provided by sklearn (226)

In order to explore and understand the classifier, two experiments have been performed on the BCI IV-2a dataset.

Binary Classification

Binary classes, meaning Left Hand/Right Hand (LH/RH), Left Hand/Feet (LH/F), Left Hand/Tongue(LH/T), Right Hand/Feet (RH/F), Right Hand/Tongue (RH/T), and Feet/Tongue(F/T) has been performed for all 3 kernels mentioned above.

One vs. All (OvA)

Here, classification for One vs. all strategy (as one class), meaning Left-Hand vs. other classes (LH/All), Right-Hand vs. other classes (RH/All), Feet vs. other classes (F/All), and Tongue vs. other classes (T/All) has been performed.

6.5.3 Evaluation Matrix

A 10×10 cross-validation procedure was conducted, and mean accuracies were reported as the evaluation metric for all experiments described in Section 6.5.2. CV corresponds to repeated 10-fold CV, where each repetition reshuffles the dataset before splitting. Hyperparameter selection is restricted strictly to the training folds of each split.

Hyperparameter tuning was performed over the ranges specified below, with the number of CSP spatial components fixed to 2. For the RBF and Matérn kernels, the length-scale (l) and signal variance (σ^2) were searched within 0.1–10.0, and the Matérn smoothness parameter (ν) within 0.5–2.5. A grid search was used to optimise kernel hyperparameters, and this tuning was nested within the CV procedure.

6.6 Results

The results of applying various Gaussian Process kernels for classification based on the dataset described in 6.5.1 are described below.

6.6.1 Comparison With Other Classifiers

The proposed CSP+GP approach yields a mean classification accuracy of 78.41%, which is higher than the accuracies obtained with CSP+LSTM, CSP+SVM, CSP+Random Forest, CSP+LSTM-CNN, and CSP+SCS-CNN (74.41%) under the same OvA strategy, as summarized in Table 6.6. These

Table 6.5: Performance Comparison Across Different Tasks and Kernels for OvA

Kernel / Task	A01	A02	A03	A04	A05	A06	A07	A08	A09	Avg
LH/All Dot Product	75.86	75.86	82.76	75.86	75.86	75.86	84.48	82.76	82.76	77.68
RH/All Dot Product	77.59	74.14	89.66	70.69	68.97	72.41	75.86	79.31	70.69	75.48
T/All Dot Product	75.86	86.21	75.86	75.86	75.86	75.86	75.86	75.86	74.14	76.82
F/All Dot Product	86.21	75.86	75.86	75.86	75.86	75.86	81.03	87.93	79.31	79.31
LH/All RBF	84.48	75.86	84.48	75.86	75.86	75.86	86.21	82.76	75.86	79.69
RH/All RBF	79.31	75.86	93.10	67.24	75.86	72.41	82.76	74.14	75.86	77.39
T/All RBF	84.48	87.93	75.86	75.86	75.86	75.86	75.86	75.86	75.86	78.16
F/All RBF	86.20	75.86	82.75	75.86	75.86	75.86	81.03	87.93	79.31	80.07
LH/All Matérn	86.21	75.86	84.48	75.86	75.86	75.86	82.76	86.21	81.03	79.36
RH/All Matérn	82.76	75.86	93.10	75.86	75.86	72.41	81.03	75.86	75.86	78.73
T/All Matérn	84.48	84.48	75.86	75.86	75.86	75.86	75.86	75.86	75.86	77.78
F/All Matérn	86.21	79.31	82.76	75.86	75.86	75.86	81.03	87.93	79.31	80.46

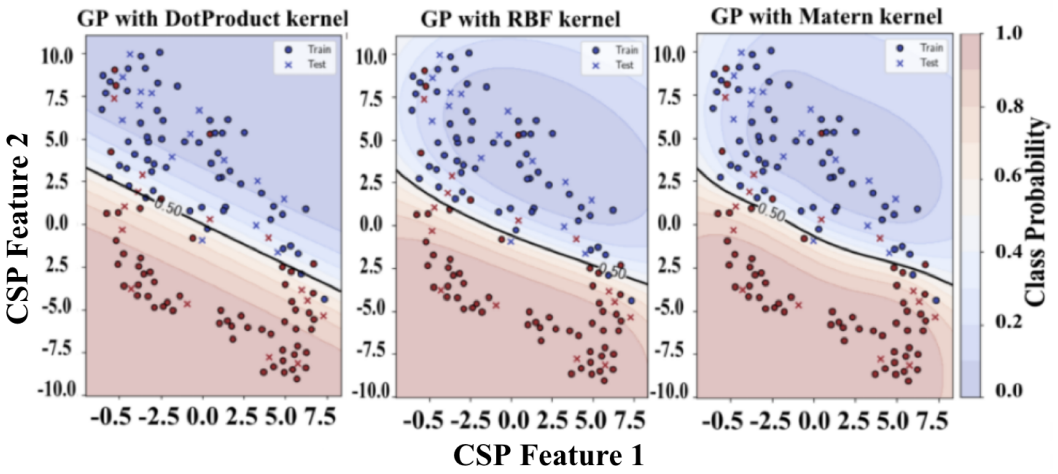

Figure 6.2: RBF, Matérn and Dot Product Kernel representation for Train and Test data together with threshold=0.5 for Subject A09

results indicate that the CSP+GP configuration demonstrates favorable performance relative to the considered baseline methods for this classification setting. The observed improvement suggests that Gaussian Process classifiers may offer advantages in modeling uncertainty and class boundaries when combined with CSP features in OvA-based MI classification.

6.6.2 Binary Classification

The performance comparison across different tasks and kernels indicates that the Matérn kernel is associated with slightly higher average accuracies than the RBF and Dot Product kernels across most tasks. Specifically, for the

Table 6.6: Comparison of Mean Accuracy(MA) (%) for BCI4-2a using CSP with different classifiers for OvA Strategy

Work	**Classifier**	**MA (%)**
Yang et al. (227)	CSP+SVM	62.23
	CSP+LSTM	66.67
Yang (228)	CSP+Random Forest	71.35
	CSP+LSTM-CNN	66.63
	CSP+SCS-CNN	74.54
Proposed Work	**CSP+GP**	**78.41**

Table 6.7: Performance Comparison Across Different Tasks and Kernels for Binary Classification

Task-Kernel	**A01**	**A02**	**A03**	**A04**	**A05**	**A06**	**A07**	**A08**	**A09**	**Avg.**
LH/RH Dot Product	62.06	27.58	82.75	72.41	44.82	75.86	62.06	56.23	82.75	62.95
LH/RH RBF	62.06	41.37	86.2	75.86	48.27	62.06	58.62	56.23	86.2	64.10
LH/RH Matérn	62.06	44.87	86.2	75.86	48.27	65.51	58.21	56.23	86.2	64.82
LH/T Dot Product	86.2	68.96	79.31	39	65.51	68.96	82.75	52.23	86.2	69.90
LH/T RBF	86.2	72.41	75.86	41.37	65.51	68.96	82.75	52.23	89.65	70.55
LH/T Matérn	89.65	72.41	75.86	41.37	65.51	68.96	82.75	52.23	89.65	70.93
LH/F Dot Product	93.1	65.51	93.1	65.51	55.17	75.86	82.75	86.2	89.65	78.54
LH/F RBF	93.1	68.95	93.1	65.51	62.06	75.86	82.75	86.2	89.65	79.69
LH/F Matérn	96.55	68.96	93.1	62.06	65.51	72.41	82.75	86.2	89.65	79.69
RH/T Dot Product	89.65	96.55	75.86	34.48	37.93	72.41	79.31	55.17	55.17	66.28
RH/T RBF	89.65	93.1	75.86	37.93	41.37	79.31	79.31	55.17	55.17	67.43
RH/T Matérn	89.65	89.65	75.86	37.93	41.37	72.41	79.31	55.17	58.62	66.66
RH/F Dot Product	93.1	55.17	86.2	41.37	41.37	75.86	89.65	82.75	79.31	71.64
RH/F RBF	93.1	62.06	82.75	41.37	48.27	72.41	89.65	82.75	75.86	72.02
RH/F Matérn	93.1	65.51	82.75	41.37	48.27	75.86	89.65	82.75	75.86	72.79
T/F Dot Product	72.41	86.2	79.31	24.13	41.37	62.06	82.7	82.7	68.96	66.65
T/F RBF	72.41	86.2	79.31	34.48	37.93	65.51	79.31	79.31	68.96	67.05
T/F Matérn	68.96	86.2	79.31	37.93	37.93	51.72	79.31	76.31	68.96	65.18

Left/Right task, the Matérn kernel achieves an average accuracy of 64.82%, which is marginally better than the RBF kernel's 64.10% and the Dot Product kernel's 62.95%. Similar trends are observed in the Left/Tongue and Left/Feet tasks, where the Matérn kernel consistently shows superior performance with average accuracies of 70.93% and 79.69%, respectively. However, the differences between kernels are subtle, indicating that all three kernels are relatively effective for the classification tasks. The most significant variance is seen in the Tongue/Feet task, where the RBF kernel performs slightly better with an average accuracy of 67.05%, compared to the Matérn kernel's 65.18% and the Dot Product kernel's 66.65%. Also within groups, the best overall performance is seen when Feet are classified with Left and Right hand individually as shown

in Table 6.7.

6.6.3 OvA

Table 6.5 shows the performance of the three kernels (RBF, Matérn, Dot Product) across the four tasks (LH/All, RH/All, T/All, F/All) for nine participants. On average, the Feet/All task consistently performed the best across all kernels, with the highest numerical accuracy reported for the Matérn kernel at 80.46%. The Dot Product kernel generally showed lower accuracies, particularly for the Right/All task, with an average of 75.48%, which is approximately 3% lower than the Matérn kernel. The RBF and Matérn kernels exhibited similar performance patterns, with only minor numerical differences (e.g., RBF slightly higher than Matérn for the Feet/All task: 80.07% vs. 79.36%). These differences represent numerical trends only, as no significant kernel effect was found ($p = 0.2068$, paired t-test).

In contrast, the effect of the task was statistically significant ($p < 0.001$), indicating that performance varied substantially across tasks regardless of kernel choice.

6.7 Discussion

Despite the GP-based classifier not yielding higher performance than the other evaluated classifiers for LH/RH classification (64.82%), for instance CSP+mLC(214) (68.36%), and state-of-the-art deep learning multiclass classifiers performing extremely well, such as Autoselected FBRCSP (229) (77.31%), EEGNet (72) (78.90%), and EEG-DBNet (230) (85.87%), the motivation to explore GP lies in its inherent ability to provide uncertainty estimates, flexibility in kernel design, and its potential for better generalization in cases where limited labeled data is available. Although GPs have been explored earlier for Motor Imagery Classification (220; 224), kernel exploration may be a viable direction for robust GP-based Deep Learning models for classification. These offline, within-session CV results suggest CSP+GP is a promising candidate for robust MI classification; future work will need to test real-time performance, session-to-session transfer, and adaptive thresholding.

6.8 Summary

In summary, this study explores and demonstrates that GPs enhance classification accuracy for OvA MI classification compared to most traditional classifiers. The Matérn kernel consistently exhibited higher performance than the other kernels across most tasks, reflecting its superior capability in handling the variability in neural data. While kernel differences were not statistically significant across the group, strong within-subject effects ($p < 0.001$) highlight the adaptability of GPs for personalized BCI. Notably, feet-related tasks achieved the highest accuracies (80.07%), suggesting task-specific advantages of GP-based models. These findings underscore the effectiveness of integrating GP with diverse kernels to improve MI-based BCI systems' performance and reliability. Future work in this field could explore GP-based classification and kernels for Deep Learning and Transfer Learning.

Chapter 7

Interfaces and their Applications

"Excellence isn't about being the best — it's about doing what's right, giving your best, and being at peace with what you've done."

- Ms. Meenal Baberwal

RQ 4: Interface Design and Real-World Application

Part A – VR-Based MI-BCI: *Can MI-BCI performance and user engagement be enhanced through immersive VR tasks, such as a 6° head-down tilt microgravity simulation, embedded within conventional MI-controlled VR paradigms for healthy individuals and SCI patients?*

Significance: Incorporating immersive, altered, valid VR environments may enhance motivation, engagement, and task-relevant MI signal generation. This is particularly important for rehabilitation, where sustained user involvement is critical, and for translating MI-BCI use to real-world contexts.

Expected Outcomes: Improved MI signal quality, higher online control accuracy, and increased user motivation.

Testing and Validation: Comparative studies between standard VR and immersive microgravity VR tasks.

Part B – Safe Interfaces for ADL: *Can continuous, interactive MI-BCI tasks, implemented via compliant and safe robotic interfaces, enable the execution of real-world ADL tasks beyond discrete interface trials?*

Significance: Real-world ADL applications require continuous, safe, and intuitive control. Compliant interfaces reduce risk, accommodate human variability, and enable effective interaction with objects in dynamic environments. This directly supports the ultimate goal of translating MI-BCIs from controlled settings to everyday use.

Expected Outcomes: Successful task execution, trajectory accuracy, and user safety and comfort.

Testing and Validation: Real-time control of robotic devices in continuous ADL tasks, with performance metrics including task completion time, error rates, and end-effector stability.

The design of effective and engaging MI-BCIs play a crucial part from laboratory experiments to meaningful real-world use. To achieve this, both the virtual and physical aspects of interaction must be optimized for engagement, safety, and functional relevance. This research question, therefore, explores two complementary directions based on engagement and soft interactions. The contributions from this chapter are:

1. Part A: To enhance MI-BCI performance and user experience through immersive VR environments that simulate realistic contexts such as microgravity

2. Part B: To develop safe, compliant robotic interfaces that allow users to perform continuous, goal-directed ADL.

Together, these studies aim to close the gap between controlled MI-BCI paradigms and practical, user-centered applications in rehabilitation and assistive technology.

Part A: VR and MI BCI

As described in Chapter 5, VR enhances the User training and engagement levels for users performing MI training. Recent advances in VR and BCI technologies have enabled increasingly immersive paradigms for training and evaluating cognitive–motor performance under altered environmental conditions. While prior research has demonstrated the efficacy of motor imagery for enhancing motor learning and adaptation in extreme contexts such as microgravity (231; 232; 233; 234), the integration of real-time neural control within valid VR environments remains largely unexplored.

Exposure to microgravity induces profound alterations in sensorimotor and proprioceptive processing, leading to disorientation, impaired postural control, and changes in muscle activation patterns. Astronaut studies have shown elevated coactivation of agonist–antagonist muscle pairs, modified tonic vibration reflexes, and reorganization of proprioceptive and vestibular integration during and after spaceflight (235; 236; 237; 238). These adaptations reflect the brain's capacity to recalibrate internal models of movement in altered gravity, providing valuable insights for neurorehabilitation contexts where sensory feedback is reduced or distorted.

Studies indicate that mental simulation of object motion and whole-body movements in weightlessness can facilitate sensorimotor adaptation and recalibrate internal models of gravity (232; 234), highlighting the potential of imagery-based interventions for functional skill transfer. Furthermore, head-down tilt (HDT) paradigms have been widely used to simulate microgravity on Earth, eliciting both physiological and cognitive changes comparable to those experienced during spaceflight (239), providing a validated analog for experimental investigations of microgravity-related effects. Despite this, there is a scarcity of research combining BCI-driven interaction with VR-based microgravity simulation to investigate task-specific performance, neural engagement, and subjective experience simultaneously, and whether this could be helpful in rehabilitation and enhancing performance among healthy people.

This study addresses these gaps by implementing a pilot study on a sequential VR paradigm consisting of a baseline "Ball Game," which is first implemented in a normal environment, then in a microgravity-simulated environment "Space Game," and followed by a repeat of the same "Ball Game" post exposure to the microgravity setting. The design emphasizes the evaluation

of BCI usability, task engagement, and neural correlates of motor imagery across standard and altered environmental contexts. By embedding the same BCI control scheme in progressively complex and immersive environments, this work enables systematic assessment of both behavioral and neural adaptation while maintaining controlled experimental conditions. The methodology further incorporates multidimensional evaluation, combining online classification performance, sensorimotor ERD analysis, and participant-reported measures of workload, presence, and imagery vividness. This comprehensive approach provides a unique perspective on the feasibility and functional impact of BCI–VR systems under simulated microgravity conditions.

This line of investigation is particularly relevant as all SCI participants presented lower-limb injuries affecting proprioceptive feedback from the feet. Proprioception contributes critically to MI vividness and sensorimotor cortical activation, as congruent sensory feedback supports the internal simulation of movement. In SCI, the disruption of afferent input from the limbs can diminish MI vividness and reduce ERD in motor-related areas. Simulated microgravity offers a controlled model of altered or reduced proprioceptive input, enabling investigation of how the central nervous system reweights sensory information and adapts under atypical body feedback conditions (233; 234). Within immersive VR, enhanced visual–vestibular cues may compensate for missing proprioceptive feedback, thereby reinforcing MI-related cortical activation and improving BCI control performance (231; 232). This provides a compelling rationale for examining MI–BCI function in simulated microgravity among individuals with proprioceptive deficits.

The main contributions of this chapter are as follows:

1. Development of a Sequential BCI–VR Paradigm:

- A novel experimental framework combining a baseline training environment (Ball Game) with a microgravity-simulated VR task (Space Game) and post-exposure evaluation.
- This design enables controlled within-subject assessment of BCI performance, neural engagement, and subjective experience across environments of extreme conditions.

2. Implementation of Real-Time EEG-Based Control in Immersive VR:

- Integration of EEG acquisition, feature extraction, and classification with Unity-based VR environments deployed on a head-mounted display.

- Continuous, online feedback allowed participants to directly control virtual objects through neural activity, supporting skill acquisition and transfer across tasks.

3. Evaluation of Neural and Behavioral Adaptation Across Contexts:

- Analysis of online BCI classification accuracy, ERD patterns over motor cortices, and Fisher ratio-based channel discrimination.
- Assessment of changes in neural engagement and performance between baseline, microgravity-simulated, and post-exposure conditions.

4. Multidimensional User Experience Assessment:

- Use of standardized questionnaires (NASA-TLX, Presence Questionnaire, Motor Imagery Vividness) alongside a customized comparative survey to capture workload, immersion, imagery vividness, and user preference.
- Provides insights into cognitive and affective responses to BCI–VR interaction beyond conventional performance metrics.

5. Proof-of-Concept for Microgravity Simulation Using HDT and VR:

- Demonstrates the feasibility of simulating altered environmental conditions with 6° HDT based VR MI-BCI for neural and behavioral studies.
- Offers a practical platform for evaluating motor imagery-based adaptation, supporting the development of training and rehabilitation applications under novel or extreme conditions.

7.1 Methodology

7.1.1 Subjects

A total of 12 participants were initially recruited for this pilot study at DCU following ethical approval: 6 individuals with SCI and 6 healthy individuals as a control group. During the course of the study, 2 SCI participants were excluded due to withdrawal prior to data collection, and 1 SCI participant exited midway through the experiment due to frustration with difficulty maintaining focus.

Despite the small sample size, a total of 6 healthy and 3 SCI participants were sufficient for this pilot investigation. The primary objective was to evaluate the feasibility and usability of a sequential BCI-VR paradigm consisting of a baseline Ball Game (Ball Game 1), followed by a Space Game in a microgravity simulation, and concluding with a repeat of the Ball Game (Ball Game 2). The design focused on within-subject comparisons and proof-of-concept assessment rather than on establishing population-level statistical inference. The pilot study allowed for testing the system workflow, participant interaction, and preliminary behavioral and subjective responses, providing essential insights for the design of larger-scale studies.

7.1.2 System design

EEG signals were acquired, processed, and classified in real time using the OpenViBE platform. The resulting control commands were transmitted via TCP/IP to the VR headset, where they were used to update the game environment and provide online feedback.

Ball Game

The Ball Game was implemented as a baseline training environment for motor imagery (MI)-based brain–computer interface (BCI) control. The game is set in a natural outdoor scene with grassy terrain, stone walls, and wooden targets, providing a calm and familiar setting. Each trial lasted eight seconds and followed the Graz BCI paradigm. From 0–3 seconds, a fixed target was displayed, followed by the appearance of a cue (a ball) at 4 seconds. Between 5–8 seconds, the participant's MI task was classified online to provide continuous feedback. Right-hand MI directed the ball toward the right-hand target, while feet MI directed the ball upward toward the central target. The score was incremented by one when the ball successfully reached the correct target, providing immediate reward for correct control. This design enabled participants to complete multiple trials per session (typically 40–60), allowing sufficient data collection for classifier adaptation while providing a low-complexity environment for learning BCI control.

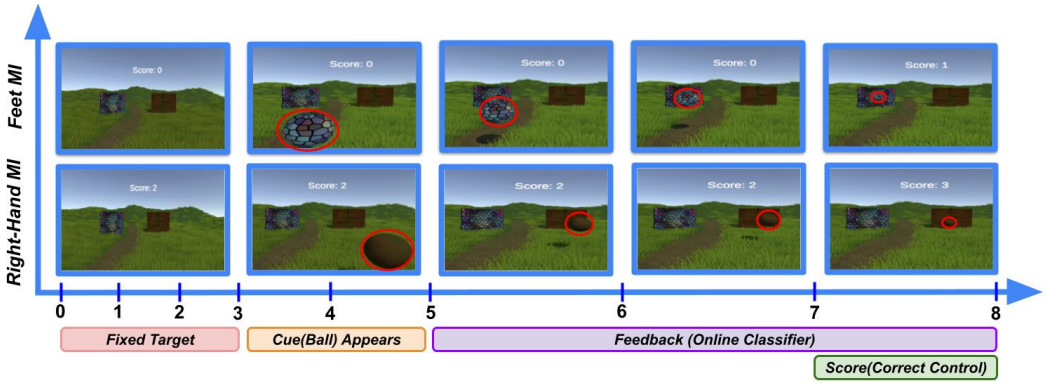

Figure 7.1: System Design for Ball Game

Space Game

The Space Game extended the same BCI control scheme into a more immersive and motivating environment, simulating operations around the International Space Station (ISS). Each experimental block began with a short introductory sequence that provided a guided virtual tour of the ISS to enhance presence and familiarize participants with the microgravity environment. The task then proceeded in trials of eight seconds, mirroring the structure of the Ball Game. From 0–3 seconds, a fixed docking point on the ISS module was displayed. At 4 seconds, a capsule cue appeared, which participants were required to collect using MI-based control. Right-hand MI moved the robotic arm toward capsules positioned laterally, whereas feet MI directed it upward toward capsules above. Between 5–8 seconds, classifier output was translated into continuous feedback through the movement of red or green robotic arms. Successful collection of a capsule increased the participant's score by one and enabled gradual vertical progression along the ISS module, creating a sense of advancement within the task. On average, each participant performed 30–40 trials per session, enabling both robust classifier training and assessment of MI performance in a challenging operational context.

The two environments were designed to complement one another within the system. The Ball Game provided a simple, nature-based task for initial training and classifier calibration, with straightforward targets and limited visual complexity. Its eight-second trial structure with clear scoring feedback facilitated skill acquisition and ensured a sufficient number of repetitions per session. In contrast, the Space Game introduced greater engagement by embedding the same BCI control scheme in a microgravity simulation.

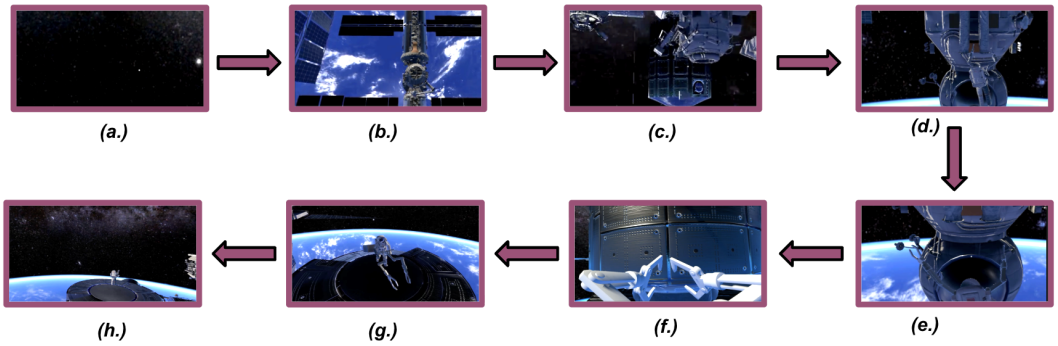

Figure 7.2: Overall System design for Space Game with (a.-e.) Exploration in space around ISS frames followed by the (f.)space game (further explained in Fig. 7.3) and (g.-h.) Post climbing ISS frames

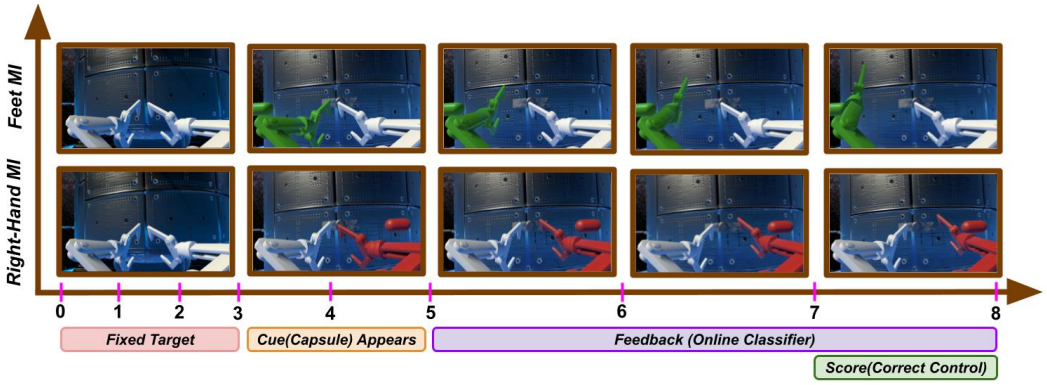

Figure 7.3: System Design for Space game.

The immersive ISS environment, capsule collection task, and sense of upward progression added motivational and cognitive dimensions while retaining the standardized eight-second trial structure. Together, the two games enabled both the reliable acquisition of MI control skills and their transfer to a more complex, motivating, and functionally relevant environment.

7.1.3 Experimental Protocol

All participants followed the same experimental sequence to ensure consistency across conditions. They first completed a training session in which they practiced MI tasks following visual cues to become familiar with the BCI system and to allow calibration. This was followed by a testing phase using the Graz MI paradigm with real-time feedback to validate each participant's ability to generate reliable control signals. Once testing was completed, participants played the first session of the VR Ball Game while seated, serving as the

baseline VR condition. Immediately after gameplay, they completed a set of questionnaires described in Section 7.2.3. Participants were then positioned in a 6° head-down tilt (HDT) posture to simulate microgravity and engaged in the VR Space Game under the same MI-BCI control. Following this condition, the same questionnaires were administered. Finally, participants returned to the seated position to play the VR Ball Game for a second time, allowing direct comparison with the initial baseline condition. As with the other sessions, the questionnaire was completed immediately after the final gameplay.

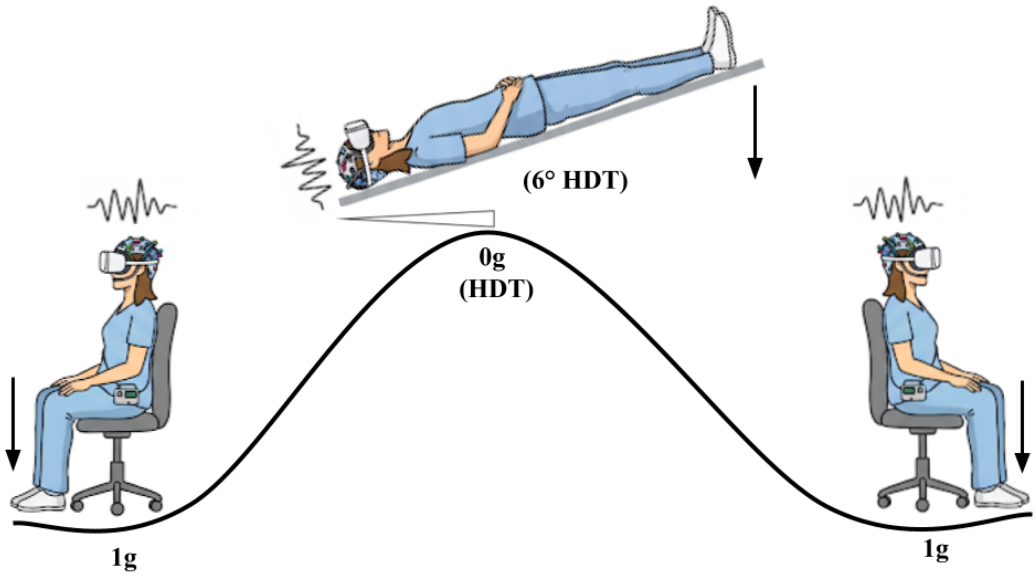

Figure 7.4: Experimental Protocol where the participants first perform the first Ball Game baseline (BG1 or Ball Game 1) Session, followed by Space Session during head-down tilt (space), and Ball Game after the space session (BG2 or Ball game 2)

7.1.4 Tools used

VR Headset

The Ball game and space game were developed in Unity and deployed on the Meta Quest 2 headset to provide an immersive and interactive environment for BCI experiments. The game integrates real-time EEG-based motor imagery inputs, allowing participants to control in-game actions through neural activity rather than conventional controllers. Designed with engaging visuals and intuitive mechanics, it supports both healthy participants and individuals with

spinal cord injury, offering a safe and motivating platform for rehabilitation-oriented training in VR.

EEG Device

In this study, EEG signals were recorded using the OpenBCI device. Sixteen active channels were utilized, specifically T3, T4, F3, F4, P4, Pz, Cz, P3, O2, O1, C4, C3, F7, T5, T6, and F8, covering frontal, central, parietal, temporal, and occipital regions to ensure comprehensive spatial representation of motor and cognitive processes. Impedance was carefully maintained below 5 kΩ for all channels to optimize signal quality and minimize noise, following standard EEG acquisition practices. To ensure that classification was not driven by eye movements or gaze direction, several controls were implemented. Target positions in the VR task were restricted so that extreme left or right placements were avoided, thereby reducing systematic gaze shifts. In addition, participants were instructed to minimise eye movements during motor imagery, as excessive gaze shifts were considered likely to reduce the neural signal quality.

7.2 Evaluation Matrix

7.2.1 Online Classification Results

EEG signal acquisition was performed throughout the experimental sessions and processed online for real-time classification. The training dataset obtained during the initial calibration phase was used to train the classifier. Feature extraction was carried out using the Common Spatial Pattern (CSP) algorithm with four spatial filters ($n = 4$) applied within the frequency band of 8–30 Hz, which is known to capture sensorimotor rhythms associated with motor imagery. The extracted features were then classified using a Linear Discriminant Analysis (LDA) classifier. A 7-fold cross-validation procedure was employed on the training dataset to evaluate classifier performance and ensure generalizability. The resulting training accuracy was computed and reported for each participant.

Following the training phase, the same feature extraction and classification pipeline was implemented for the online sessions. First, participants performed the Graz BCI task with real-time visual feedback, which provided an initial measure of online performance outside the VR environment. The same classifier settings were then applied to the three subsequent VR conditions: the seated

VR Ball Game (Session 1), the Space Game in 6° head-down tilt (HDT), and the seated VR Ball Game (Session 2). Online classification accuracies were recorded for each condition to assess BCI performance across different contexts and postures.

To evaluate differences in performance across conditions, statistical analyses were conducted on the classification accuracies. A repeated-measures ANOVA was applied to determine whether condition (Graz BCI, Ball Game 1, Space Game, Ball Game 2) had a significant effect on classification accuracy. Where assumptions of normality were violated, a non-parametric equivalent (Friedman test) was used. Post-hoc pairwise comparisons with Bonferroni correction were carried out to identify specific differences between conditions. This analysis enabled examination of whether simulated microgravity (6° HDT) or task context influenced online BCI performance relative to baseline and post-exposure seated conditions.

7.2.2 Event-Related Desynchronization (ERD) Analysis

In addition to classification accuracy, ERD patterns were analyzed to characterize neural activity over the sensorimotor cortex during motor imagery tasks. ERD was computed in the μ (8–12 Hz) and β (13–30 Hz) frequency bands, which are known to be modulated by motor-related processes. Power spectral densities were estimated using band-pass filtered EEG signals, and ERD ratios were calculated relative to a baseline period according to the standard formula:

$$ERD\% = \frac{P_{\text{task}} - P_{\text{baseline}}}{P_{\text{baseline}}} \times 100 \tag{7.1}$$

where P_{baseline} corresponds to the mean spectral power during the baseline interval, and P_{task} denotes the mean spectral power during the motor imagery interval. Negative values indicate desynchronization (i.e., power suppression), while positive values correspond to synchronization.

For detailed examination, ERD ratios were specifically extracted from channels C3, Cz, and C4, which are located over the left, central, and right motor cortices, respectively. These channels are of primary interest due to their established involvement in motor imagery of the upper and lower limbs. The ERD dynamics across these channels were compared between tasks and conditions (training, Graz feedback, Ball Game 1, Space Game, Ball Game 2) to investigate changes in cortical activation.

To further quantify the discriminative power of EEG channels, Fisher's ratio (FR) was applied across all electrodes based on their ERD values. Fisher's ratio measures the class separability by comparing between-class variance to within-class variance, and is defined as:

$$FR_c = \frac{\sum_{i=1}^{K} n_i \left(\mu_{i,c} - \mu_c\right)^2}{\sum_{i=1}^{K} n_i \sigma_{i,c}^2} \tag{7.2}$$

where FR_c is the Fisher ratio for channel c, K is the number of classes, n_i is the number of trials in class i, $\mu_{i,c}$ is the mean ERD value of class i at channel c, μ_c is the overall mean ERD value across classes at channel c, and $\sigma_{i,c}^2$ is the variance of ERD values for class i at channel c.

Channels with higher Fisher ratio values indicate greater discriminative potential for separating motor imagery classes. This analysis was used to validate the relevance of C3, Cz, and C4 while also identifying additional electrodes that contributed significantly to classification performance.

7.2.3 Questionnaire Data

To assess subjective experience during the experiment, participants completed a set of questionnaires after each VR condition (Ball Game 1, Space Game, Ball Game 2). The questionnaires were selected to capture multiple dimensions of workload, immersion, and motor imagery vividness.

Presence Questionnaire (PQ): A customized version of the Presence Questionnaire was administered, covering 22 items related to sense of presence, control, environmental responsiveness, naturalness of interaction and movement, visual and auditory involvement, and consistency with real-world experience. Example items included ratings of control over events, naturalness of self-motion, and degree of concentration on the task. **NASA Task Load Index:** Subjective workload was assessed using the NASA-TLX, which measures six dimensions: mental demand, physical demand, temporal demand, performance, effort, and frustration. Scores were reported for each subscale after every VR session.

Motor Imagery Vividness Questionnaire: A motor imagery questionnaire adapted from the KVIQ/MIQ-RS was used to evaluate vividness and controllability of motor imagery. Participants rated vividness of imagery and system responsiveness for both feet and hand imagery, as well as their

confidence and focus during the task.

Personalized Comparative Questionnaire: In addition, participants completed a short, study-specific questionnaire designed to compare the two VR environments. This included questions on game preference, perceived ease of MI control, sense of immersion, physical comfort, mental demand, perceived success, and experienced discomfort. Responses provided qualitative insights into user experience beyond standardized measures.

Together, this series of questionnaires enabled a multidimensional assessment of workload, immersion, imagery vividness, and subjective preference across the experimental conditions.

7.3 Results

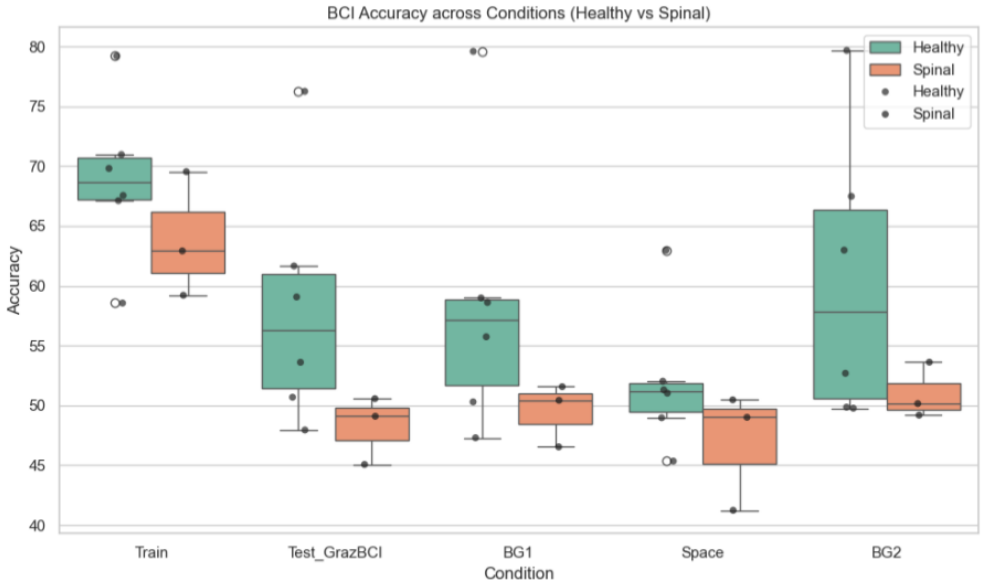

Figure 7.5: Mean accuracy trajectories across Train, Test(Graz BCI), Ball Game at baseline (BG1), Space Game during head-down tilt (space), and Ball Game after the space session (BG2) datasets.

7.3.1 Accuracy (Objective Performance)

Accuracy was significantly affected by Game (BG1, Space, BG2), as indicated by a within-subjects ANOVA, $F(2, 16) = 5.76$, $p = 0.013$, $\eta_p^2 = 0.419$, reflecting a large effect. Post-hoc paired comparisons (all meeting the assumptions of a

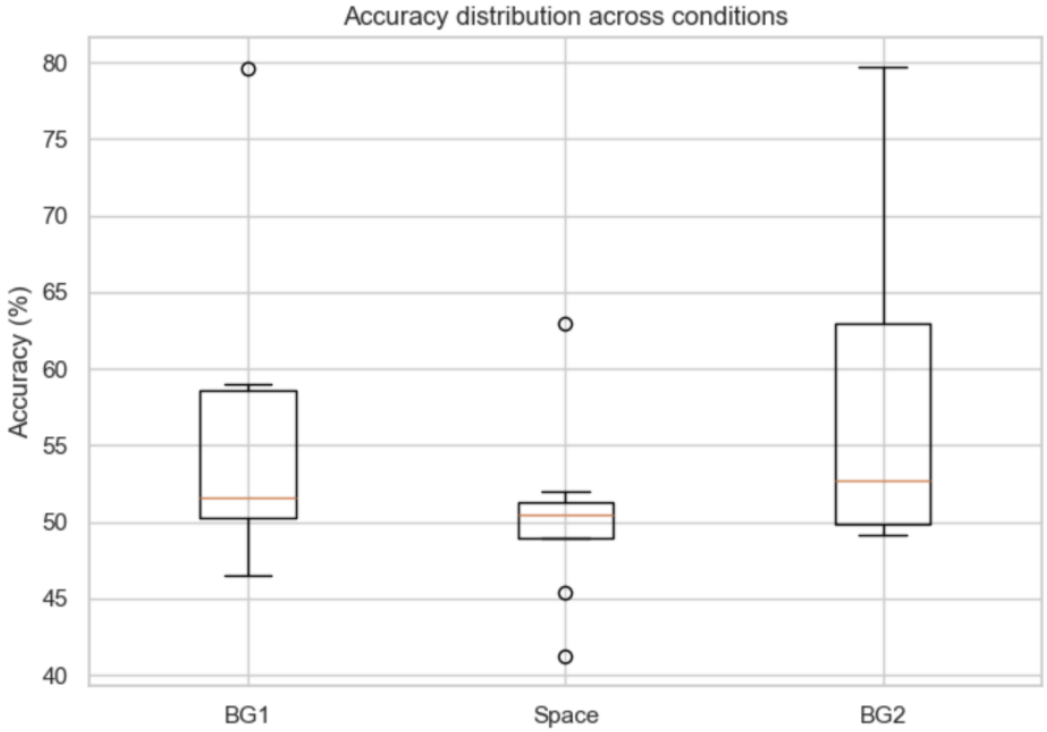

Figure 7.6: Mean accuracy trajectories across games

paired t-test; normality of difference scores was verified using Shapiro–Wilk tests, all $p > 0.10$) revealed a trend toward lower accuracy in the Space game compared to BG1 ($t(8) = 2.17$, $p = 0.062$, $dz = 0.72$), and a significant rebound in BG2 relative to Space ($t(8) = -2.83$, $p = 0.022$, $dz = -0.94$), whereas the difference between BG1 and BG2 was not significant ($t(8) = -1.32$, $p = 0.223$, $dz = -0.44$). These comparisons followed a significant omnibus ANOVA, and since the paired samples satisfied test assumptions, the uncorrected paired t-tests are appropriate for interpreting the direction and magnitude of effects. These findings indicate that participants' accuracy dropped during the Space condition and partially recovered in BG2, consistent with a carryover or adaptation effect. Figure 7.12 illustrates mean accuracy trajectories across games, showing a pronounced U-shaped pattern for Healthy participants and a less pronounced recovery for SCI participants.

Table 7.1: Within-subjects ANOVA for Accuracy

Effect	F	p	η_p^2
Game	5.76	0.013	0.419

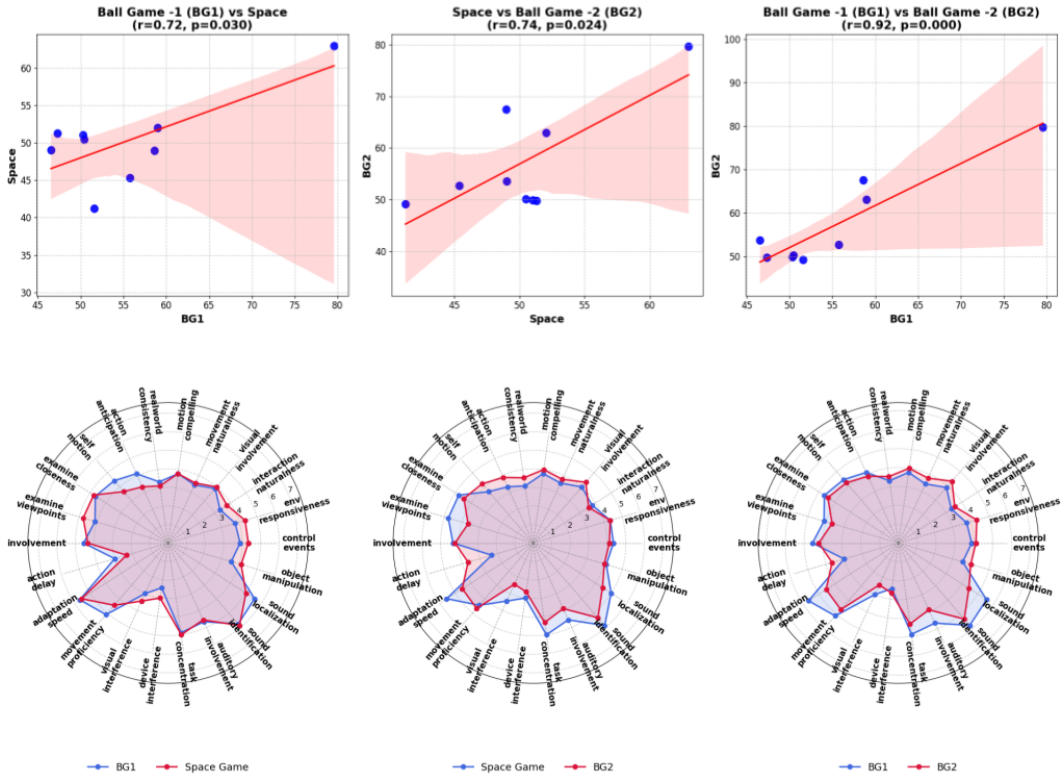

Figure 7.7: Overall correlation analysis between Ball Game at baseline (BG1) and Space Game during head-down tilt (space), Ball Game after the space session (BG2) and Space Game during head-down tilt (space),Ball Game at baseline (BG1) and Ball Game after the space session (BG2)

Table 7.2: Pairwise Paired Comparisons (Uncorrected) for Accuracy

Comparison	t	p	dz
BG1 vs Space	2.17	0.062	0.72
BG1 vs BG2	-1.32	0.223	-0.44
Space vs BG2	-2.83	0.022	-0.94

Responder analysis revealed that five participants (H02, H03, H05, H06, S01) improved in BG2 relative to BG1. Some of these responders reported that the Space game provided better control or immersion, suggesting that subjective experience may align with performance improvements.

7.3.2 Mixed-Effects Regression

A mixed-effects model predicting accuracy from Game, Group, and participant random intercepts confirmed a significant drop in Space relative to BG1 ($\beta = -6.48$, $p = 0.007$) and indicated partial recovery in BG2. The Group main effect

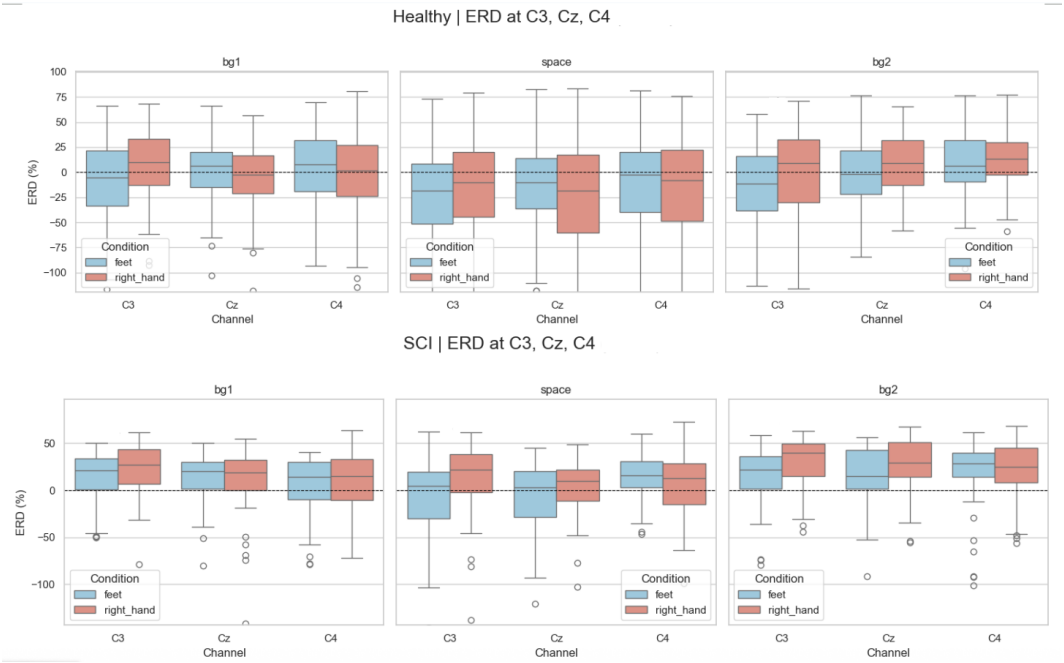

Figure 7.8: Mean ERD values for Healthy and SCI participants across the three game conditions: Ball Game at baseline (BG1), Space Game during head-down tilt (space), and Ball Game after the space session (BG2) for channel C3, Cz, C4 w.r.t feet and right hand classification. Error bars represent the standard error of the mean.

(SCI lower accuracy) trended toward significance ($\beta = -8.91$, $p = 0.102$), and no significant Game × Group interaction was observed. Table 7.3 summarizes selected coefficients.

Table 7.3: Mixed-Effects Regression Predicting Accuracy

Predictor	β	SE	z	p
Intercept	46.45	11.39	4.08	< 0.001
Game (Space vs BG1)	-5.19	2.00	-2.59	0.010
Presence total	0.018	0.105	0.18	0.861
Confidence (mean)	3.40	2.92	1.16	0.245
Effort (mean)	-0.53	0.56	-0.95	0.343

7.3.3 Between-Group Comparisons (Healthy vs SCI)

Independent t-tests showed consistently higher accuracy in Healthy participants across all games, with medium-to-large effect sizes (Cohen's $d \approx 0.9$–1.0), though differences were not statistically significant (Table 7.4).

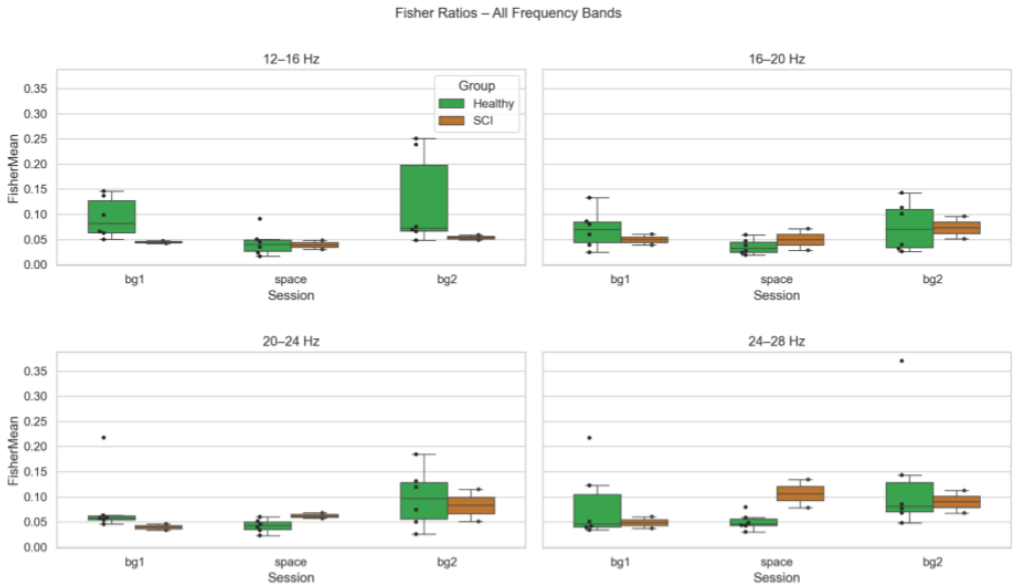

Figure 7.9: Mean Fisher Ratio w.r.t frequency bands for Healthy and SCI participants across the three game conditions: Ball Game at baseline (BG1), Space Game during head-down tilt (space), and Ball Game after the space session (BG2). Error bars represent the standard error of the mean.

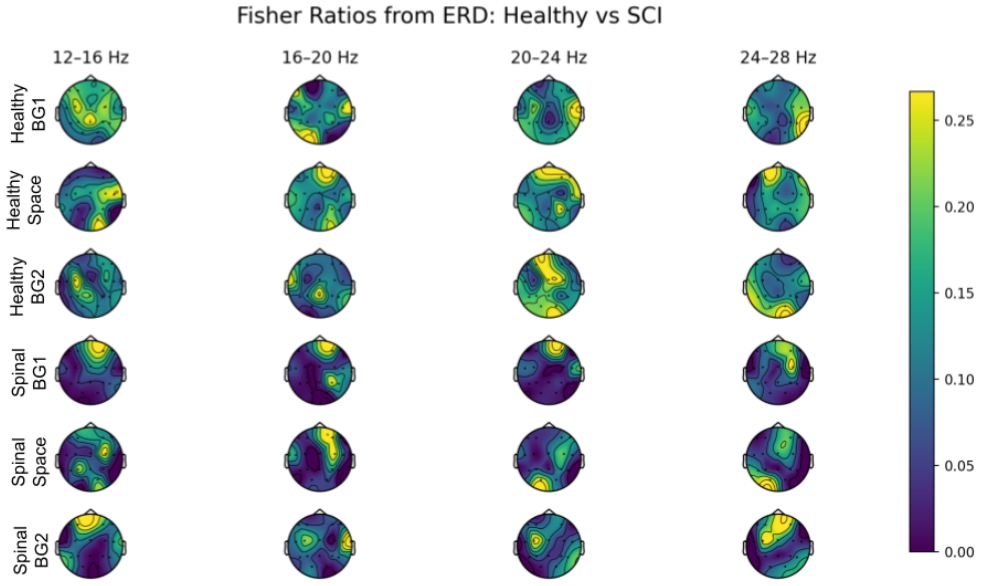

Figure 7.10: Fisher Ratio from ERD data for Healthy and SCI participants across the three game conditions: Ball Game at baseline (BG1), Space Game during head-down tilt (Space), and Ball Game after the space session (BG2). Error bars represent the standard error of the mean.

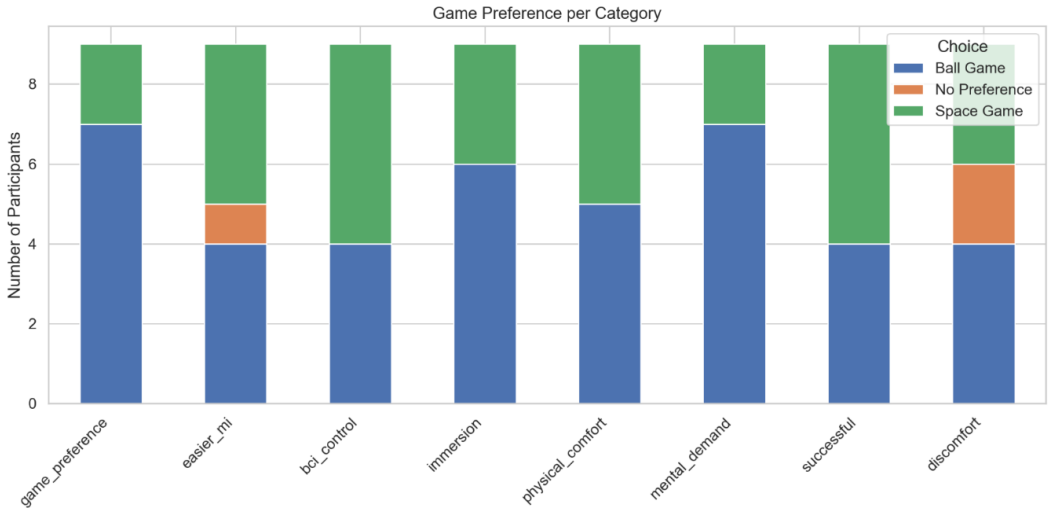

Figure 7.11: Personal Preference of the participants w.r.t. Ball and Space game

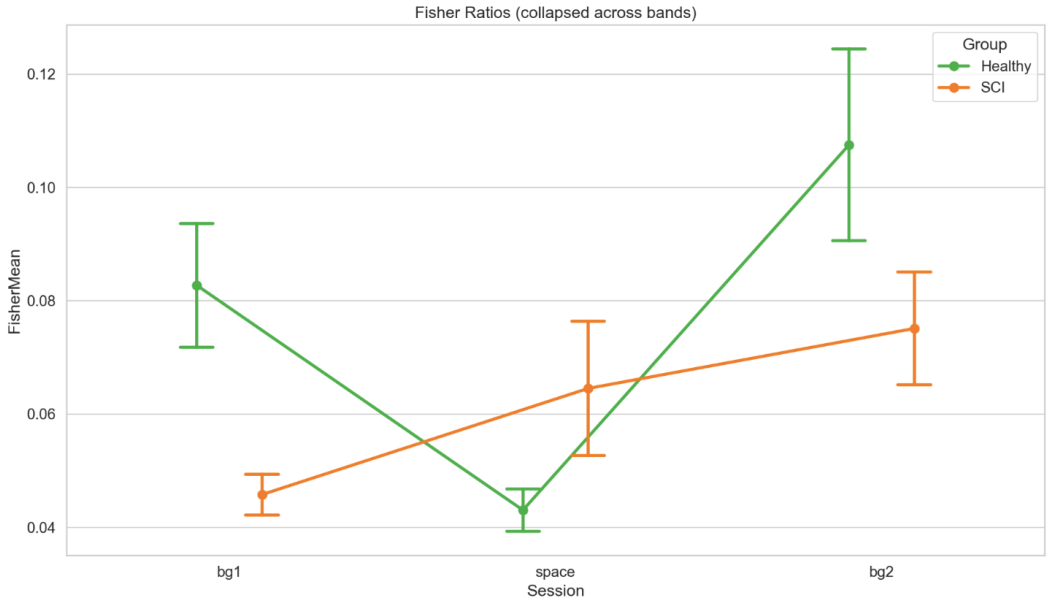

Figure 7.12: Mean Fisher's Ratio for Healthy and SCI participants across the three game conditions: Ball Game at baseline (b1), Space Game during head-down tilt (space), and Ball Game after the space session (b2). Error bars represent the standard error of the mean.

7.3.4 Subjective Measures

Presence. Presence questionnaires demonstrated high internal consistency (Cronbach's α = .820–.906). Mean presence scores per game are shown in Table 7.5. Presence tended to be slightly higher in Space and BG2 compared to BG1, but correlations with accuracy were small and non-significant (all

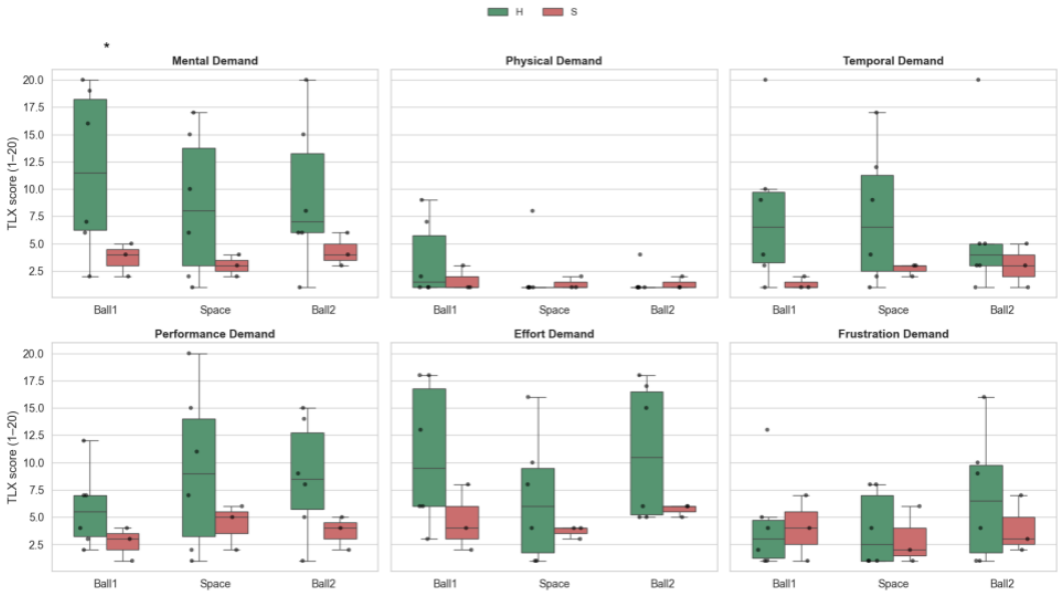

Figure 7.13: NASA-TLX scores for Healthy and SCI participants across the three game conditions: Ball Game at baseline (Ball1), Space Game during head-down tilt (Space), and Ball Game after the space session (Ball2). Error bars represent the standard error of the mean.

Table 7.4: Between-Group Comparisons (Healthy vs SCI)

Measure	t	p	Mean Healthy	Mean SCI	d
BG1	1.82	.118	58.42	49.51	0.92
Space	1.34	.238	51.94	46.91	0.89
BG2	1.86	.114	60.41	50.99	0.93
Test_GrazBCI	2.22	0.066	58.21	48.25	1.02

$|r| < .43$, $p > .25$).

Table 7.5: Mean Presence Scores (Across Participants)

Game	Mean ± SE
BG1	4.17 ± 0.22
Space	4.43 ± 0.21
BG2	4.28 ± 0.23

Vividness. Mean vividness (Confidence + Focus) per game is shown in Table 7.6. Patterns are variable, but several participants who improved in BG2 also reported higher vividness during Space.

Table 7.6: Mean Vividness Scores (Confidence + Focus) per Game

Game	Mean ± SE
BG1	4.00 ± 0.31
Space	4.11 ± 0.28
BG2	4.06 ± 0.29

NASA-TLX. Mean TLX effort per game is shown in Table 7.7. Effort ratings were highest in Space, consistent with a greater cognitive load during the 6° HDT condition.

Table 7.7: Mean NASA-TLX Effort per Game

Game	Mean ± SE
BG1	7.44 ± 1.81
Space	9.44 ± 2.09
BG2	6.44 ± 1.65

7.3.5 Preferences

Collapsed game preference data showed that the majority of Healthy participants preferred the Ball game (5/6, 83.3%), whereas SCI participants also mostly preferred Ball (2/3, 66.7%). Fisher's swexact test confirmed no significant association between group and preference ($\chi^2 = 0.75$, $p = .861$).

To summarize the results, accuracy decreased in the Space game and rebounded in BG2, consistent with a carryover/adaptation effect. Effect sizes for the Space drop and Space to BG2 recovery were large (partial $\eta^2 = 0.419$, $dz \approx 0.94$), emphasizing practical significance. Responder analysis identified participants for whom Space influenced subsequent performance, while group-level differences favored Healthy participants but were not statistically significant. Subjective measures (presence, vividness, TLX) did not strongly predict accuracy, suggesting that the Space to BG2 effect is primarily reflected in objective performance. Figure 7.12 shows mean trajectories of accuracy across games.

7.4 Discussion

These between-group trends should be interpreted very cautiously due to the small n (6 healthy, 3 SCI). This pilot study evaluated the feasibility

and preliminary effects of a sequential BCI–VR paradigm consisting of a baseline Ball Game (BG1), a microgravity-simulated Space Game, and a post-exposure Ball Game (BG2). The results indicate that participants' performance, measured as online classification accuracy, was significantly influenced by the game context. Accuracy decreased during the Space game and partially rebounded in BG2, forming a U-shaped trajectory for Healthy participants, with a less pronounced recovery in SCI participants. Mixed-effects regression confirmed the significant drop in accuracy during the Space condition and partial recovery in BG2, while group differences favored Healthy participants but did not reach statistical significance. These findings suggest a carryover or adaptation effect, in which exposure to the novel microgravity-simulated environment temporarily challenged motor imagery control, followed by partial re-adaptation when returning to the baseline VR task. Responder analysis further revealed that some participants who experienced performance gains in BG2 also reported higher subjective control and immersion during the Space game, indicating that engagement and motivation may contribute to subsequent improvements in objective performance. SCI participants may exhibit lower BCI accuracy due to impaired corticospinal pathways, reduced motor imagery consistency, and altered sensorimotor rhythms (45), although stronger ERD does not necessarily translate to higher accuracy because classifier performance also depends on signal stability, separability between classes, and noise characteristics. Subjective measures of presence, vividness, and cognitive workload provided complementary insights. Presence scores tended to be higher in the Space and BG2 conditions compared to BG1, demonstrating that the immersive VR environment successfully engaged participants. Vividness ratings showed variability across individuals, and NASA-TLX effort ratings were highest during the Space game, consistent with the increased cognitive demands associated with performing motor imagery under 6° head-down tilt. However, correlations between subjective measures and accuracy were generally small and non-significant, suggesting that performance effects were primarily driven by task complexity and environmental challenges rather than participants' self-reported experience.

The findings demonstrate the feasibility of the sequential BCI–VR paradigm for eliciting measurable changes in performance and neural engagement. The observed accuracy drop during the Space game and subsequent recovery in BG2 highlight the potential of immersive VR to challenge and recalibrate

motor imagery-based control, supporting skill adaptation and transfer. These preliminary results indicate that embedding BCI control in progressively complex environments (231; 234) may be a promising approach for training and rehabilitation applications, particularly in scenarios requiring adaptation to altered or extreme conditions.

It is important to acknowledge the limitations of this study. As a pilot investigation, the sample size was small (n = 9 after exclusions), which limits statistical power and generalizability. The within-subject design and sequential exposure to tasks may introduce order effects, and the study did not include repeated sessions to evaluate longer-term adaptation or learning. Additionally, performance and subjective measures were collected only once per condition, restricting the assessment of sustained effects or learning trajectories. Despite these constraints, the study successfully validated the experimental workflow, real-time EEG acquisition, BCI integration with VR, and usability of the system, providing essential insights for future investigations.

These preliminary findings highlight the potential for developing more robust and adaptive BCI–VR systems. Future work in the field should include larger sample sizes, repeated sessions to assess learning and adaptation over time, and variations in task complexity and microgravity simulation. Incorporating richer neurophysiological metrics and adaptive algorithms could further optimize BCI performance and user experience. Ultimately, this approach offers a practical platform for investigating motor imagery-based adaptation in challenging environments and has the potential to inform the design of next-generation BCI–VR systems for training, rehabilitation, and operational applications.

7.5 Summary

To summarize, Part-A of the chapter presented a pilot study investigating the feasibility of a sequential BCI–VR paradigm combining a baseline Ball Game, a microgravity-simulated Space Game, and a post-exposure Ball Game. The study demonstrated that participants' performance was temporarily challenged during the Space game and partially recovered in BG2, indicating adaptation effects. Subjective measures of presence, vividness, and workload complemented these findings, revealing engagement and cognitive demand without strongly predicting performance. Despite the small sample size and single-session design, the results validate the experimental workflow and system usability. Overall,

this chapter establishes the proof-of-concept for integrating real-time EEG-based BCI control with immersive VR, providing a foundation for future studies and the development of adaptive BCI–VR systems for training, rehabilitation, and operational applications in altered environments.

Part B: Soft Robots and MI BCI

Soft robots, with their adaptable and pliable nature, have opened new avenues for exploration in human-machine interaction. Soft exoskeletons are highly dependent on their design, which gives researchers the freedom and creativity to design and manufacture exosuits for different regions of the body that require support. Pavone and Cafolla designed a 3D-printed soft finger exoskeleton and further explained the conceptual study of possibly using the exoskeleton with MI-based BCI (240).

Since the field is new and still holds many opportunities to be explored, the majority of the work to date has focused on upper limb robotics and exoskeletons. A full-body exo-suit or a lower limb exosuit, and operating soft robots operated through a BCI still largely remains to be explored and evaluated (241). As discussed in Chapter 4 on how MI training and exoskeleton intervention enhanced Steps Per Minute during exoskeleton intervention for SCI patients, possibly, a hybrid BCI system (EEG and other vitals) combined with soft exosuits may bring this research out of laboratories in real-life environments.

Soft robots can be manufactured in laboratories and are comparatively inexpensive compared to traditional exoskeletons, which may bring exosuits as a feasible implementation for daily use. However, there are still challenges in bringing these systems into risky situations where rigid support is required for walking, for instance, for people suffering from ALS/SCI or in the field of stroke rehabilitation. Exploring hybrid exoskeletons (a combination of traditional and soft exosuits) for supporting people with ALS/SCI may be helpful, considering the cost, safety, and flexibility of using exoskeletons in the real world.

While BCI-based assistance has been investigated with a focus on soft exosuits assisting hand-rehabilitation (118) or with strenuous arm acitivites (242), it is still an open challenge how BMI can be used for controlling soft manipulators. In this section, the first step towards solving this challenge is made by proposing a pipeline that lets the user steer a soft robot's end-effector in Cartesian space in an asynchronous manner. Asynchronous BCI refers to a type of neural interface that enables users to interact with external devices or systems without the need for synchronized timing between their brain activity and the output of the interface. This allows for more flexible and naturalistic control, as users can initiate commands or actions at their own pace, independent of specific temporal cues. The two key ingredients are a novel

mapping strategy transforming the brain signals into meaningful references and Cartesian impedance control. The latter is essential because it allows for preserving the robot's compliance in closed-loop (243). The proposed BMI pipeline is built around an HSA soft robot (244; 245), which relies on architected metamaterials and electrical actuation to elongate, bend, and twist. This makes the control problem especially challenging because of the peculiarity of these systems' dynamics, namely, underactuation and non-affinity in control. Motor imagery-based control gives the computational controller access to the privileged information of setpoints, which can be considered to be an upper bound on performance. This work presents a proof-of-concept engineering demonstration with a single participant (n=1).

The contributions of this work are:

1. Demonstrating BCI control for continuum soft robots with a single participant. This strategy is supported by experiments in which setpoint regulation was performed with a planar HSA robot and motor imagery

2. A Cartesian impedance controller for HSA robots, which is experimentally validated on a simple ADL task involving environment interaction: the user needs to steer the end-effector towards the tip of a hairspray container, apply force to release the fluid, and finally let the robot retreat from the contact.
3. Designing the experimental protocol and integrating the BCI with the soft robotic platform, enabling real-time control and evaluation of human-robot interaction.

7.6 Methodology

7.6.1 Experimental Protocol

The participant was given brief instructions about Motor Imagery signals and asked to imagine rest and right-hand movements. Following this, they went through training without feedback. This data was used to train the algorithm, followed by real-time feedback in the testing phase to get the algorithm's accuracy. This trial kept repeating until an accuracy of 65 % was obtained. Once an accuracy of 65 % or more is achieved, the participant could move the HSA in real-time.

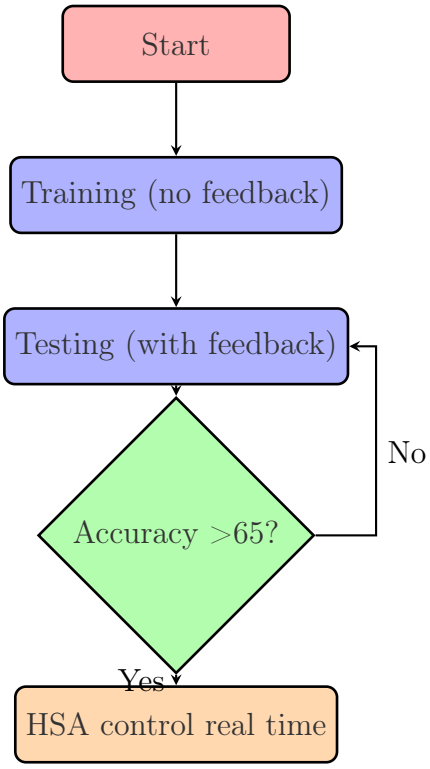

Figure 7.14: Protocol design of the Real-time HSA control

Once an accuracy level greater than 65% is achieved, the participant operates the HSA robot in real-time. A randomly generated dot is displayed with regard to the HSA robot, and the objective is to envision moving the HSA robot to the left or right to reach the position of the projected dot (setpoint regulation).

7.6.2 Tools used

Handed Shearing Auxetic (HSA) Setup

A robot consisting of four HSA rods, which were 3D printed via digital projection lithography is consideredfrom the photopolymer resin Carbon FPU 50. Each HSA rod is electrically actuated by a Dynamixel M-28 servo up to a maximum twist angle of $\phi_{\max} = 3.49\,\text{rad}$. The robot is attached platform-down to a motion capture cage with eight Optitrack Prime X13 cameras tracking at 200 Hz the pose of reflective markers attached to the end-effector of the HSA robot. It is estimated that the current Cartesian-space velocity of the end-effector with a Savitzky-Golay filter. Subsequently, a closed-form expression of the inverse kinematics of a CS model (245) to compute the current configuration q of the robot were leveraged. An image of the current shape of the robot is

considered, together with the present end-effector position (white dot), the attractor planned by the user (green square), the operational workspace (grey, see also Fig. 7.15) and if applicable, the goal position (red dot). The currently active axis of movement e_a with a double arrow and project the resulting image onto a black screen in the background of the motion capture cage were specified. The robot is operated with a ROS2 software framework[1]. The predicted and classified brain signals were received via TCP at a frequency of 18 Hz and move the attractor subsequently with $\Delta_x = 0.2\,\text{mm}$. The Cartesian impedance controller was evaluated using the gains $K_p = 300\,\text{N/m}$, $K_d = 1.5\,\text{Ns/m}$ at a frequency of 50 Hz and finally send the desired motor positions to the servos.

The entire control pipeline from measuring EEG signals to sending the actuation commands to the motors exhibits a maximum latency of (i.e., is upper-bounded by) 130 ms. For safety, the robot was operated at a distance within a closed environment, and the EEG-based BCI control was designed to break automatically if the participant's eyes remained closed continuously, preventing unintended robot movement.

EEG Device Setup

The data collection process utilized the flexEEG Neuroconcise device, seamlessly integrated with the OpenVibe software through the Lab Streaming Layer (LSL). This configuration facilitated data recording and cue presentation. To maintain accuracy, the sampling frequency was set at 250 Hz.

During EEG data acquisition, electrode impedance couldn't be assessed due to the limitations of the equipment. However, a meticulous approach was adopted to identify artifacts. Before data collection, a manual-guided protocol was followed, encompassing tests like jaw clenching and eye blinks. Subsequently, various artifact mitigation techniques were employed, including Independent Component Analysis (ICA) and bandpass filtering, to eliminate noisy signals.

The conductive gel was applied to minimize contact impedance and promote scalp interface stability to ensure optimal signal quality.

[1] https://github.com/tud-phi/ros2-hsa

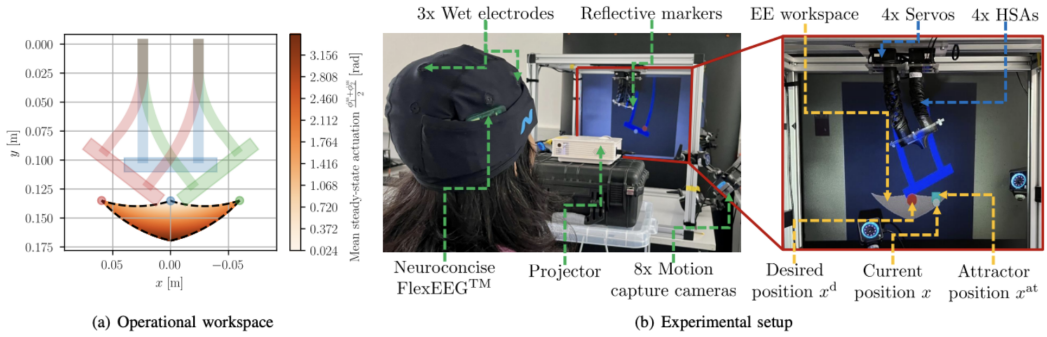

Figure 7.15: Experimental Setup with EEG and HSA robot.

7.7 Evaluation Matrix

7.7.1 Online Processing

EEG data processing

The 3-channel flexEEG Neuroconcise device was integrated with the OpenVibe software to acquire the EEG data and process it in real-time. This configuration facilitates data recording and cue presentation. The EEG signals were sampled at a frequency of 125 Hz with a pipeline that involves three bi-polar channels around the motor cortex: FC3-CP3, FCZ-CPZ, and FC4-CP4. After a notch filter of 50 Hz, Independent Component Analysis (ICA) was applied to extract three independent components from the recorded EEG data, which is represented by the equation $S(t) = W\,X(t)$, where $S(t)$ are the extracted independent components and W represents the unmixing matrix, allowing us to separate eye blink artefacts in EEG signals, which is critical for enhancing the accuracy. Subsequently, a Butterworth filter bank is applied to isolate specific frequency bands of interest, including 8-15 Hz and 15-42 Hz. The general equation for a Butterworth filter of order N for a given frequency range (e.g., 8-15 Hz) is

$$H(f) = \frac{1}{1 + \left(\frac{f}{f_c}\right)^{2N}}, \tag{7.3}$$

where $H(f)$ represents the frequency response of the filter, f is the frequency of the EEG signal, N is the filter order, and f_c is the critical frequency (i.e., center frequency) of the desired frequency band.

This enhances the ability to analyze EEG data by isolating and examining different frequency band components within the EEG signals. Once the signals

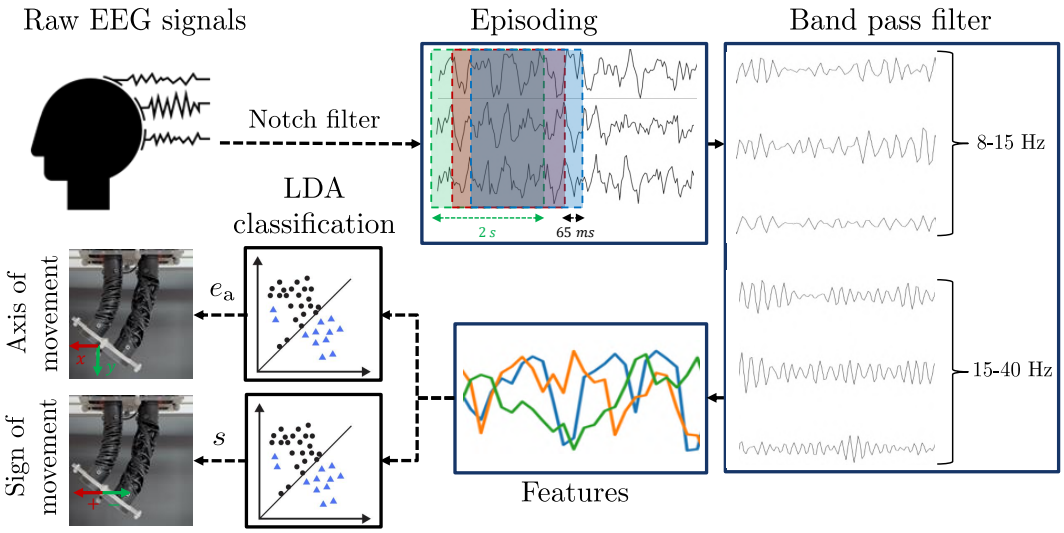

Figure 7.16: EEG data processing pipeline: The EEG data is acquired in real-time, pre-processed, and divided into episodes and subbands. Next, the extracted power features are extracted and passed to two LDA classifiers: the first outputs the axis of movement (for example, moving along the x- or y-axis), and the second provides the sign of movement (for example, positive or negative movement along the active axis). These commands are then used to move the attractor in Cartesian space.

are filtered in sub-bands and epoched with a duration of 2 s and time interval of 0.065 s, the features are extracted by the log of the power: $L_i(t) = \log(P_i(t))$, where the power $P_i(t) = |E_i(t)|^2$ is represented by square of magnitude of the EEG signal $E_i(t)$ at time instance t. These features are then provided to a classifier, LDA, due to its simplicity (21).

A second classifier is implemented with the same pipeline, where jaw clenching is provided as a muscle artefact that is classified v/s raw EEG data.

Setpoint Regulation

Nine setpoints were randomly generated within the operational workspace of the robot and displayed to the user as red circles over a duration of 540 seconds. The user was able to freely move the attractor to reach and maintain the end-effector at each setpoint(Fig. 7.15). Additionally, an experiment was conducted in which the computational controller had access to normally privileged information, allowing it to regulate the robot immediately toward the setpoints. By removing the BCI from the control loop, this provided a reference for the expected performance of the computational controller and served as a performance upper bound.

7.8 Results

First, the ERD/ERS behavior with respect to rest vs. motor imagination in Fig. 7.18 is analyzed. It is evident that the baseline of rest remained the same in both scenarios when the participant did not perform motor imagery, but as soon as the cue is presented at 0.0 s, a shift in power for the right-hand motor imagery with comparison to the rest state is noticeable.

With Setpoint Regulation, it is observed that the participant can reach the proximity of the setpoint within the allotted time of 60s in six out of nine times (i.e., 66.6%). For the successful steps, the average response time is 21.5 s. For the successful steps, the average response time is 21.5 s. However, as the protocol does not contain a command to let the attractor rest, it is challenging to keep the end-effector at the setpoint, and it is observed oscillations, particularly with respect to the x-coordinate. In the third experiment, the Cartesian impedance controller is asked to track the setpoints directly. The fast response time, a well-known characteristic of model-based control approaches, is evident. However,

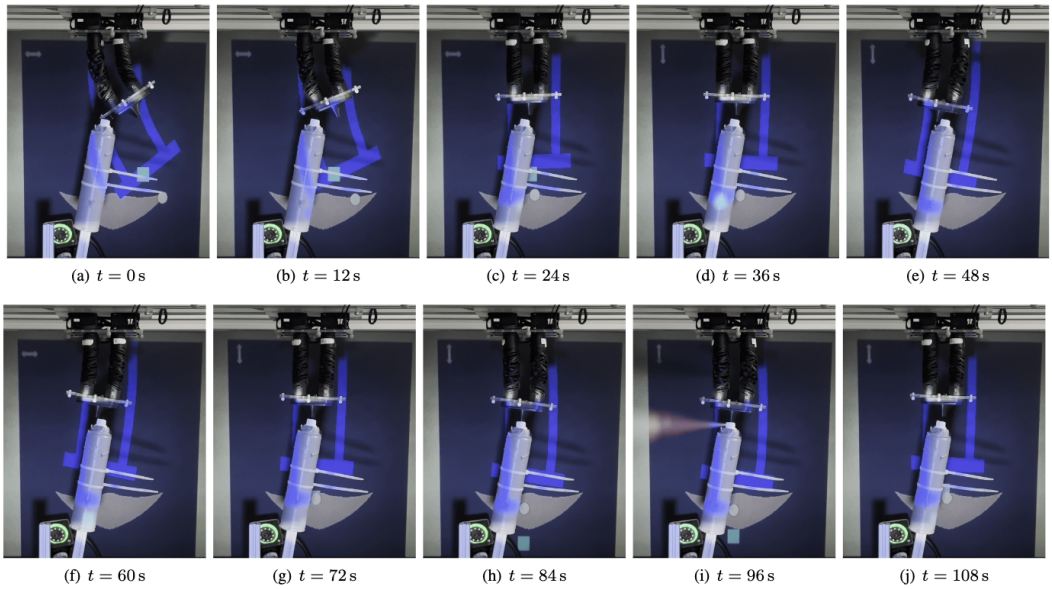

(a) $t = 0\,\mathrm{s}$ (b) $t = 12\,\mathrm{s}$ (c) $t = 24\,\mathrm{s}$ (d) $t = 36\,\mathrm{s}$ (e) $t = 48\,\mathrm{s}$

(f) $t = 60\,\mathrm{s}$ (g) $t = 72\,\mathrm{s}$ (h) $t = 84\,\mathrm{s}$ (i) $t = 96\,\mathrm{s}$ (j) $t = 108\,\mathrm{s}$

Figure 7.17: Sequence of still shots for completing a basic Activity of Daily Living (ADL) by controlling the robot with EEG-based motor imagery.

the errors in the model (for example, caused by hysteresis or unmodelled nonlinearities) (245), together with the lack of integral action, lead to steady-state errors.

Finally, the ADL task is considered to release hair spray using the end-effector of the HSA robot. A sequence of still shots is presented in Fig. 7.17. Already during the first attempt, the participant can steer the end-effector toward the button, apply force, and release the fluid within 86 s; when the manipulator is in contact with the object at time 74 s to 104 s.

Also, it is noticed that the end-effector does not need to be perfectly aligned with the centre of the button and can still complete the task successfully due to the compliance of the closed-loop system in the tangential direction.

7.9 Discussion

part-B of this chapter presents a pilot demonstration of integrating motor imagery-based BCI control with a soft continuum robot (HSA) in a real-time setting. The results indicate that a participant can successfully steer the end-effector in Cartesian space, regulate setpoints, and perform a simple ADL task, such as pressing the button of a hairspray container. The asynchronous BCI paradigm, combined with a Cartesian impedance controller, allowed the robot

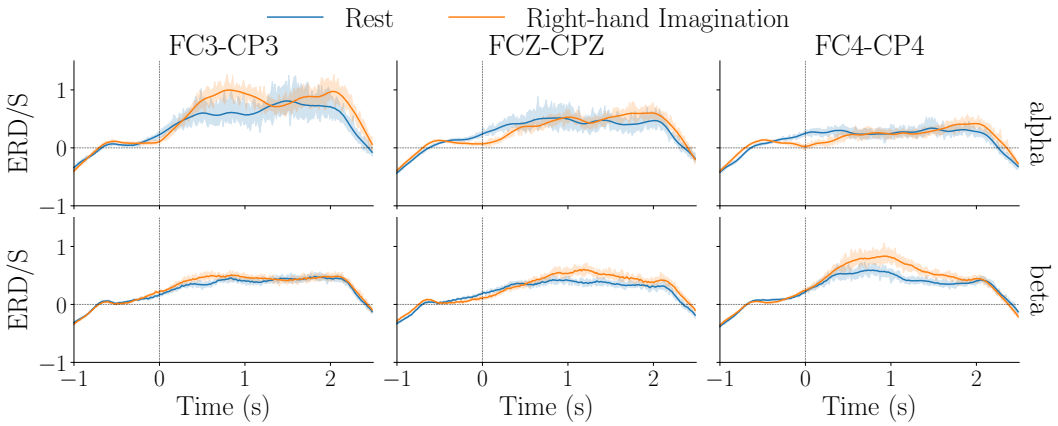

Figure 7.18: Event Related Synchronization/Desynchronization for rest v/s right-hand imagination during training.

to retain compliance, compensating for small misalignments and unmodelled dynamics, which is a critical advantage of soft robotic systems over rigid counterparts. The observed oscillations in setpoint tracking highlight the challenges of using BCI control for soft robots, including the limited precision of neural signals, the lack of integral action in the controller, and the inherent nonlinearity and underactuation of the HSA system. Nonetheless, the participant was able to complete the ADL task, demonstrating that even imperfect control can be functional in practice.

Given that this study is based on a single participant, the findings should be interpreted as preliminary and proof-of-concept rather than definitive evidence. Limitations include the small sample size, absence of a control group, and the simplicity of the task relative to real-world applications. Moreover, EEG-based MI control remains subject to variability in neural signal quality, training duration, and participant engagement, which may influence performance. Despite these constraints, the study demonstrates the feasibility of combining BCI with soft robots for practical manipulation tasks, suggesting that such systems could be extended to assist individuals with motor impairments in rehabilitation or daily activities. Future work should explore multi-participant studies, longer-term training, hybrid BCI paradigms combining EEG with other physiological signals, and more complex multi-DOF tasks to improve generalizability and robustness.

Overall, these preliminary findings indicate that soft robotic systems controlled via MI-based BCIs have the potential to provide safe, flexible, and

adaptive interfaces for assistive technology. By leveraging the inherent compliance of soft robots and asynchronous neural control, this approach could bridge the gap between laboratory demonstrations and real-world applications, laying the foundation for future neuro-robotic systems that support rehabilitation, skill training, and everyday activities.

7.10 Summary

To summarize Part-B of this chapter, it demonstrated the feasibility of real-time motor imagery-based BCI control of a soft continuum robot. Using an asynchronous BCI paradigm and Cartesian impedance control, the participant successfully performed setpoint regulation and a simple ADL task, highlighting the adaptability and compliance of soft robots. While the study is limited by a single participant and simplified tasks, it establishes a proof-of-concept for combining BCI with soft robotic manipulators. These results provide a foundation for future research on multi-participant studies, hybrid BCI systems, and complex task execution, paving the way toward practical applications in rehabilitation and assistive technology.

Chapter 8

Conclusion

""Research is a team sport" and "It takes a village to raise a child." - Anonymous. Although a PhD is a very personal journey and an individual accomplishment, usually, there is a team in the background supporting you to get to the milestone. This could be your supervisors, other PhDs or postdocs, either in your research group or just in the same lab, your friends and of course your family."

- Prof. Noel O' Connor, on behalf of ML-Labs at DCU

8.1 Contribution of the thesis

This PhD thesis set out to investigate whether systematic enhancements across the key components of MI-BCI systems—encompassing signal acquisition, user training, algorithmic processing, and interface design—can enable reliable, motivating, and practical MI-BCI use outside laboratory settings, thereby supporting ADL for both healthy individuals and people with neuromuscular conditions such as spinal cord injury. The findings of this work demonstrate that MI-BCIs can indeed transition from controlled experimental paradigms to real-world applicability through a combined approach of carefully optimizing each subsystem (User Training, Algorithms, Interface and their application) within the BCI set-up. These contributions are listed chapterwise below:

1. Chapter 4 contributes to testing the hypothesis that engaging in MI practice before and after exoskeleton-assisted walking can enhance the efficacy of exoskeleton-based rehabilitation. It further evaluates whether exoskeleton-assisted walking modulates post-intervention MI performance, thereby revealing a potential bidirectional relationship between MI training and robotic rehabilitation. By examining MI-related EEG activity across pre- and post-training sessions, this chapter explores how integrating MI sessions around exoskeleton use may foster mutual enhancement and lay the groundwork for future closed-loop MI–BCI–exoskeleton rehabilitation frameworks. The characterization of MI signals in SCI participants confirmed that, despite motor impairments, reliable neurophysiological activity can be elicited and classified. ERD/ERS patterns and classification accuracy metrics demonstrated that SCI individuals retain the neural substrates necessary for MI–BCI control. These findings validate the feasibility of MI-based interventions to support rehabilitation outcomes in clinical populations and establish a foundation for subsequent developments in user training, algorithmic optimization, and interface design.

2. Chapter 5 emphasizes the critical role of training optimization in enhancing motor imagery (MI) skill acquisition. Through comparative analysis of visual, auditory, and immersive VR instructional modalities, this chapter demonstrates that immersive VR environments significantly improve both MI signal quality and participant engagement. The contributions of this

chapter include conducting an extensive user study to examine the impact of varied cue presentation mediums with respect to their relevance to ADL and MI training; performing comprehensive qualitative and quantitative analyses to assess user preferences and validate the underlying hypothesis through multiple evaluation metrics; and implementing analyses using only three EEG channels to minimize hardware requirements—thereby promoting the feasibility of MI–BCI training for practical, real-world applications.

3. Chapter 6 presents the algorithmic advancements that strengthen the practicality and real-world applicability of motor imagery–based brain–computer interfaces (MI–BCIs). By combining Fisher Ratio and Pearson Correlation techniques, this chapter demonstrates effective single-channel classification, thereby reducing the number of required electrodes without compromising performance. This simplification enhances hardware efficiency and user comfort, promoting the feasibility of portable and user-friendly MI–BCI systems. Additionally, the implementation of advanced classifiers, including Gaussian Process (GP) models, provided robust real-time control under conditions of inter-subject variability and environmental noise, ensuring smoother and more reliable MI–BCI operation. The contributions of this chapter include: (Part A) evaluating the robustness of single-channel–based feature extraction methods across datasets and identifying the most informative electrode sites; and (Part B) exploring adaptive classifier concepts and threshold-setting mechanisms through emerging algorithms such as Gaussian Process models, and reporting their offline classification accuracies. These algorithmic innovations collectively advance the portability, robustness, and usability of MI–BCI systems for everyday and rehabilitation contexts.

4. Chapter 7 highlights the critical importance of interface design for translating motor imagery–based brain–computer interfaces (MI–BCIs) into real-world applications. Immersive virtual reality (VR) environments, including microgravity simulations, were shown—through preliminary pilot data—to enhance user engagement following the Space Game and improve MI signal discriminability. These findings demonstrate the value of embedding MI tasks within ecologically valid, engaging contexts that reflect real-life scenarios. Complementarily, the development of safe, compliant

robotic interfaces enabled continuous, interactive control for executing functional activities of daily living (ADL), thereby extending MI–BCI use beyond discrete, trial-based paradigms toward sustained, goal-directed interaction. The contributions of this chapter include: (Part A) enhancing MI–BCI performance and user experience through immersive VR environments that replicate realistic contexts such as microgravity; and (Part B) developing safe and compliant robotic systems that facilitate continuous, goal-oriented ADL execution. Together, these studies bridge the gap between controlled laboratory paradigms and practical, user-centered MI–BCI applications in rehabilitation and assistive technology.

The integration of robust algorithms, realistic VR simulations, and compliant robotics collectively demonstrates that real-world MI–BCI applications are achievable when all subsystems are optimized in concert. The merit of this thesis lies in its holistic approach. By addressing training, algorithmic processing, and interface design, this work bridges the gap between laboratory MI-BCI research and practical deployment. It provides a methodological framework for developing MI-BCI systems that are not only technically robust but also motivating, safe, and user-centered, supporting both rehabilitation and daily living. The contributions span multiple subsystems: identifying reliable MI signals in SCI, designing immersive training protocols, developing robust single-channel and advanced classifiers, and implementing interfaces capable of continuous and safe task execution. Together, these advances lay the groundwork for MI-BCIs that can meaningfully support independence and quality of life.

While this research represents a significant step toward practical MI-BCI deployment, future work can expand its impact by exploring multiple real-world scenarios in home environments, integrating multimodal biosignals for greater robustness, and conducting longitudinal studies to assess skill retention and functional outcomes. Extending these approaches to diverse participant populations will further ensure inclusivity and generalizability.

In conclusion, this thesis demonstrates that enhancing MI-BCI subsystems in an integrated manner enables reliable, motivating, and functional use outside laboratory settings. By systematically addressing signal acquisition, user training, algorithmic robustness, and interface design, it provides both empirical evidence and practical strategies for translating MI-BCI research into real-world

applications that support ADL for healthy individuals and persons with SCI.

8.2 Future of MI-BCI Systems

There are some limitations to the studies conducted in this thesis, which open up future directions for this research:

- **Incorporation of Haptic Feedback:** The current user studies were conducted with visual and auditory media only. Future work can integrate haptic feedback mechanisms to enhance immersion and sensorimotor engagement. Haptics may also strengthen the link between imagined and perceived movement, potentially improving motor imagery (MI) performance and user embodiment within the system.

- **Transition from Offline to Online Implementation:** The algorithms developed in this work were evaluated in an offline setting. Future research should focus on real-time (online) implementation to assess system adaptability and responsiveness during live interaction. Moreover, integrating these algorithms into deep learning frameworks could enhance classification robustness, temporal generalization, and model interpretability for real-world use.

- **Large-Scale Validation:** The current applications and interfaces were evaluated in pilot studies with a limited sample size. Future studies should include larger and more diverse populations to evaluate scalability, usability, and clinical effectiveness. Longitudinal trials (over a period of months) could also provide insight into learning effects, retention, and long-term rehabilitation outcomes.

- **Exploration of Alternative and Hybrid Devices:** As discussed in Chapter 3, different MI acquisition devices could be investigated, such as dry-electrode EEG systems, wearable EEG headsets, or hybrid setups combining EEG with other modalities. To bring MI-BCI systems beyond laboratory environments, future studies should explore more user-friendly and adaptive interfaces that integrate wearable sensors, eye-tracking, speech-based commands, or soft robotics. Such systems could provide multimodal feedback — combining neural, visual, auditory, and

proprioceptive cues — to create an immersive and personalized experience. This would improve comfort, reduce setup time, and increase practicality in home-based or clinical environments. This also opens up a vision with state-of-art interfaces for excellent and safe user experience depicted in Figure 8.1

- **Soft Robotics and Wearable Exosuits:** Soft robotic exosuits represent a promising avenue due to their flexibility, light weight, and comfort. Future research could explore the integration of MI-BCI systems with soft exosuits for upper or lower limb rehabilitation, leveraging recent advancements in flexible actuators and smart textiles. These systems could enable continuous and safe at-home rehabilitation while adapting to users' movement intentions in real time.

- **Gamified and VR-Enhanced Rehabilitation:** The incorporation of gamification and virtual reality (VR) elements can enhance motivation and engagement during MI training. Future developments should explore personalized VR environments, adaptive difficulty levels, and reward systems that encourage consistent practice. Such systems can be extended to home-based rehabilitation platforms, providing real-time feedback and remote monitoring by clinicians.

- **System-Level Integration Toward Comprehensive Rehabilitation:** Ultimately, each subsystem developed in this research — including MI decoding, feedback presentation, and interface control — can be integrated into a holistic rehabilitation ecosystem. This would bridge neurotechnology, virtual environments, and assistive robotics into a unified platform for daily living and therapy, moving MI-BCI from controlled experiments toward practical, home-based clinical use.

Finally, a conceptual home-based setup is expressed in Fig. 8.2 with a vision that this technology becomes part of daily living to assist humans in best possible ways.

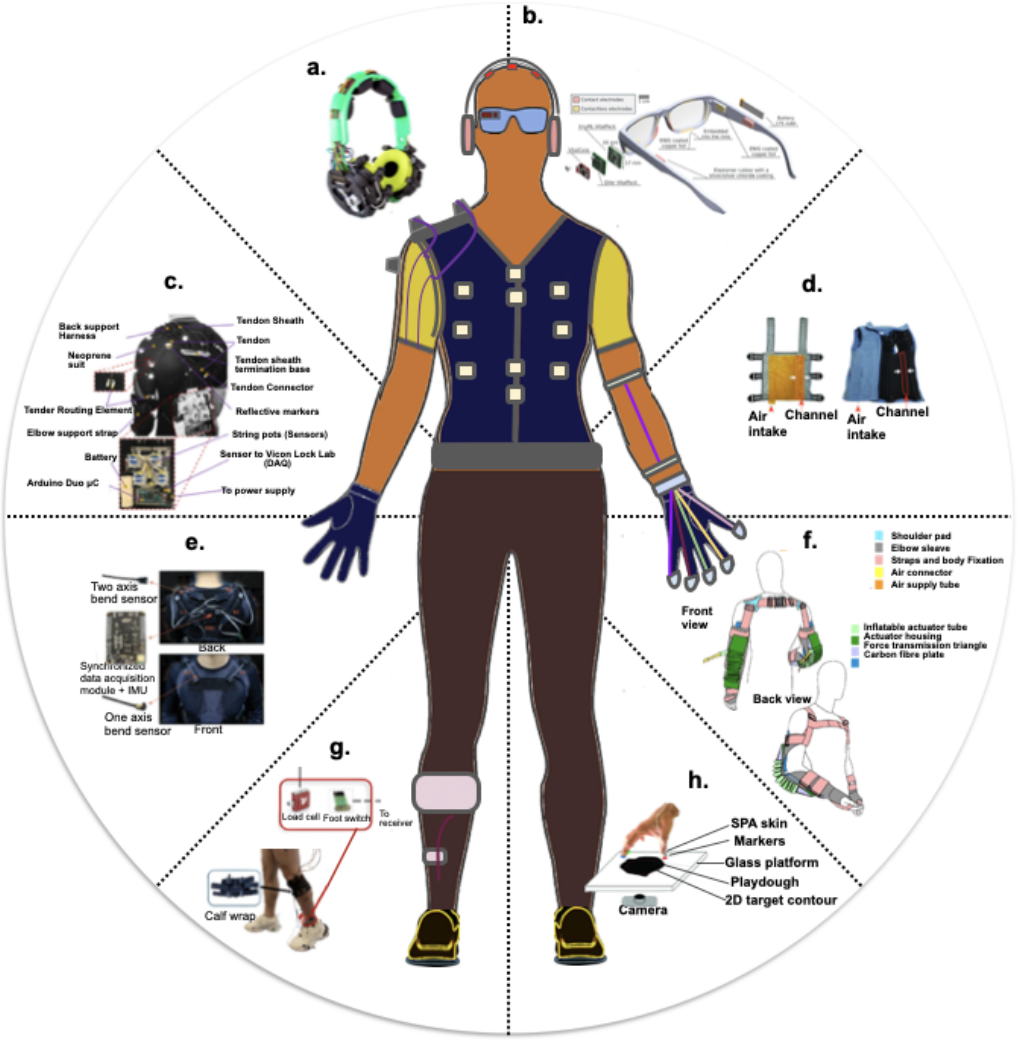

Figure 8.1: Possible future interfaces for MI. (a.) Wearable electrodes integrated in headphones, from ref (158) with permission copyright©2024, The Authors (b.) Smart glasses from ref (246) with permission Copyright ©2020 American Chemical Society (c.) Soft shoulder exoskeleton adopted from ref(140) with permission copyright©2020, IEEE. (d.) Smart Hug Vest adopted from ref(141) with permission copyright©2021, IEEE. (e.) Wearable textile IMU sensors reprinted from ref(163) with permission copyright©2024, IEEE. (f.)Elbow exoskeleton reprinted from ref(162) published with CC-BY 4.0 Copyright©2021, The Author(s). (g.) Wearable ankle exoskeleton reprinted from ref(161) published with CC-BY 4.0 copyright©2024, The Authors. (h.) Wearable haptics (soft pneumatic actuators) for fingers reprinted from ref(159) published with CC-BY4.0, copyright©, The Authors.

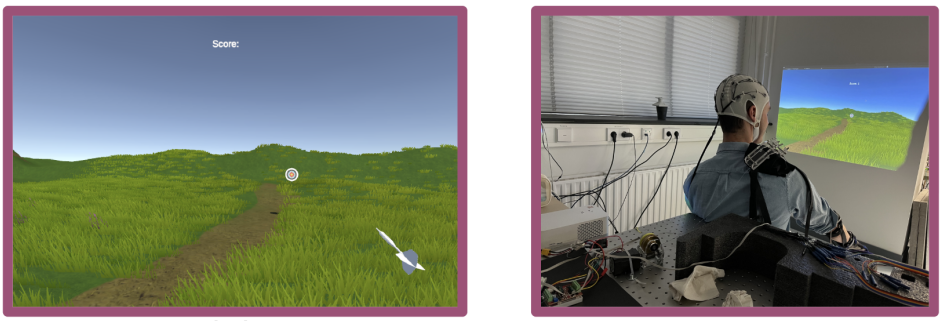

Figure 8.2: Conceptual Wearable Setup incorporating (a.)game-based rehabilitation with (b.) soft wearable exosuit (139) for Home-based Setup

"You only live once, but if you do it right, once is enough"
- Mr. Ghanshyamji Joshi, On behalf of my Maternal Family.

Bibliography

[1] S. Varona-Moya, F. Velasco-Alvarez, S. Sancha-Ros, Á. Fernández-Rodríguez, M. J. Blanca, and R. Ron-Angevin, "Wheelchair navigation with an audio-cued, two-class motor imagery-based brain-computer interface system," in *2015 7th International IEEE/EMBS Conference on Neural Engineering (NER)*, pp. 174–177, IEEE, 2015.

[2] M. Barsotti, D. Leonardis, C. Loconsole, M. Solazzi, E. Sotgiu, C. Procopio, C. Chisari, M. Bergamasco, and A. Frisoli, "A full upper limb robotic exoskeleton for reaching and grasping rehabilitation triggered by MI-BCI," in *2015 IEEE international conference on rehabilitation robotics (ICORR)*, pp. 49–54, IEEE, 2015.

[3] R. A. Ramadan and A. V. Vasilakos, "Brain computer interface: control signals review," *Neurocomputing*, vol. 223, pp. 26–44, 2017.

[4] G. Schalk and E. C. Leuthardt, "Brain-computer interfaces using electrocorticographic signals," *IEEE reviews in biomedical engineering*, vol. 4, pp. 140–154, 2011.

[5] R. Sitaram, A. Caria, R. Veit, T. Gaber, G. Rota, A. Kuebler, and N. Birbaumer, "FMRI brain-computer interface: a tool for neuroscientific research and treatment," *Computational intelligence and neuroscience*, vol. 2007, 2007.

[6] S. M. Coyle, T. E. Ward, and C. M. Markham, "Brain–computer interface using a simplified functional near-infrared spectroscopy system," *Journal of neural engineering*, vol. 4, no. 3, p. 219, 2007.

[7] J. Mellinger, G. Schalk, C. Braun, H. Preissl, W. Rosenstiel, N. Birbaumer, and A. Kübler, "An MEG-based brain–computer interface (BCI)," *Neuroimage*, vol. 36, no. 3, pp. 581–593, 2007.

[8] R. Sharma and H. K. Meena, "Emerging trends in EEG signal processing: A systematic review," *SN Computer Science*, vol. 5, no. 4, p. 415, 2024.

[9] F. L. Da Silva, "EEG: origin and measurement," in *EEG-fMRI: physiological basis, technique, and applications*, pp. 23–48, Springer, 2023.

[10] H. Altaheri, G. Muhammad, M. Alsulaiman, S. U. Amin, G. A. Altuwaijri, W. Abdul, M. A. Bencherif, and M. Faisal, "Deep learning techniques for classification of electroencephalogram (EEG) motor imagery (MI) signals: A review," *Neural Computing and Applications*, vol. 35, no. 20, pp. 14681–14722, 2023.

[11] V. More and K. George, "Incorporating Motor Imagery-Controlled Gaming into Paralysis Rehabilitation," in *2024 IEEE First International Conference on Artificial Intelligence for Medicine, Health and Care (AIMHC)*, pp. 72–77, IEEE, 2024.

[12] J. W. Choi, B. H. Kim, S. Huh, and S. Jo, "Observing actions through immersive virtual reality enhances motor imagery training," *IEEE Transactions on Neural Systems and Rehabilitation Engineering*, vol. 28, no. 7, pp. 1614–1622, 2020.

[13] W. Li, Y. Ma, K. Shao, Z. Yi, W. Cao, M. Yin, T. Xu, and X. Wu, "The Human-Machine Interface Design Based on sEMG and Motor Imagery EEG for Lower Limb Exoskeleton Assistance System," *IEEE Transactions on Instrumentation Measurement*, vol. 73, p. 3375980, 2024.

[14] J. R. Wolpaw, N. Birbaumer, D. J. McFarland, G. Pfurtscheller, and T. M. Vaughan, "Brain–computer interfaces for communication and control," *Clinical neurophysiology*, vol. 113, no. 6, pp. 767–791, 2002.

[15] B. U. Forstmann, M. C. Keuken, and A. Alkemade, "An introduction to human brain anatomy," in *An introduction to model-based cognitive neuroscience*, pp. 71–89, Springer, 2015.

[16] M. A. Reslan, M. Tabet, Y. Yehya, A. Shaito, and F. Kobeissy, "The brain and exercise: in sickness and in health," *Front. Young Minds*, vol. 10, 2022.

[17] Lymphlassie, "Neuroplasticity and Body Image," 2020.

[18] R. Shriram, M. Sundhararajan, and N. Daimiwal, "EEG based cognitive workload assessment for maximum efficiency," *Int. Organ. Sci. Res. IOSR*, vol. 7, pp. 34–38, 2013.

[19] S.-H. Kim, O.-K. Lee, and D. J. Kim, "Study of Practical Method for International 10 20 Electrode System," *Korean Journal of Clinical Laboratory Science*, vol. 53, no. 1, pp. 60–67, 2021.

[20] G. Pfurtscheller and C. Neuper, "Motor imagery activates primary sensorimotor area in humans," *Neuroscience letters*, vol. 239, no. 2-3, pp. 65–68, 1997.

[21] F. Lotte, "A tutorial on EEG signal-processing techniques for mental-state recognition in brain–computer interfaces," *Guide to brain-computer music interfacing*, pp. 133–161, 2014.

[22] G. Pfurtscheller, C. Neuper, G. Muller, B. Obermaier, G. Krausz, A. Schlogl, R. Scherer, B. Graimann, C. Keinrath, D. Skliris, *et al.*, "Graz-BCI: state of the art and clinical applications," *IEEE Transactions on neural systems and rehabilitation engineering*, vol. 11, no. 2, pp. 177–180, 2003.

[23] T.-j. Luo, "Dual selections based knowledge transfer learning for cross-subject motor imagery EEG classification," *Frontiers in Neuroscience*, vol. 17, p. 1274320, 2023.

[24] H. Alkadhi, P. Brugger, S. H. Boendermaker, G. Crelier, A. Curt, M.-C. Hepp-Reymond, and S. S. Kollias, "What disconnection tells about motor imagery: evidence from paraplegic patients," *Cerebral cortex*, vol. 15, no. 2, pp. 131–140, 2005.

[25] M. Jeannerod, "Mental imagery in the motor context," *Neuropsychologia*, vol. 33, no. 11, pp. 1419–1432, 1995.

[26] G. R. Müller-Putz, R. Scherer, G. Pfurtscheller, and R. Rupp, "EEG-based neuroprosthesis control: a step towards clinical practice," *Neuroscience letters*, vol. 382, no. 1-2, pp. 169–174, 2005.

[27] G. Prasad, P. Herman, D. Coyle, S. McDonough, and J. Crosbie, "Applying a brain-computer interface to support motor imagery practice in

people with stroke for upper limb recovery: a feasibility study," *Journal of neuroengineering and rehabilitation*, vol. 7, no. 1, pp. 1–17, 2010.

[28] C. S. L. Tsui, J. Q. Gan, and H. Hu, "A self-paced motor imagery based brain-computer interface for robotic wheelchair control," *Clinical EEG and neuroscience*, vol. 42, no. 4, pp. 225–229, 2011.

[29] K. Lee, D. Liu, L. Perroud, R. Chavarriaga, and J. d. R. Millán, "A brain-controlled exoskeleton with cascaded event-related desynchronization classifiers," *Robotics and Autonomous Systems*, vol. 90, pp. 15–23, 2017.

[30] D. J. McFarland and J. R. Wolpaw, "Brain–computer interface use is a skill that user and system acquire together," *PLoS biology*, vol. 16, no. 7, p. e2006719, 2018.

[31] S. Sreeja, J. Rabha, K. Nagarjuna, D. Samanta, P. Mitra, and M. Sarma, "Motor imagery EEG signal processing and classification using machine learning approach," in *2017 International Conference on New Trends in Computing Sciences (ICTCS)*, pp. 61–66, IEEE, 2017.

[32] A. Capozio, M. Graham, R. Ichiyama, and S. L. Astill, "A single session of motor imagery paired with spinal stimulation improves manual dexterity and increases cortical excitability after spinal cord injury," *Clinical Neurophysiology*, 2025.

[33] S. Saha, K. A. Mamun, K. Ahmed, R. Mostafa, G. R. Naik, S. Darvishi, A. H. Khandoker, and M. Baumert, "Progress in brain computer interface: Challenges and opportunities," *Frontiers in systems neuroscience*, vol. 15, p. 578875, 2021.

[34] R. Lindsay, A. Kittel, and M. Spittle, "Motor imagery and action observation: a case for the integration of 360 VR," *Frontiers in Psychology*, vol. 13, p. 880185, 2022.

[35] X. J. Liu, S. Ge, A. Cordova, Z. Yaghi, B. Y. Jiang, G. H. Yue, and W. X. Yao, "Elderly may benefit more from motor imagery training in gaining muscle strength than young adults: a systematic review and Meta-analysis," *Frontiers in Psychology*, vol. 13, p. 1052826, 2023.

[36] S. Tinaz, S. Kamel, S. S. Aravala, M. Elfil, A. Bayoumi, A. Patel, D. Scheinost, R. Sinha, and M. Hampson, "Neurofeedback-guided kinesthetic motor imagery training in Parkinson's disease: Randomized trial," *NeuroImage: Clinical*, vol. 34, p. 102980, 2022.

[37] J. A. Binks, J. R. Emerson, M. W. Scott, C. Wilson, P. Van Schaik, and D. L. Eaves, "Enhancing upper-limb neurorehabilitation in chronic stroke survivors using combined action observation and motor imagery therapy," *Frontiers in Neurology*, vol. 14, p. 1097422, 2023.

[38] R. S. Lindsay, P. Larkin, A. Kittel, and M. Spittle, "Mental imagery training programs for developing sport-specific motor skills: a systematic review and meta-analysis," *Physical Education and Sport Pedagogy*, vol. 28, no. 4, pp. 444–465, 2023.

[39] R. Zhang, S. Feng, N. Hu, S. Low, M. Li, X. Chen, and H. Cui, "Hybrid Brain-Computer Interface Controlled Soft Robotic Glove for Stroke Rehabilitation," *IEEE Journal of Biomedical and Health Informatics*, 2024.

[40] J. Zhang and M. Wang, "A survey on robots controlled by motor imagery brain-computer interfaces," *Cognitive Robotics*, vol. 1, pp. 12–24, 2021.

[41] S. Aggarwal and N. Chugh, "Review of machine learning techniques for EEG based brain computer interface," *Archives of Computational Methods in Engineering*, vol. 29, no. 5, pp. 3001–3020, 2022.

[42] M. Z. Baig, N. Aslam, and H. P. Shum, "Filtering techniques for channel selection in motor imagery EEG applications: a survey," *Artificial intelligence review*, vol. 53, no. 2, pp. 1207–1232, 2020.

[43] V. Kohli, U. Tripathi, V. Chamola, B. K. Rout, and S. S. Kanhere, "A review on Virtual Reality and Augmented Reality use-cases of Brain Computer Interface based applications for smart cities," *Microprocessors and Microsystems*, vol. 88, p. 104392, 2022.

[44] A. Kawala-Sterniuk, N. Browarska, A. Al-Bakri, M. Pelc, J. Zygarlicki, M. Sidikova, R. Martinek, and E. J. Gorzelanczyk, "Summary of over fifty years with brain-computer interfaces—a review," *Brain Sciences*, vol. 11, no. 1, p. 43, 2021.

[45] S. C. Cramer, E. L. Orr, M. J. Cohen, and M. G. Lacourse, "Effects of motor imagery training after chronic, complete spinal cord injury," *Experimental brain research*, vol. 177, no. 2, pp. 233–242, 2007.

[46] E. Opsommer, O. Chevalley, and N. Korogod, "Motor imagery for pain and motor function after spinal cord injury: a systematic review," *Spinal cord*, vol. 58, no. 3, pp. 262–274, 2020.

[47] V. Quiles, L. Ferrero, E. Iáñez, M. Ortiz, Á. Megía, N. Comino, Á. M. Gil-Agudo, and J. M. Azorín, "Usability and acceptance of using a lower-limb exoskeleton controlled by a bmi in incomplete spinal cord injury patients: a case study," in *2020 42nd Annual International Conference of the IEEE Engineering in Medicine & Biology Society (EMBC)*, pp. 4737–4740, IEEE, 2020.

[48] K. C. Davis, B. Meschede-Krasa, I. Cajigas, N. W. Prins, C. Alver, S. Gallo, S. Bhatia, J. H. Abel, J. A. Naeem, L. Fisher, *et al.*, "Design-development of an at-home modular brain–computer interface (BCI) platform in a case study of cervical spinal cord injury," *Journal of neuroengineering and rehabilitation*, vol. 19, no. 1, p. 53, 2022.

[49] Z. Cui, Y. Li, S. Huang, X. Wu, X. Fu, F. Liu, X. Wan, X. Wang, Y. Zhang, H. Qiu, *et al.*, "BCI system with lower-limb robot improves rehabilitation in spinal cord injury patients through short-term training: a pilot study," *Cognitive Neurodynamics*, vol. 16, no. 6, pp. 1283–1301, 2022.

[50] F. Zahra, "BCI-Based Upper Limb Motor Remodeling Training System Post-Spinal Cord Injury," *Injury and Rehabilitation Care*, vol. 1, no. 1, pp. 1–12, 2025.

[51] E. R. S. Serafini, C. D. Guerrero-Mendez, T. F. Bastos-Filho, A. Cotrina-Atencio, A. F. de Azevedo Dantas, D. Delisle-Rodriguez, and C. C. do Espírito-Santo, "Gait training-based motor imagery and EEG neurofeedback in Lokomat: A clinical intervention with complete spinal cord injury individuals," *IEEE Transactions on Neural Systems and Rehabilitation Engineering*, vol. 32, pp. 1896–1905, 2024.

[52] C. F. Blanco-Diaz, E. R. da Silva Serafini, T. Bastos-Filho, A. F. O. de Azevedo Dantas, C. C. do Espirito Santo, and D. Delisle-Rodriguez,

"A gait imagery-based brain-computer interface with visual feedback for spinal cord injury rehabilitation on lokomat," *IEEE Transactions on Biomedical Engineering*, 2024.

[53] D. Ma, R. R. Zeng, S. S. Chan, Y. Pan, and J. J. Zhang, "Case report: Movement-related neuroplasticity in a patient after spinal cord injury in response to task-oriented bimanual training," *Frontiers in Human Neuroscience*, vol. 18, p. 1502517, 2025.

[54] L. Toni, V. de Seta, S. Romeni, V. Mendez, L. Pollina, D. Emedoli, L. Albano, S. Iannaccone, P. Mortini, and S. Micera, "Decoding Lower Limb Motor Attempts from EEG Signals in a Spinal Cord Injury Patient with Epidural Electrical Implant," in *International Conference on NeuroRehabilitation*, pp. 68–72, Springer, 2024.

[55] F. Xu, M. Liu, X. Chen, Y. Yan, J. Zhao, Y. Liu, J. Zhao, S. Pang, S. Yin, J. Leng, *et al.*, "Time–frequency–space transformer EEG decoding for spinal cord injury," *Cognitive Neurodynamics*, vol. 18, no. 6, pp. 3491–3506, 2024.

[56] M. S. I. Joy, M. H. Chowdhury, K. Hasan, S. Mutsuddi, and Q. D. Hossain, "Spiking Neural Network Approach for Binary Classification of Hand Movements of Spinal Cord Injured Patients," in *2025 International Conference on Electrical, Computer and Communication Engineering (ECCE)*, pp. 1–5, IEEE, 2025.

[57] F. Xu, Y. Lou, Y. Deng, Z. Lun, P. Zhao, D. Yan, Z. Han, Z. Wu, C. Feng, L. Chen, *et al.*, "Motor imagery EEG decoding based on TS-former for spinal cord injury patients," *Brain Research Bulletin*, vol. 224, p. 111298, 2025.

[58] B. M. Dekleva, R. H. Chowdhury, A. P. Batista, S. M. Chase, B. M. Yu, M. L. Boninger, and J. L. Collinger, "Motor cortex retains and reorients neural dynamics during motor imagery," *Nature human behaviour*, vol. 8, no. 4, pp. 729–742, 2024.

[59] R. Kumari, A. Dybus, M. Purcell, and A. Vučković, "Motor priming to enhance the effect of physical therapy in people with spinal cord injury," *The Journal of Spinal Cord Medicine*, vol. 48, no. 2, pp. 312–326, 2025.

[60] M. A. Hasan, P. Sattar, S. A. Qazi, M. Fraser, and A. Vuckovic, "Brain networks with modified connectivity in patients with neuropathic pain and spinal cord injury," *Clinical EEG and Neuroscience*, vol. 55, no. 1, pp. 88–100, 2024.

[61] N. Hesam-Shariati, L. Alexander, K. Y. Chen, A. Craig, P. A. Glare, M. P. Jensen, C.-T. Lin, J. H. McAuley, J. W. Middleton, G. L. Moseley, *et al.*, "A home-based self-directed EEG neurofeedback intervention for people with chronic neuropathic pain following spinal cord injury (the StoPain Trial): description of the intervention," *Spinal Cord*, vol. 62, no. 11, pp. 658–666, 2024.

[62] C. Brunner, R. Leeb, G. Müller-Putz, A. Schlögl, and G. Pfurtscheller, "BCI Competition 2008–Graz data set A," *Institute for Knowledge Discovery (Laboratory of Brain-Computer Interfaces), Graz University of Technology*, vol. 16, pp. 1–6, 2008.

[63] A. Korik, N. Du Bois, G. Campbell, E. O'Neill, L. Hay, S. Gilbert, M. Grealy, and D. Coyle, "Real-time feedback improves imagined 3D primitive object classification from EEG," *Brain-Computer Interfaces*, vol. 11, no. 1-2, pp. 61–85, 2024.

[64] P. Arpaia, D. Coyle, F. Donnarumma, A. Esposito, A. Natalizio, and M. Parvis, "Visual and haptic feedback in detecting motor imagery within a wearable brain–computer interface," *Measurement*, vol. 206, p. 112304, 2023.

[65] P. Arpaia, D. Coyle, A. Esposito, A. Natalizio, M. Parvis, M. Pesola, and E. Vallefuoco, "Motor imagery-based brain-computer interface with dry sensors and multimodal feedback: towards tele-rehabilitation," 2023.

[66] R. Chaisaen, P. Autthasan, N. Mingchinda, P. Leelaarporn, N. Kunaseth, S. Tammajarung, P. Manoonpong, S. C. Mukhopadhyay, and T. Wilaiprasitporn, "Decoding EEG rhythms during action observation, motor imagery, and execution for standing and sitting," *IEEE sensors journal*, vol. 20, no. 22, pp. 13776–13786, 2020.

[67] A. Adham, H. Bessaguet, L. Struber, D. Rimaud, E. Ojardias, and P. Giraux, "Distinct and additive effects of visual and vibratory feedback

for motor rehabilitation: an EEG study in healthy subjects," *Journal of NeuroEngineering and Rehabilitation*, vol. 21, no. 1, p. 158, 2024.

[68] H. Bashashati, R. K. Ward, G. E. Birch, and A. Bashashati, "Comparing different classifiers in sensory motor brain computer interfaces," *PloS one*, vol. 10, no. 6, p. e0129435, 2015.

[69] H. Ramoser, J. Muller-Gerking, and G. Pfurtscheller, "Optimal spatial filtering of single trial EEG during imagined hand movement," *IEEE transactions on rehabilitation engineering*, vol. 8, no. 4, pp. 441–446, 2000.

[70] Y. Wang, S. Gao, and X. Gao, "Common spatial pattern method for channel selelction in motor imagery based brain-computer interface," in *2005 IEEE engineering in medicine and biology 27th annual conference*, pp. 5392–5395, IEEE, 2006.

[71] K. K. Ang, Z. Y. Chin, H. Zhang, and C. Guan, "Filter bank common spatial pattern (FBCSP) in brain-computer interface," in *2008 IEEE international joint conference on neural networks (IEEE world congress on computational intelligence)*, pp. 2390–2397, IEEE, 2008.

[72] V. J. Lawhern, A. J. Solon, N. R. Waytowich, S. M. Gordon, C. P. Hung, and B. J. Lance, "EEGNet: a compact convolutional neural network for EEG-based brain–computer interfaces," *Journal of neural engineering*, vol. 15, no. 5, p. 056013, 2018.

[73] W. Zhao, X. Jiang, B. Zhang, S. Xiao, and S. Weng, "CTNet: a convolutional transformer network for EEG-based motor imagery classification," *Scientific Reports*, vol. 14, no. 1, p. 20237, 2024.

[74] N. Tibrewal, N. Leeuwis, and M. Alimardani, "Classification of motor imagery EEG using deep learning increases performance in inefficient BCI users," *Plos one*, vol. 17, no. 7, p. e0268880, 2022.

[75] D. Milanés-Hermosilla, R. Trujillo Codorniú, R. López-Baracaldo, R. Sagaró-Zamora, D. Delisle-Rodriguez, J. J. Villarejo-Mayor, and J. R. Núñez-Álvarez, "Monte carlo dropout for uncertainty estimation and motor imagery classification," *Sensors*, vol. 21, no. 21, p. 7241, 2021.

[76] S. U. Amin, M. Alsulaiman, G. Muhammad, M. A. Mekhtiche, and M. S. Hossain, "Deep Learning for EEG motor imagery classification based on multi-layer CNNs feature fusion," *Future Generation computer systems*, vol. 101, pp. 542–554, 2019.

[77] Y. El Ouahidi, V. Gripon, B. Pasdeloup, G. Bouallegue, N. Farrugia, and G. Lioi, "A Strong and Simple Deep Learning Baseline for BCI Motor Imagery decoding," *IEEE Transactions on Neural Systems and Rehabilitation Engineering*, 2024.

[78] P. Wang, A. Jiang, X. Liu, J. Shang, and L. Zhang, "LSTM-based EEG classification in motor imagery tasks," *IEEE transactions on neural systems and rehabilitation engineering*, vol. 26, no. 11, pp. 2086–2095, 2018.

[79] Z. Khademi, F. Ebrahimi, and H. M. Kordy, "A transfer learning-based CNN and LSTM hybrid deep learning model to classify motor imagery EEG signals," *Computers in biology and medicine*, vol. 143, p. 105288, 2022.

[80] A. Subasi and S. Mian Qaisar, "The Ensemble Machine Learning-Based Classification of Motor Imagery Tasks in Brain-Computer Interface," *Journal of Healthcare Engineering*, vol. 2021, no. 1, p. 1970769, 2021.

[81] R. Chatterjee, A. Datta, and D. K. Sanyal, "Ensemble learning approach to motor imagery EEG signal classification," in *Machine Learning in Bio-Signal Analysis and Diagnostic Imaging*, pp. 183–208, Elsevier, 2019.

[82] M. Parvan, A. R. Ghiasi, T. Y. Rezaii, and A. Farzamnia, "Transfer learning based motor imagery classification using convolutional neural networks," in *2019 27th Iranian Conference on Electrical Engineering (ICEE)*, pp. 1825–1828, IEEE, 2019.

[83] K. Zhang, N. Robinson, S.-W. Lee, and C. Guan, "Adaptive transfer learning for EEG motor imagery classification with deep convolutional neural network," *Neural Networks*, vol. 136, pp. 1–10, 2021.

[84] D. Wu, X. Jiang, and R. Peng, "Transfer learning for motor imagery based brain–computer interfaces: A tutorial," *Neural Networks*, vol. 153, pp. 235–253, 2022.

[85] F. Xu, Y. Miao, Y. Sun, D. Guo, J. Xu, Y. Wang, J. Li, H. Li, G. Dong, F. Rong, *et al.*, "A transfer learning framework based on motor imagery rehabilitation for stroke," *Scientific Reports*, vol. 11, no. 1, p. 19783, 2021.

[86] B. Sharma, P. T. Phan, J. Davies, T. T. Hoang, C. C. Nguyen, A. Ji, K. Zhu, E. Nicotra, N. H. Lovell, and T. N. Do, "Soft Upper-Limb Wearable Robotic Devices: Technology and Applications," *Advanced Intelligent Systems*, vol. 6, no. 12, p. 2400266, 2024.

[87] S. Bhujel and S. Hasan, "A comparative study of end-effector and exoskeleton type rehabilitation robots in human upper extremity rehabilitation," *Human-Intelligent Systems Integration*, vol. 5, no. 1, pp. 11–42, 2023.

[88] Z. Li, Y. Yuan, L. Luo, W. Su, K. Zhao, C. Xu, J. Huang, and M. Pi, "Hybrid brain/muscle signals powered wearable walking exoskeleton enhancing motor ability in climbing stairs activity," *IEEE Transactions on Medical Robotics and Bionics*, vol. 1, no. 4, pp. 218–227, 2019.

[89] A. L. Benabid, T. Costecalde, A. Eliseyev, G. Charvet, A. Verney, S. Karakas, M. Foerster, A. Lambert, B. Morinière, N. Abroug, *et al.*, "An exoskeleton controlled by an epidural wireless brain–machine interface in a tetraplegic patient: a proof-of-concept demonstration," *The Lancet Neurology*, vol. 18, no. 12, pp. 1112–1122, 2019.

[90] M. Lin, J. Huang, J. Fu, Y. Sun, and Q. Fang, "A VR-based motor imagery training system with EMG-based real-time feedback for post-stroke rehabilitation," *IEEE Transactions on Neural Systems and Rehabilitation Engineering*, vol. 31, pp. 1–10, 2022.

[91] F. Škola and F. Liarokapis, "Embodied VR environment facilitates motor imagery brain–computer interface training," *Computers & Graphics*, vol. 75, pp. 59–71, 2018.

[92] F. Škola and F. Liarokapis, "Virtual reality embodiment in motor imagery brain–computer interface training," *SN Computer Science*, vol. 4, no. 1, p. 17, 2022.

[93] M. Mahmood, S. Kwon, H. Kim, Y.-S. Kim, P. Siriaraya, J. Choi, B. Otkhmezuri, K. Kang, K. J. Yu, Y. C. Jang, *et al.*, "Wireless Soft Scalp Electronics and Virtual Reality System for Motor Imagery-Based

Brain–Machine Interfaces," *Advanced Science*, vol. 8, no. 19, p. 2101129, 2021.

[94] M. Kashif, A. Ahmad, M. A. M. Bandpei, S. A. Gilani, A. Hanif, and H. Iram, "Combined effects of virtual reality techniques and motor imagery on balance, motor function and activities of daily living in patients with parkinson's disease: a randomized controlled trial," *BMC geriatrics*, vol. 22, no. 1, p. 381, 2022.

[95] X. Xu, X. Fan, J. Dong, X. Zhang, Z. Song, W. Li, and F. Pu, "Event-related EEG desynchronization reveals enhanced motor imagery from the third person perspective by manipulating sense of body ownership with virtual reality for stroke patients," *IEEE Transactions on Neural Systems and Rehabilitation Engineering*, 2024.

[96] H. Alsuradi, J. Hong, A. Sarmadi, R. Volcic, H. Salam, S. F. Atashzar, F. Khorrami, and M. Eid, "Neural signatures of motor imagery for a supernumerary thumb in VR: an EEG analysis," *Scientific Reports*, vol. 14, no. 1, p. 21558, 2024.

[97] K. Wang, F. Tian, L. Pan, M. Xu, M. Li, B. Dong, and D. Ming, "Virtual Reality Game-Based Adaptive Neurofeedback Training for Motor Imagery," in *Asian-Pacific Conference on Medical and Biological Engineering*, pp. 296–303, Springer, 2023.

[98] A. Vourvopoulos and S. Bermúdez i Badia, "Motor priming in virtual reality can augment motor-imagery training efficacy in restorative brain-computer interaction: a within-subject analysis," *Journal of neuroengineering and rehabilitation*, vol. 13, pp. 1–14, 2016.

[99] A. Vourvopoulos, J. E. M. Cardona, and S. B. i Badia, "Optimizing motor imagery neurofeedback through the use of multimodal immersive virtual reality and motor priming," in *2015 International Conference on Virtual Rehabilitation (ICVR)*, pp. 228–234, IEEE, 2015.

[100] L. Ferrero, M. Ortíz, V. Quiles, E. Iáñez, and J. M. Azorín, "Improving motor imagery of gait on a brain–computer interface by means of virtual reality: A case of study," *Ieee Access*, vol. 9, pp. 49121–49130, 2021.

[101] J. W. Choi, S. Huh, and S. Jo, "Improving performance in motor imagery BCI-based control applications via virtually embodied feedback," *Computers in Biology and Medicine*, vol. 127, p. 104079, 2020.

[102] L. N. Awad, J. Bae, K. O'donnell, S. M. De Rossi, K. Hendron, L. H. Sloot, P. Kudzia, S. Allen, K. G. Holt, T. D. Ellis, *et al.*, "A soft robotic exosuit improves walking in patients after stroke," *Science translational medicine*, vol. 9, no. 400, p. eaai9084, 2017.

[103] R. W. Nuckols, S. Lee, K. Swaminathan, D. Orzel, R. D. Howe, and C. J. Walsh, "Individualization of exosuit assistance based on measured muscle dynamics during versatile walking," *Science robotics*, vol. 6, no. 60, p. eabj1362, 2021.

[104] M. Pan, C. Yuan, X. Liang, T. Dong, T. Liu, J. Zhang, J. Zou, H. Yang, and C. Bowen, "Soft actuators and robotic devices for rehabilitation and assistance," *Advanced Intelligent Systems*, vol. 4, no. 4, p. 2100140, 2022.

[105] E. Tricomi, G. Piccolo, F. Russo, X. Zhang, F. Missiroli, S. Ferrari, L. Gionfrida, F. Ficuciello, M. Xiloyannis, and L. Masia, "Leveraging Geometric Modeling-based Computer Vision for Context Aware Control in a Hip Exosuit," *IEEE Transactions on Robotics*, 2025.

[106] M. Xiloyannis, R. Alicea, A.-M. Georgarakis, F. L. Haufe, P. Wolf, L. Masia, and R. Riener, "Soft robotic suits: State of the art, core technologies, and open challenges," *IEEE Transactions on Robotics*, vol. 38, no. 3, pp. 1343–1362, 2021.

[107] J. Piao, M. Kim, J. Kim, C. Kim, S. Han, I. Back, J.-s. Koh, and S. Koo, "Development of a comfort suit-type soft-wearable robot with flexible artificial muscles for walking assistance," *Scientific reports*, vol. 13, no. 1, p. 4869, 2023.

[108] H. Zhang and H. Shea, "Clutchable Fabric Actuator for Energy-Efficient Wearable Robots," *Advanced Functional Materials*, vol. 35, no. 6, p. 2415099, 2025.

[109] J. L. Samper-Escudero, A. Gimenez-Fernandez, M. A. Sanchez-Uran, and M. Ferre, "A cable-driven exosuit for upper limb flexion based on fibres compliance," *IEEE Access*, vol. 8, pp. 153297–153310, 2020.

[110] C. T. O'Neill, C. M. McCann, C. J. Hohimer, K. Bertoldi, and C. J. Walsh, "Unfolding textile-based pneumatic actuators for wearable applications," *Soft Robotics*, vol. 9, no. 1, pp. 163–172, 2022.

[111] E. P. Sridhar, V. Erel, A. Nasirian, M. B. Wijesundara, and M. Rahman, "Design, development, and evaluation of a pneumatically actuated soft wearable robotic elbow exoskeleton for reducing muscle activity and perceived workload," *Journal of Rehabilitation and Assistive Technologies Engineering*, vol. 12, p. 20556683251347517, 2025.

[112] B. Ugurlu, H. Oshima, E. Sariyildiz, T. Narikiyo, and J. Babic, "Active compliance control reduces upper body effort in exoskeleton-supported walking," *IEEE Transactions on Human-Machine Systems*, vol. 50, no. 2, pp. 144–153, 2020.

[113] R. Hidayah, D. Sui, K. A. Wade, B.-C. Chang, and S. Agrawal, "Passive knee exoskeletons in functional tasks: Biomechanical effects of a SpringExo coil-spring on squats," *Wearable Technologies*, vol. 2, p. e7, 2021.

[114] X. Yang, T.-H. Huang, H. Hu, S. Yu, S. Zhang, X. Zhou, A. Carriero, G. Yue, and H. Su, "Spine-inspired continuum soft exoskeleton for stoop lifting assistance," *IEEE Robotics and Automation Letters*, vol. 4, no. 4, pp. 4547–4554, 2019.

[115] P. A. Vargas, F. L. Brasil, A. C. McConnell, M. Vallejo, D. W. Corne, A. A. Stokes, and R. C. Moioli, "Combining soft robotics and brain-machine interfaces for stroke rehabilitation," in *Converging Clinical and Engineering Research on Neurorehabilitation II: Proceedings of the 3rd International Conference on NeuroRehabilitation (ICNR2016), October 18-21, 2016, Segovia, Spain*, pp. 1257–1262, Springer, 2017.

[116] A. C. McConnell, M. Vallejo, R. C. Moioli, F. L. Brasil, N. Secciani, M. P. Nemitz, C. P. Riquart, D. W. Corne, P. A. Vargas, and A. A. Stokes, "SOPHIA: soft orthotic physiotherapy hand interactive aid," *Frontiers in Mechanical Engineering*, vol. 3, p. 3, 2017.

[117] W. Li, J. Xu, X. Yan, C. Lin, and C. Fu, "Motor Imagery Intention Recognition Based on Common Spatial Pattern for Manipulator Grasping,"

in *International Conference on Intelligent Robotics and Applications*, pp. 125–135, Springer, 2022.

[118] J. Zhang, B. Wang, C. Zhang, Y. Xiao, and M. Y. Wang, "An EEG/EMG/EOG-based multimodal human-machine interface to real-time control of a soft robot hand," *Frontiers in neurorobotics*, vol. 13, p. 7, 2019.

[119] H. Kwon, C. Hwang, and S. Jo, "Vision combined with mi-based bci in soft robotic glove control," in *2022 10th International Winter Conference on Brain-Computer Interface (BCI)*, pp. 1–5, IEEE, 2022.

[120] P. Mukherjee and A. H. Roy, "EEG sensor driven assistive device for elbow and finger rehabilitation using deep learning," *Expert Systems with Applications*, vol. 244, p. 122954, 2024.

[121] N. Gao, P. Chen, and L. Liang, "BCI–VR-based hand soft rehabilitation system with its applications in hand rehabilitation after stroke," *International Journal of Precision Engineering and Manufacturing*, vol. 24, no. 8, pp. 1403–1424, 2023.

[122] Y. Li, J. Zhang, C. Zhang, Y. Xiao, J. Hong, M. Y. Wang, and Y. Li, "Design of isometric and isotonic soft hand for rehabilitation combining with noninvasive brain machine interface," in *2018 15th International Conference on Ubiquitous Robots (UR)*, pp. 749–754, IEEE, 2018.

[123] L. Schiatti, J. Tessadori, G. Barresi, L. S. Mattos, and A. Ajoudani, "Soft brain-machine interfaces for assistive robotics: A novel control approach," in *2017 International Conference on Rehabilitation Robotics (ICORR)*, pp. 863–869, IEEE, 2017.

[124] N. Cheng, K. S. Phua, H. S. Lai, P. K. Tam, K. Y. Tang, K. K. Cheng, R. C.-H. Yeow, K. K. Ang, C. Guan, and J. H. Lim, "Brain-computer interface-based soft robotic glove rehabilitation for stroke," *IEEE Transactions on Biomedical Engineering*, vol. 67, no. 12, pp. 3339–3351, 2020.

[125] W. Zhang, A. Song, H. Hu, M. Miao, and B. Xu, "The application of vibration tactile stimulation in hand motor imagery paradigm: a pilot study," *Brain-Apparatus Communication: A Journal of Bacomics*, vol. 3, no. 1, p. 2383862, 2024.

[126] Z. Tang, L. Zhang, X. Chen, J. Ying, X. Wang, and H. Wang, "Wearable supernumerary robotic limb system using a hybrid control approach based on motor imagery and object detection," *IEEE Transactions on Neural Systems and Rehabilitation Engineering*, vol. 30, pp. 1298–1309, 2022.

[127] R. S. Araujo, C. R. Silva, S. P. Netto, E. Morya, and F. L. Brasil, "Development of a low-cost EEG-controlled hand exoskeleton 3D printed on textiles," *Frontiers in Neuroscience*, vol. 15, p. 661569, 2021.

[128] J. J. González-España, L. Sánchez-Rodríguez, M. A. Pacheco-Ramírez, J. Feng, K. Nedley, S.-H. Chang, G. E. Francisco, and J. L. Contreras-Vidal, "At-Home Stroke Neurorehabilitation: Early Findings with the NeuroExo BCI System," *Sensors*, vol. 25, no. 5, p. 1322, 2025.

[129] M. Zeydabadinezhad, J. Jowers, D. Buhl, B. Cabaniss, and B. Mahmoudi, "A personalized earbud for non-invasive long-term EEG monitoring," *Journal of Neural Engineering*, vol. 21, no. 2, p. 026026, 2024.

[130] N.-D. Mai and W.-Y. Chung, "On-Chip Mental Stress Detection: Integrating a Wearable Behind-the-Ear EEG Device with Embedded Tiny Neural Network," *IEEE Journal of Biomedical and Health Informatics*, 2024.

[131] T. L. Goh and L.-S. Peh, "Walkingwizard-a truly wearable eeg headwear for everyday use," in *2024 IEEE/ACM Conference on Connected Health: Applications, Systems and Engineering Technologies (CHASE)*, pp. 212–213, IEEE, 2024.

[132] M. Sheeraz, A. R. Aslam, E. M. Drakakis, H. Heidari, M. A. B. Altaf, and W. Saadeh, "A Closed-Loop Ear-Worn Wearable EEG System with Real-Time Passive Electrode Skin Impedance Measurement for Early Autism Detection," *Sensors (Basel, Switzerland)*, vol. 24, no. 23, p. 7489, 2024.

[133] K. Schäffer, Y. Ozkan-Aydin, and M. M. Coad, "Soft wrist exosuit actuated by fabric pneumatic artificial muscles," *IEEE Transactions on Medical Robotics and Bionics*, 2024.

[134] K. Zhu, B. Sharma, P. T. Phan, J. Davies, M. T. Thai, T. T. Hoang, C. C. Nguyen, A. Ji, E. Nicotra, N. H. Lovell, *et al.*, "Development of a

Smart Textile-Driven Soft Spine Exosuit for Lifting Tasks in Industrial Applications," in *2024 IEEE/SICE International Symposium on System Integration (SII)*, pp. 13–18, IEEE, 2024.

[135] T. Lei, J. Seo, K. Liang, J. Xu, H. Li, Y. Zhou, M. Khan, and K. H. Heung, "Lightweight active soft back exosuit for construction workers in lifting tasks," *Journal of Construction Engineering and Management*, vol. 150, no. 7, p. 04024073, 2024.

[136] H. Su, F. Missiroli, X. Zhang, C. Becchio, H.-S. Park, and L. Masia, "Advanced Soft Wearable Robotics for Rehabilitation: Incorporating Forearm Rotation in a Glove Exosuit to Augment Grasping Capabilities and Improve Therapeutic Outcomes," in *2024 10th IEEE RAS/EMBS International Conference for Biomedical Robotics and Biomechatronics (BioRob)*, pp. 1011–1016, IEEE, 2024.

[137] S. Thakur, N. D. Armas, J. Adegite, R. Pandey, J. Mead, P. M. Rao, and C. D. Onal, "A Tetherless Soft Robotic Wearable Haptic Human Machine Interface for Robot Teleoperation," in *2024 IEEE/RSJ International Conference on Intelligent Robots and Systems (IROS)*, pp. 12226–12233, IEEE, 2024.

[138] R. F. Natividad, T. Miller-Jackson, and R. Y. Chen-Hua, "A 2-DOF shoulder exosuit driven by modular, pneumatic, fabric actuators," *IEEE Transactions on Medical Robotics and Bionics*, vol. 3, no. 1, pp. 166–178, 2020.

[139] T. Verburg, S. Joshi, A. Seth, and C. Della Santina, "Development of a Variable Stiffness Mechanism with a Linear Output for Exosuit Integration," in *2024 10th IEEE RAS/EMBS International Conference for Biomedical Robotics and Biomechatronics (BioRob)*, pp. 1738–1745, IEEE, 2024.

[140] R. J. Varghese, B. P. L. Lo, and G.-Z. Yang, "Design and prototyping of a bio-inspired kinematic sensing suit for the shoulder joint: Precursor to a multi-dof shoulder exosuit," *IEEE Robotics and Automation Letters*, vol. 5, no. 2, pp. 540–547, 2020.

[141] H. Brown, E. Shannon, and N. T. Fitter, "Design and preliminary evaluation of the aid vest: An automatic inflatable wearable device for anxiety

reduction," in *2021 IEEE World Haptics Conference (WHC)*, pp. 745–750, IEEE, 2021.

[142] M. D. Permanasari, M. Shavira, F. Trivan, H. Azka, M. Maira, N. Zulfa, R. Karnita, E. Noviana, *et al.*, "PELÜK: Deep-touch-pressure (DTP) Sensory Vest to Reduce Anxiety," *Rekayasa Hijau: Jurnal Teknologi Ramah Lingkungan*, vol. 8, no. 3, pp. 309–319, 2024.

[143] L. Luo, "Behave-Knit: Sustainable Integration of Pneumatic Actuators in Knitted Wearables," in *Proceedings of the Nineteenth International Conference on Tangible, Embedded, and Embodied Interaction*, pp. 1–4, 2025.

[144] A. G. Hassabo, B. M. Hegazy, H. M. Elmorsy, N. Gamal, A. Sedik, F. Saad, and H. A. Othman, "Intelligent smart textiles: Wearable textile devices for solar cells," *Journal of Art, Design and Music*, vol. 3, no. 2, p. 10, 2024.

[145] J. Martins, S. M. Cerqueira, A. W. Catarino, A. F. da Silva, A. M. Rocha, J. Vale, M. Ângelo, and C. P. Santos, "Integrating sEMG and IMU sensors in an e-Textile smart vest for forward posture monitoring: First steps," *Sensors*, vol. 24, no. 14, p. 4717, 2024.

[146] H. Choi and S. Yoo, "Development of human-touch smart armband for tele-haptic communication using a fabric-based soft pneumatic actuator," *Fashion and Textiles*, vol. 10, no. 1, p. 31, 2023.

[147] Y. Ma, T. Xie, P. Zhang, H. Kim, and S. Je, "AirPush: A Pneumatic Wearable Haptic Device Providing Multi-Dimensional Force Feedback on a Fingertip," in *Proceedings of the 2024 CHI Conference on Human Factors in Computing Systems*, pp. 1–13, 2024.

[148] K. Yao, Q. Zhuang, Q. Zhang, J. Zhou, C. K. Yiu, J. Zhang, D. Ye, Y. Yang, K. W. Wong, L. Chow, *et al.*, "A fully integrated breathable haptic textile," *Science Advances*, vol. 10, no. 42, p. eadq9575, 2024.

[149] J. Qi, L. Yu, E. T. Khoo, K. W. Ng, Y. Gao, A. W. C. Kow, J. C. Yeo, and C. T. Lim, "Bridging the digital–physical divide using haptic and wearable technologies," *Nature Electronics*, vol. 7, no. 12, pp. 1098–1110, 2024.

[150] B. A. MacGavin, J. L. Tennison, T. Edwards, and J. L. Gorlewicz, "The CHAT System: A Wearable Haptic System For Facilitating Tactile Communication," *IEEE Transactions on Haptics*, 2025.

[151] D. Leonardis, D. Chiaradia, G. Santamato, C. Camardella, and A. Frisoli, "Rendering Fine Tactile Feedback With a Novel Hydraulic Actuation Method for Wearable Haptic Devices," *IEEE Access*, 2024.

[152] M. Kruijthoff, A. El Ali, H. Verma, S. Günther, and K. Jansen, "MobiTouch: Enhancing Pneumatic Wearable Haptics with Vibrotactile Actuation," in *Proceedings of the International Conference on Mobile and Ubiquitous Multimedia*, pp. 516–518, 2024.

[153] P. B. Banyarani, B. Tarvirdizadeh, and A. Hadi, "Design and fabrication of a soft wearable robot using a novel pleated fabric pneumatic artificial muscle (pfPAM) to assist walking," *Sensors and Actuators A: Physical*, vol. 370, p. 115278, 2024.

[154] T. Liu and J. Realmuto, "A Soft Robotic Exosuit For Knee Extension Using Hyper-Bending Actuators," *arXiv preprint arXiv:2410.02802*, 2024.

[155] N.-Y. Liu, P. M. R. Erpenback, S. O. Arriagada, P.-H. Su, P. A. Tuan, C.-H. Yu, and B.-S. Chang, "A Rigid-Soft Switchable Lower Body Exosuit for Lifting," in *2024 International Conference on Advanced Robotics and Intelligent Systems (ARIS)*, pp. 1–6, IEEE, 2024.

[156] H. Ju, Z. Guan, S. Guo, Z. Liu, Q. Zhang, T. Zheng, J. Zhao, and Y. Zhu, "JHT-EXO: A Soft Ankle Exosuit for Assisting Walking in Patients with Post-Stroke Foot Inversion," in *2024 IEEE International Conference on Robotics and Biomimetics (ROBIO)*, pp. 161–165, IEEE, 2024.

[157] Y. Han, D. Shi, Y. Shao, Y. Feng, X. Ding, and W. Zhang, "Design and Evaluation of a Soft Knee Exosuit for Reducing Knee Medial Compartment Load During Walking," *IEEE Transactions on Biomedical Engineering*, 2024.

[158] M. T. Knierim, C. Zimny, G. Ivucic, and T. Röddiger, "Advancing Wearable BCI: Headphone EEG for Cognitive Load Detection in Lab and Field," *Proceedings of the ACM on Interactive, Mobile, Wearable and Ubiquitous Technologies*, vol. 9, no. 1, pp. 1–26, 2025.

[159] H. A. Sonar, J.-L. Huang, and J. Paik, "Soft touch using soft pneumatic actuator–skin as a wearable haptic feedback device," *Advanced Intelligent Systems*, vol. 3, no. 3, p. 2000168, 2021.

[160] A. Bontula, K. Jones, S. Buchmeier, C. Wilson, and N. T. Fitter, "Evaluating a Soft Robotic Vest's Ability to Reduce General Anxiety," in *2024 33rd IEEE International Conference on Robot and Human Interactive Communication (ROMAN)*, pp. 1538–1543, IEEE, 2024.

[161] X. Zhang, Y.-X. Liu, R. Wang, and E. M. Gutierrez-Farewik, "Soft ankle exoskeleton to counteract dropfoot and excessive inversion," *Frontiers in Neurorobotics*, vol. 18, p. 1372763, 2024.

[162] J. Nassour, G. Zhao, and M. Grimmer, "Soft pneumatic elbow exoskeleton reduces the muscle activity, metabolic cost and fatigue during holding and carrying of loads," *Scientific Reports*, vol. 11, no. 1, p. 12556, 2021.

[163] R. Liu, Q. Song, T. Ma, and H. Pan, "Remapping Movement of Shoulder with Soft Sensors: A Non-invasive Wearable Body-Machine Interface," *IEEE Sensors Journal*, vol. 24, no. 20, pp. 33101–33111, 2024.

[164] R. Nawaz, H. Suen, R. Ullah, M. Purcell, S. Diggin, E. McCaughey, and A. Vuckovic, "Electroencephalography Longitudinal Markers of Central Neuropathic Pain Intensity in Spinal Cord Injury: A Home-Based Pilot Study," *Biomedicines*, vol. 12, no. 12, p. 2751, 2024.

[165] J. Choi, K. T. Kim, J. H. Jeong, L. Kim, S. J. Lee, and H. Kim, "Developing a motor imagery-based real-time asynchronous hybrid BCI controller for a lower-limb exoskeleton," *Sensors*, vol. 20, no. 24, p. 7309, 2020.

[166] Y. He, Y. Xu, M. Hai, Y. Feng, P. Liu, Z. Chen, and W. Duan, "Exoskeleton-assisted rehabilitation and neuroplasticity in spinal cord injury," *World Neurosurgery*, vol. 185, pp. 45–54, 2024.

[167] F. Patarini, F. Tamburella, S. Mohebban, F. Pichiorri, N. Tagliamonte, A. Ranieri, M. Lorusso, G. Serratore, A. Bigioni, A. Ciaramidaro, *et al.*, "Assessing Therapist-Mediated Visual Feedback in Robot-Assisted Gait Training Through Eye-Tracking and HD-EEG," in *International Conference on NeuroRehabilitation*, pp. 195–198, Springer, 2024.

[168] Z. Al-Qaysi, M. Ahmed, N. M. Hammash, A. F. Hussein, A. Albahri, M. Suzani, and B. Al-Bander, "A systematic rank of smart training environment applications with motor imagery brain-computer interface," *Multimedia Tools and Applications*, vol. 82, no. 12, pp. 17905–17927, 2023.

[169] K. Kostoglou and G. R. Müller-Putz, "Motor-Related EEG Analysis Using a Pole Tracking Approach," *IEEE Transactions on Neural Systems and Rehabilitation Engineering*, 2024.

[170] J. Leng, L. Gao, X. Jiang, Y. Lou, Y. Sun, C. Wang, J. Li, H. Zhao, C. Feng, F. Xu, *et al.*, "A multi-feature fusion graph attention network for decoding motor imagery intention in spinal cord injury patients," *Journal of Neural Engineering*, vol. 21, no. 6, p. 066044, 2024.

[171] M. Liu, Y. Liu, W. Shi, Y. Lou, Y. Sun, Q. Meng, D. Wang, F. Xu, Y. Zhang, L. Zhang, *et al.*, "EMPT: a sparsity Transformer for EEG-based motor imagery recognition," *Frontiers in Neuroscience*, vol. 18, p. 1366294, 2024.

[172] A. Gonzalez-Cely, C. Blanco-Diaz, D. Delisle-Rodriguez, and T. Bastos-Filho, "EEG-Based Multi-Class Classification for Recognizing Pedaling Velocities: A Promising Approach for Brain-Computer Interface-Enhanced Lower-Limb Robotic Rehabilitation," in *2024 10th IEEE RAS/EMBS International Conference for Biomedical Robotics and Biomechatronics (BioRob)*, pp. 223–228, IEEE, 2024.

[173] J. Feng, S. Gao, Y. Hu, G. Sun, and W. Sheng, "Brain-computer interface for patients with spinal cord injury: A bibliometric study," *World Neurosurgery*, vol. 192, pp. 170–187, 2024.

[174] T. T. Roberts, G. R. Leonard, and D. J. Cepela, "Classifications in brief: American spinal injury association (ASIA) impairment scale," *Clinical Orthopaedics and Related Research®*, vol. 475, no. 5, pp. 1499–1504, 2017.

[175] E. B. Inc., "EksoNR: Robotic Exoskeleton for Rehabilitation and Mobility." https://eksobionics.com/, 2023. FDA-approved exoskeleton for lower limb rehabilitation.

[176] A. Wiśniowska-Szurlej, N. Wołoszyn, J. Brożonowicz, G. Ciąpała, K. Pietryka, J. Grzegorczyk, J. Leszczak, A. Ćwirlej-Sozańska, B. Sozański, and B. Korczowski, "Enhanced rehabilitation outcomes of robotic-assisted gait training with EksoNR lower extremity exoskeleton in 19 stroke patients," *Medical Science Monitor: International Medical Journal of Experimental and Clinical Research*, vol. 29, pp. e940511–1, 2023.

[177] ANT Neuro, "ANT Neuro – Enschede, The Netherlands." https://www.ant-neuro.com/, 2025. Accessed: 2025-10-08.

[178] R. Leeb, C. Brunner, G. Müller-Putz, A. Schlögl, and G. Pfurtscheller, "BCI Competition 2008–Graz data set B," *Graz University of Technology, Austria*, vol. 16, pp. 1–6, 2008.

[179] G. Pfurtscheller, "Event-related synchronization (ERS): an electrophysiological correlate of cortical areas at rest," *Electroencephalography and clinical neurophysiology*, vol. 83, no. 1, pp. 62–69, 1992.

[180] G. Pfurtscheller and F. L. Da Silva, "Event-related EEG/MEG synchronization and desynchronization: basic principles," *Clinical neurophysiology*, vol. 110, no. 11, pp. 1842–1857, 1999.

[181] Y. Hu and K. Chen, "Feature extraction of EEG signal based on EMD in OVR-CSP,"

[182] A. M. Roy, "A multi-scale fusion CNN model based on adaptive transfer learning for multi-class MI-classification in BCI system," *BioRxiv*, pp. 2022–03, 2022.

[183] A. Nanbancha, C. Mawhinney, and K. Sinsurin, "The effect of motor imagery and action observation in the rehabilitation of lower limb injuries: A scoping review," *Clinical Rehabilitation*, vol. 37, no. 2, pp. 145–161, 2023.

[184] F. Velasco-Álvarez, R. Ron-Angevin, L. da Silva-Sauer, and S. Sancha-Ros, "Audio-cued motor imagery-based brain–computer interface: Navigation through virtual and real environments," *Neurocomputing*, vol. 121, pp. 89–98, 2013.

[185] P. Arpaia, D. Coyle, G. D'Errico, E. De Benedetto, L. T. De Paolis, N. du Bois, S. Grassini, G. Mastrati, N. Moccaldi, and E. Vallefuoco, "Virtual reality enhances EEG-based neurofeedback for emotional self-regulation," in *International Conference on Extended Reality*, pp. 420–431, Springer, 2022.

[186] C. Gao, M. Xia, Z. Zhang, Y. Han, and Y. Gu, "Improving the Brain-Computer Interface Learning Process with Gamification in Motor Imagery: A Review," *Gamification-Analysis, Design, Development and Ludification*, 2022.

[187] L. Zhang, L. Chen, Z. Wang, X. Zhang, X. Liu, and D. Ming, "Enhancing Visual-Guided Motor Imagery Performance via Sensory Threshold Somatosensory Electrical Stimulation Training," *IEEE Transactions on Biomedical Engineering*, vol. 70, no. 2, pp. 756–765, 2022.

[188] Q. Zhou, R. Cheng, L. Yao, X. Ye, and K. Xu, "Neurofeedback training of alpha relative power improves the performance of motor imagery brain-computer interface," *Frontiers in Human Neuroscience*, vol. 16, p. 831995, 2022.

[189] P. Sepulveda, R. Sitaram, M. Rana, C. Montalba, C. Tejos, and S. Ruiz, "How feedback, motor imagery, and reward influence brain self-regulation using real-time fMRI," *Human brain mapping*, vol. 37, no. 9, pp. 3153–3171, 2016.

[190] G. Freeman, "Complete Latin squares and related experimental designs," *Journal of the Royal Statistical Society Series B: Statistical Methodology*, vol. 41, no. 2, pp. 253–262, 1979.

[191] "Neuroconcise technology," https://www.neuroconcise.co.uk/,"

[192] N. Du Bois, R. Beveridge, N. McShane, T. Moore, and D. Coyle, "Signal Quality Assessment of a Wearable Electroencephalography (EEG) Device Built on a Flexible Printed Circuit: FlexEEG," in *2022 IEEE International Conference on Metrology for Extended Reality, Artificial Intelligence and Neural Engineering (MetroXRAINE)*, pp. 679–684, IEEE, 2022.

[193] S. N. Resalat and V. Saba, "A study of various feature extraction methods on a motor imagery based brain computer interface system," *Basic and clinical neuroscience*, vol. 7, no. 1, p. 13, 2016.

[194] L. Pan, K. Wang, L. Xu, X. Sun, W. Yi, M. Xu, and D. Ming, "Riemannian geometric and ensemble learning for decoding cross-session motor imagery electroencephalography signals," *Journal of Neural Engineering*, vol. 20, no. 6, p. 066011, 2023.

[195] S. G. Hart, "NASA task load index (TLX)," 1986.

[196] P. Arpaia, D. Coyle, F. Donnarumma, A. Esposito, A. Natalizio, and M. Parvis, "Non-immersive versus immersive extended reality for motor imagery neurofeedback within a brain-computer interfaces," in *International Conference on Extended Reality*, pp. 407–419, Springer, 2022.

[197] L. Li, Y. Zhang, L. Fan, J. Zhao, J. Guo, C. Li, J. Wang, and T. Liu, "Activation of the brain during motor imagination task with auditory stimulation," *Frontiers in Neuroscience*, vol. 17, p. 1130685, 2023.

[198] Z. Emami and T. Chau, "The effects of visual distractors on cognitive load in a motor imagery brain-computer interface," *Behavioural brain research*, vol. 378, p. 112240, 2020.

[199] D. Zapała, P. Francuz, E. Zapała, N. Kopiś, P. Wierzgała, P. Augustynowicz, A. Majkowski, and M. Kołodziej, "The impact of different visual feedbacks in user training on motor imagery control in BCI," *Applied psychophysiology and biofeedback*, vol. 43, pp. 23–35, 2018.

[200] A. A. Frolov, O. Mokienko, R. Lyukmanov, E. Biryukova, S. Kotov, L. Turbina, G. Nadareyshvily, and Y. Bushkova, "Post-stroke rehabilitation training with a motor-imagery-based brain-computer interface (BCI)-controlled hand exoskeleton: a randomized controlled multicenter trial," *Frontiers in neuroscience*, vol. 11, p. 400, 2017.

[201] L.-W. Ko, S. Ranga, O. Komarov, and C.-C. Chen, "Development of single-channel hybrid BCI system using motor imagery and SSVEP," *Journal of healthcare engineering*, vol. 2017, 2017.

[202] J. Camacho and V. Manian, "Real-time single channel EEG motor imagery based Brain Computer Interface," in *2016 World Automation Congress (WAC)*, pp. 1–6, IEEE, 2016.

[203] S. Kanoga, A. Kanemura, and H. Asoh, "A comparative study of features and classifiers in single-channel EEG-based motor imagery BCI," in *2018 IEEE Global Conference on Signal and Information Processing (GlobalSIP)*, pp. 474–478, IEEE, 2018.

[204] K. P. Thomas, C. Guan, C. T. Lau, A. P. Vinod, and K. K. Ang, "A new discriminative common spatial pattern method for motor imagery brain–computer interfaces," *IEEE transactions on biomedical engineering*, vol. 56, no. 11, pp. 2730–2733, 2009.

[205] K. P. Thomas, N. Robinson, and A. P. Vinod, "Utilizing subject-specific discriminative EEG features for classification of motor imagery directions," in *2019 IEEE 10th International Conference on Awareness Science and Technology (iCAST)*, pp. 1–5, IEEE, 2019.

[206] K. P. Thomas, N. Robinson, and V. A. Prasad, "Separability of motor imagery directions using subject-specific discriminative EEG features," *IEEE Transactions on Human-Machine Systems*, vol. 51, no. 5, pp. 544–553, 2021.

[207] R. Dhiman *et al.*, "Electroencephalogram channel selection based on pearson correlation coefficient for motor imagery-brain-computer interface," *Measurement: Sensors*, vol. 25, p. 100616, 2023.

[208] J. Yu and Z. L. Yu, "Cross-correlation based discriminant criterion for channel selection in motor imagery BCI systems," *Journal of Neural Engineering*, vol. 18, no. 4, p. 046083, 2021.

[209] P. Gaur, K. McCreadie, R. B. Pachori, H. Wang, and G. Prasad, "An automatic subject specific channel selection method for enhancing motor imagery classification in EEG-BCI using correlation," *Biomedical Signal Processing and Control*, vol. 68, p. 102574, 2021.

[210] V. Jusas and S. G. Samuvel, "Classification of motor imagery using a combination of user-specific band and subject-specific band for brain-computer interface," *Applied Sciences*, vol. 9, no. 23, p. 4990, 2019.

[211] M. Meng, Z. Dong, Y. Gao, and Q. She, "Optimal channel and frequency band-based feature selection for motor imagery electroencephalogram classification," *International Journal of Imaging Systems and Technology*, vol. 33, no. 2, pp. 670–679, 2023.

[212] Y. Yang, I. Bloch, S. Chevallier, and J. Wiart, "Subject-specific channel selection using time information for motor imagery brain–computer interfaces," *Cognitive Computation*, vol. 8, pp. 505–518, 2016.

[213] S. Hu, H. Wang, J. Zhang, W. Kong, and Y. Cao, "Causality from Cz to C3/C4 or between C3 and C4 revealed by Granger causality and new causality during motor imagery," in *2014 International joint conference on neural networks (IJCNN)*, pp. 3178–3185, IEEE, 2014.

[214] V. P. Oikonomou, S. Nikolopoulos, and I. Kompatsiaris, "A multitask bayesian framework for the analysis of motor imagery EEG data," in *2022 30th European Signal Processing Conference (EUSIPCO)*, pp. 1308–1312, IEEE, 2022.

[215] M. Kodama, S. Iwama, M. Morishige, and J. Ushiba, "Thirty-minute motor imagery exercise aided by EEG sensorimotor rhythm neurofeedback enhances morphing of sensorimotor cortices: a double-blind sham-controlled study," *Cerebral Cortex*, vol. 33, no. 11, pp. 6573–6584, 2023.

[216] X. Tang, C. Yang, X. Sun, M. Zou, and H. Wang, "Motor imagery EEG decoding based on multi-scale hybrid networks and feature enhancement," *IEEE Transactions on Neural Systems and Rehabilitation Engineering*, vol. 31, pp. 1208–1218, 2023.

[217] Z. Miao and M. Zhao, "Time–space–frequency feature Fusion for 3-channel motor imagery classification," *Biomedical Signal Processing and Control*, vol. 90, p. 105867, 2024.

[218] A. Kumari, D. R. Edla, R. R. Reddy, S. Jannu, A. Vidyarthi, A. Alkhayyat, and M. S. G. de Marin, "EEG-based motor imagery channel selection and classification using hybrid optimization and two-tier deep learning," *Journal of Neuroscience Methods*, vol. 409, p. 110215, 2024.

[219] M. J. Rosenfelder, M. Spiliopoulou, B. Hoppenstedt, R. Pryss, P. Fissler, M. della Piedra Walter, I.-T. Kolassa, and A. Bender, "Stability of mental

motor-imagery classification in EEG depends on the choice of classifier model and experiment design, but not on signal preprocessing," *Frontiers in computational neuroscience*, vol. 17, p. 1142948, 2023.

[220] B. Wang, F. Wan, P. U. Mak, P. I. Mak, and M. I. Vai, "Eeg signals classification for brain computer interfaces based on gaussian process classifier," in *Proceedings of the 7th international conference on Information, communications and signal processing*, pp. 784–788, 2009.

[221] H. Ban, E. H. Riemens, and R. T. Rajan, "Malleable Kernel Interpolation for Scalable Structured Gaussian Process," 2023.

[222] M. N. Gibbs and D. J. MacKay, "Variational Gaussian process classifiers," *IEEE Transactions on Neural Networks*, vol. 11, no. 6, pp. 1458–1464, 2000.

[223] C. K. Williams and C. E. Rasmussen, *Gaussian processes for machine learning*, vol. 2. MIT press Cambridge, MA, 2006.

[224] M. Zhong, F. Lotte, M. Girolami, and A. Lécuyer, "Classifying EEG for brain computer interfaces using Gaussian processes," *Pattern Recognition Letters*, vol. 29, no. 3, pp. 354–359, 2008.

[225] A. Gramfort, M. Luessi, E. Larson, D. A. Engemann, D. Strohmeier, C. Brodbeck, R. Goj, M. Jas, T. Brooks, L. Parkkonen, *et al.*, "MEG and EEG data analysis with MNE-Python," *Frontiers in Neuroinformatics*, vol. 7, p. 267, 2013.

[226] F. Pedregosa, "Scikit-learn: Machine learning in python Fabian," *Journal of machine learning research*, vol. 12, p. 2825, 2011.

[227] Y. An, H. K. Lam, and S. H. Ling, "Multi-classification for EEG motor imagery signals using data evaluation-based auto-selected regularized FBCSP and convolutional neural network," *Neural Computing and Applications*, vol. 35, no. 16, pp. 12001–12027, 2023.

[228] Y. An, *Development of advanced machine learning based EEG robot for disabled people*. University of Technology Sydney (Australia), 2022.

[229] Y. An, S. H. Han, and S. H. Ling, "Multi-classification for EEG Motor Imagery Signals using Auto-selected Filter Bank Regularized Common

Spatial Pattern," in *2022 IEEE 16th International Symposium on Medical Information and Communication Technology (ISMICT)*, pp. 1–6, IEEE, 2022.

[230] X. Lou, X. Li, H. Meng, J. Hu, M. Xu, J. Yang, and Z. Li, "EEG-DBNet: A Dual-Branch Network for Motor-Imagery Brain-Computer Interfaces," *arXiv preprint arXiv:2405.16090*, 2024.

[231] A. Guillot and U. Debarnot, "Benefits of motor imagery for human space flight: a brief review of current knowledge and future applications," *Frontiers in Physiology*, vol. 10, p. 396, 2019.

[232] S. Gravano, F. Lacquaniti, and M. Zago, "Mental imagery of object motion in weightlessness," *npj Microgravity*, vol. 7, no. 1, p. 50, 2021.

[233] C. Papaxanthis, T. Pozzo, R. Kasprinski, and A. Berthoz, "Comparison of actual and imagined execution of whole-body movements after a long exposure to microgravity," *Neuroscience letters*, vol. 339, no. 1, pp. 41–44, 2003.

[234] D. Rannaud Monany, M. Barbiero, F. Lebon, J. Babič, G. Blohm, D. Nozaki, and O. White, "Motor imagery helps updating internal models during microgravity exposure," *Journal of Neurophysiology*, vol. 127, no. 2, pp. 434–443, 2022.

[235] A. Van Ombergen, A. Demertzi, E. Tomilovskaya, B. Jeurissen, J. Sijbers, I. B. Kozlovskaya, P. M. Parizel, P. H. Van de Heyning, S. Sunaert, S. Laureys, *et al.*, "The effect of spaceflight and microgravity on the human brain," *Journal of neurology*, vol. 264, no. Suppl 1, pp. 18–22, 2017.

[236] J. Roll, K. Popov, V. Gurfinkel, M. Lipshits, C. André-Deshays, J. Gilhodes, and C. Quoniam, "Sensorimotor and perceptual function of muscle proprioception in microgravity," *Journal of Vestibular Research*, vol. 3, no. 3, pp. 259–273, 1993.

[237] G. Clément, "Using your head: cognition and sensorimotor functions in microgravity," *Gravitational and Space Biology*, vol. 20, no. 2, pp. 65–78, 2007.

[238] J. R. Lackner and P. DiZio, "Motor function in microgravity: movement in weightlessness," *Current Opinion in Neurobiology*, vol. 6, no. 6, pp. 744–750, 1996.

[239] A. Chouker, M. Thiel, V. Baranov, D. Meshkov, A. Kotov, K. Peter, K. Messmer, and F. Christ, "Simulated microgravity, psychic stress, and immune cells in men: observations during 120-day 6 HDT," *Journal of Applied Physiology*, vol. 90, no. 5, pp. 1736–1743, 2001.

[240] L. Pavone and D. Cafolla, "A Tailored BCI Controlled Soft Finger Exoskeleton for Patient's Needs: A Conceptual Design," *Biomedical Journal of Scientific & Technical Research*, vol. 19, no. 3, pp. 14288–14292, 2019.

[241] B. Quinlivan, S. Lee, P. Malcolm, D. Rossi, M. Grimmer, C. Siviy, N. Karavas, D. Wagner, A. Asbeck, I. Galiana, *et al.*, "Assistance magnitude versus metabolic cost reductions for a tethered multiarticular soft exosuit," *Science Robotics*, vol. 2, no. 2, 2017.

[242] N. Tacca, J. Nassour, S. K. Ehrlich, N. Berberich, and G. Cheng, "Neurocognitive assessment of intentional control methods for a soft elbow exosuit using error-related potentials," *Journal of NeuroEngineering and Rehabilitation*, vol. 19, no. 1, p. 124, 2022.

[243] C. Della Santina, M. Bianchi, G. Grioli, F. Angelini, M. Catalano, M. Garabini, and A. Bicchi, "Controlling soft robots: balancing feedback and feedforward elements," *IEEE Robotics & Automation Magazine*, vol. 24, no. 3, pp. 75–83, 2017.

[244] M. Stölzle, L. Chin, R. L. Truby, D. Rus, and C. Della Santina, "Modelling Handed Shearing Auxetics: Selective Piecewise Constant Strain Kinematics and Dynamic Simulation," in *2023 IEEE International Conference on Soft Robotics (RoboSoft)*, pp. 1–8, IEEE, 2023.

[245] M. Stölzle, D. Rus, and C. D. Santina, "An Experimental Study of Model-based Control for Planar Handed Shearing Auxetics Robots," in *Experimental Robotics: The 18th International Symposium*, Springer, 2023.

[246] N. Schärer, F. Villani, A. Melatur, S. Peter, T. Polonelli, and M. Magno, "Electrasight: Fully onboard eye tracking for smart glasses with hybrid eog (heog)," *IEEE Internet of Things Journal*, 2025.